TIN WHISKERS MITIGATION BY CO-ELECTROPLATING ANTIMONY

by

LEI ZHANG

A dissertation submitted in partial fulfillment of the
requirements for the degree of

DOCTOR OF PHILOSOPHY IN MECHANICAL ENGINEERING

2024

Oakland University
Rochester, Michigan

Doctoral Advisory Committee:

Xia Wang, Ph.D., Chair
Hongwei Qu, Ph.D., Co-Chair
Gary Barber, Ph.D.
Ankun Yang, Ph.D.

To Wenhui and Rongguang

No words could properly convey my appreciation for the

love, care, inspiration, and motivation you have given me.

ACKNOWLEDGMENTS

Foremost, I would like to express my sincere gratitude to my co-advisors Dr. Hongwei Qu and Dr. Xia Wang for the continuous support of my doctoral study and research, and their patience, motivation, enthusiasm, and immense knowledge. Their dynamism, vision, and sincerity have deeply inspired me. I could not have finished my research without their trust in me and the authority they gave me. I would also like to thank them for their friendship and great sense of humor. It is a great privilege and honor to work and study under their guidance.

I would also like to thank Dr. Gary Barber and Dr. Ankun Yang for their encouragement, and insightful comments on this dissertation work.

My sincere thanks also go to Mr. Sherin Bhassyvasantha for offering me the necessary testing materials and leading me to work on analyzing projects. Our discussions and his guidance on materials characterizations greatly helped me throughof the research.

Last but not least, I would like to acknowledge with gratitude the support and love of my parents and my dearest wife. They have been keeping me moving forward with courage and love.

Lei Zhang

PREFACE

Spontaneous tin whiskers are filament-type structures grown from bulk or thin film tin with a very high aspect ratio. In Sn coating, this phenomenon is considered as internal stress-driven diffusion behavior. Sn whiskers can cause short-circuiting by bridging adjacent electronic components. In the past, doping lead into tin plating was the most popular method of inhibiting tin whisker growth. Due to environmental concerns, lead, however, has been banned from electronic products by the European legislation on Restriction of Hazardous Substances (RoHS), and this old issue has reemerged ever since. Thus, Sn whiskers are now receiving significant attention in academia and industries. Unfortunately, even today there is a lack of understanding of the mechanism for Sn whisker growth. This dissertation work tries to address this issue with additives and optimized conditions in electroplating of tin films.

ABSTRACT

TIN WHISKERS MITIGATION BY CO-ELECTROPLATING ANTIMONY

by

LEI ZHANG

Advisers: Xia Wang, Ph.D. and Hongwei Qu, Ph.D.

Electroplating Sn coatings are used extensively in the electronics industry because of their excellent solderability, ductility, electrical conductivity, and corrosion resistance. However, tin whiskers have been observed to grow spontaneously from the electroplating tin coatings for over 70 years. This filament-type structure can lead to short circuits and device failures by bridging adjacent electronics. Over the last several decades, adding a small amount of lead (Pb) has been the most widely adopted method for mitigating Sn whiskers growth. However, this 70-year-old issue of whisker growth has reemerged due to the ban on the use of Pb from Sn-based plating and solders enforced by the European legislation on Restriction of Hazardous Substances (RoHS).

The actual mitigation provided by the co-electroplating lead remains unclear. Some have attributed the mitigation to the formation of equiaxial grains in a Sn-Pb plating process. Others have attributed it to reducing stress buildup in the film while doping Pb.

This study proposes an innovative controllable way to mitigate Sn whiskers growth by electroplating Sn-xSb alloys (x=3 wt.%, 10 w.t%, 15 wt.%.). In effect validation, a fixture was designed to apply high wide-plane compressive stress rather than

using a hardness indenter to accelerate whisker growth. The results revealed that no whisker growth was observed on any Sn-xSb surface, while pure Sn samples produced whiskers up to 200 um under the same conditions. Adding a minor quantity of Sb could refine the Sn grains, however, the Sn grain size was not further refined with the increase in Sb content. In correspondence, the mitigation effect on whiskers growth was not further improved with the increase in Sb content. As confirmed by a series of EBSD studies, the addition of Sb changed the grain structure from a monolayer columnar structure to a multilayer equiaxed structure, which is favorable in whisker mitigation. The inhibition effect of Sb addition on whisker growth can be ascribed to the assistance of dynamic recrystallization and produces horizontal grain boundaries of Sn grains.

This dissertation details the following studies: background of tin whisker problems; development and validation of an effective co-electroplating recipe for tin whisker mitigation using advanced analysis tools; identification of the primary mechanisms of the whisker growth mitigation.

TABLE OF CONTENTS

TABLE OF CONTENTS—Continued

TABLE OF CONTENTS—Continued

LIST OF TABLES

LIST OF FIGURES

LIST OF FIGURES—Continued

LIST OF FIGURES—Continued

LIST OF ABBREVIATIONS

EBSD	Electron backscattering diffraction
IMC	Intermetallic compound
DRX	Dynamic recrystallization
SEM	Scanning electron microscopy
EDS	Energy dispersive spectroscopy
WEEE	Waste Electrical and Electronic Equipment
ROHS	Restriction of Hazardous Substances
MVA	Metal Vapor Arc
KAM	Kernel Average Misorientation
MSA	Methanesulfonic acid
PEG	Polyethylene glycol
GNDs	Geometrically Necessary Dislocations
LAGBs	Low-angle grain boundaries
HAGBs	High-angle grain boundaries

CHAPTER ONE

INTRODUCTION

1.1 Background

Metallic whiskers are electrically conductive, needle-like crystalline structures that spontaneously grow from a metallic finish (especially an electroplated finish). People sometimes confuse the term “whiskers” with a more familiar phenomenon known as “dendrites” which form during electrochemical migration processes. In contrast, whiskers are formed by the migration of atoms caused by the internal stress of the material, and whisker growth is considered to be a process of releasing internal stress.

The phenomenon of metallic whiskers has been recognized as a critical issue in electronics reliability since the 1940s. This recognition was propelled by incidents such as the short-circuiting of condenser plates due to the growth of cadmium whiskers, as documented by Cobb [1] in his pioneering studies. These conductive crystalline structures can attain lengths of several hundred micrometers, substantially elevating the risk of electrical failure through short-circuiting or metal arcing.

Extensive research has been dedicated to understanding the whisker growth phenomena across a range of metals, including tin (Sn) and its alloys, bismuth (Bi), zinc (Zn), indium (In), and others [2-4]. Among these, tin is of paramount interest to the electronics manufacturing sector due to its prevalent use. Tin’s attributes—such as its low melting point, affordability, exceptional electrical conductivity, high resistance to corrosion, and excellent solderability—make it the metal of choice for over half of the global production of electronic solder used in the assembly of circuit boards.

Consequently, the study of tin whiskers occupies a central role in ongoing research efforts aimed at enhancing the reliability and longevity of electronic devices and systems by developing strategies to mitigate whisker formation and its associated challenges.

Tin whiskers have been a serious threat in terms of electronic reliability for more than 70 years [5-7]. The first published reports of Sn whiskers date back to the 1950s [8]. In 1959, Arnold first reported that it was effective to mitigate Sn whiskers growth by adding at least 3 wt.% Pb [9]. Hereafter, the addition of a small amount of Pb to tin plating became the predominant mitigation strategy of whisker growth for more than 50 years. However, in 2006, the European Union passed the Waste Electrical and Electronic Equipment (WEEE) and Restriction of Hazardous Substances (RoHS) legislation, which banned the use of Pb in electronic products due to environmental concerns [10]. Several other nations such as Japan and some states in the USA had issued similar legislation to eliminate the use of Pb. This rapidly growing lead-free movement currently affects nearly all electronic products. Sn whiskers have therefore re-emerged as a major reliability concern in electronic and electrical systems. The problem has further been exacerbated by the continuous industry demands for smaller and faster devices, with higher packing densities and smaller critical dimensions. Under these conditions, whiskers pose even more of a threat, forcing the industry to seek alternatives to mitigate tin whiskers growth.

1.2 Tin whiskers basics

1.2.1 Driving Forces and Growth Mechanisms for Whiskers Formation

There is currently no consensus on the underlying mechanism of whisker incubation and growth. The research on whiskering is still being conducted in various communities, at all levels. A great deal of controversy and contradictory information

regarding the key factors that affect whisker formation still exists. Most researchers agree that the internal compressive stress and the diffusion of Sn atoms are the two key factors to induce Sn whisker formation.

As early as 1954, Fisher R.M. reported that the application of mechanical stress to the Sn layer resulted in the whiskers formation from the surface [11]. The paper showed that the whisker growth rate is accelerated by the application of mechanical stress. Other studies [12-14] have repeatedly confirmed that mechanical stress can enhance whiskers growth. To date, five main sources of driving forces for whisker formation have been reported, including:

a. mechanical stress (bending, clamping, etc.),
b. residual stress due to initial plating [15,16],
c. thermal-expansion mismatch during thermal cycling [17],
d. electromigration [18],
e. and intermetallic compound (IMC) formation (Cu6Sn5, etc.) [19-20].

In addition to these driving forces, parameters such as the texture of Sn films, humidity [21], and corrosion [22], will also influence whisker formation and growth.

It is also worth mentioning that since Tu proposed the "crack oxide theory" in 1994 [23], studies on the effect of the Sn oxide layer on whisker formation have also been carried out. Related studies suggest that the Sn oxide layer plays a key role in inhibiting homogeneous stress relaxation. The protective or tenacious oxide layer prevents vacancies from being generated at the metal-oxide interface, thereby preventing in-plane stress relaxation by transport of vacancies to the Sn intermetallic region where compressive stress is largest. The oxide-based theories all require some form of breakage

of the oxide layer that would allow whiskers to be extruding out in response to the in-plane compressive stress. To date, whether the oxide layer is necessary for whisker formation remains questionable.

There are currently two principal whisker models that are widely accepted to describe whisker formation. One is Vianco and Rejent's dynamic recrystallization (DRX) whisker growth model [24]. They propose that the underlying mechanism behind whisker growth is DRX. The theory states that creep deformation induced by compressive stress initiates DRX and then provides the mass transport necessary to sustain the grain growth of DRX. The compressive stress generates plastic deformation and increases strain energy, which initiates DRX. Hence whisker formation from the surface is the result of the DRX. The DRX process begins with the build-up of defects caused by deformation, and once the resulting increasing strain energy exceeds a limit, needle grains are generated. These new grains grow under the driving force and once the grain size is commensurate with other grains, there is a constraint on further growth into the material. Outward grain growth, so-called whiskers, will happen until the stress is removed from the material.

Therefore, whisker development, as a form of DRX (Fig. 1.1), is a serial process comprising deformation that increases the strain energy, new grain initiation, and then grain growth (which is responsible for the whisker formation). The sustained deformation under compressive stress drives the mass transport mechanism. The compressive stress creates dislocations that pile up at pre-existing grain boundaries and the resulting strain energy increases to the point where new grains are initiated.

The other whisker model is proposed by Smetana [6]. In Smetana's model, recrystallization and vacancies at the whisker's base are two key factors for whisker formation. When columnar grains are subjected to compressive stress, oblique grain boundaries will be created after recrystallization as shown in Fig. 1.2. These oblique grain boundaries are shown to have lower stress levels than the vertical boundaries. The Sn atoms diffuse into the oblique grain boundaries from surrounding grains due to the stress gradient. As more Sn atoms diffuse into the oblique boundaries, some of the atoms will move into the whisker grain. Since the boundaries are not fixed, grain boundary sliding occurs along the boundaries, which produces whisker growth directed upward. How the whisker protrudes out from the surface (straight, bent, kinked, etc.) depends on where the Sn atoms are introduced into the whisker grain and if there are any pinned grain boundaries.

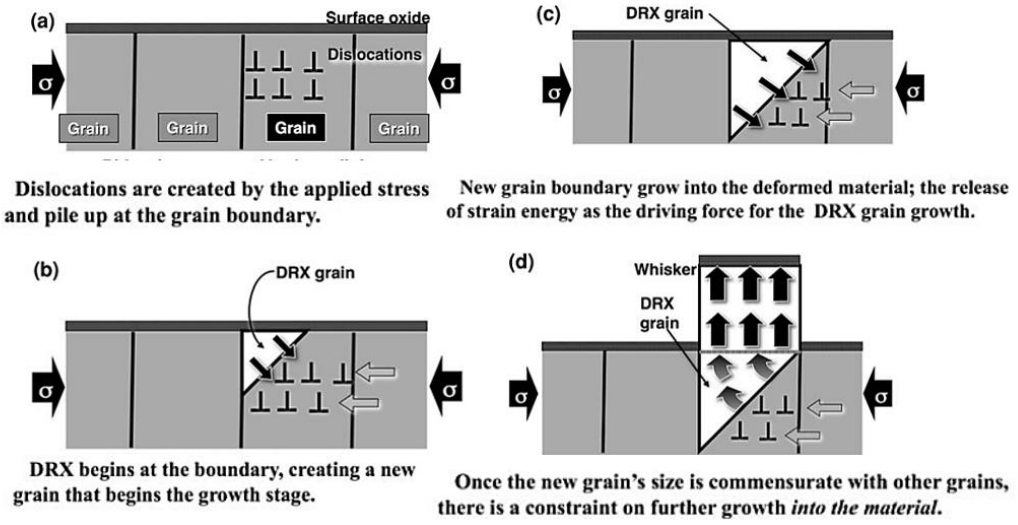

Figure 1.1 Schematic showing whisker growth under the DRX model [24]

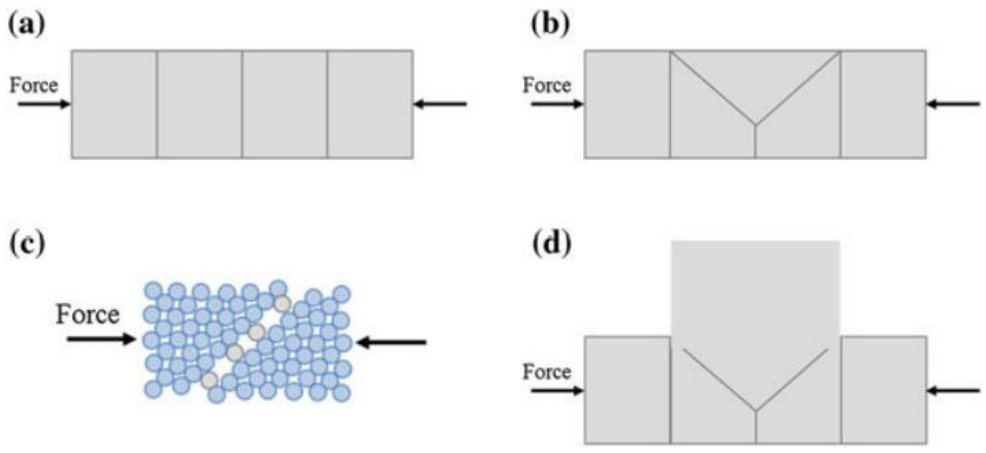

Figure 1.2 Schematic of Smetana whisker model [6]

In this study, a steady-state growth model of Sn whisker growth was used as a fundamental mechanism [57]. A steady-state growth rate ($\Delta h/\Delta t$) of a whisker with constant radius can be calculated by:

$$\frac{\Delta h}{\Delta t} = \frac{\Omega J A_{accum}}{\pi a^2} \tag{1.1}$$

Where h is the height(length) increase of the whisker due to atomic accumulation over time Δt, J is flux, A_{accum} is the area of the grain surface that flux enters, Ω is the molar volume of Sn ($1.7 \times 10^{-5} m^3 mol^{-1}$) and a is the radius of the equivalent circle of the surface grain.

The stress gradient, $\nabla\sigma$, drives atomic flux toward the whisker base (σ_l is the stress at distance l away from the whisker center, which decreases toward the whiskers adge). In this whisker formation model, two mechanisms are important: atoms accrete on the grain boundary plane perpendicular to the growth direction through Coble creep

(A_{accum}), which causes grain boundary shearing and grain boundary sliding on the plane parallel to the whisker growth direction (A_{slide}).

J and $\nabla\sigma$ are given by

$$J = \frac{D_{eff}\nabla\sigma}{RT} \tag{1.2}$$

Where D_{eff} is the effective diffusion coefficient, R is the gas constant, and T is the temperature.

$$\nabla^2\sigma = \frac{\partial^2\sigma}{\partial r^2} + \frac{1}{r}\frac{\partial\sigma}{\partial r} = 0 \tag{1.3}$$

$$\nabla\sigma|_{r=a} = \frac{\partial\sigma}{\partial r}|_{r=a} = \frac{\Delta\sigma}{a\ln(\frac{l}{a})} \tag{1.4}$$

The surface grain geometry is modeled as a stepped cone shape (as shown in Fig.1.3) with constant radius a, depth ℓ and a cone angle of θ with effective accumulation area A_{accum}, where $A_{accum} = \pi a^2$. For a straight whisker growing normal to the film surface, sliding occurs on the planes normal to the film surface with a total area of $\pi a\ell$. The sliding area $A_{slide} = \frac{\pi a^2}{tan\theta}$. The stress gradient drives atoms to flow to the base of the surface grains. The shear stress caused by the pile-up must overcome the grain boundary sliding friction $\sigma_{friction}$. In the presence of an oxide layer, the shear stress caused by the pile-up must also crack the surface oxide before grain boundary sliding can occur. The back stress in the base of a whisker is given by Equation 1.5.

$$\Delta\sigma = \sigma_m - \sigma_f\frac{A_{slide}}{A_{accum}} - \frac{2t}{a}\tau \tag{1.5}$$

Where t is the thickness of the surface oxide and τ is the strength of the surface oxide. Thus, the critical factors in the whisker growth rate analysis are $\sigma_{friction}$, the in-

plane compressive stress σ_m, the surface grain radius a , surface grain geometry θ , and the stress to produce a circumferential crack in the oxide of thickness t.

In summary, the whisker growth rate with a constant radius, driven from the two-dimensional continuity equation can be calculated by:

$$\frac{\Delta h}{\Delta t} = \left(\frac{\Omega D_{eff}}{RT \ln\left(\frac{a}{l}\right)}\right)\left(\frac{1}{a}\right)\left[\sigma_m - \left(\frac{1}{\tan\theta}\right)\sigma_{friction} - 2\left(\frac{t}{a}\right)\tau_{oxide}^{fraction}\right] \qquad (1.6)$$

The implication of this steady-state growth model is the existence of a critical surface grain geometry for a given grain boundary sliding coefficient and oxide layer thickness. This critical geometry determines whether a surface grain will grow out of the plane through grain boundary sliding and Coble creep, ultimately forming a whisker. Assuming that the effect of surface oxide thickness is relatively small, a normalized growth rate can be calculated as a function of surface grain depth and the ratio of grain boundary sliding friction to applied stress $\sigma_{friction}/\sigma_m$, as illustrate in Fig.1.4.

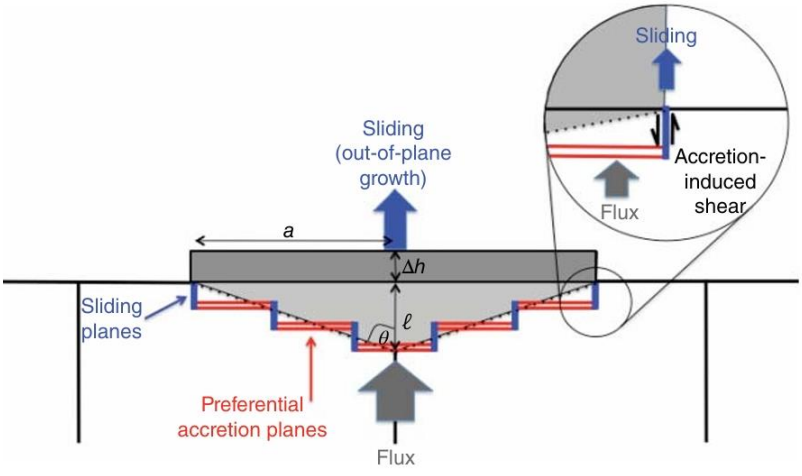

Figure 1.3 Schematic of a steady-state whisker growth model [57]

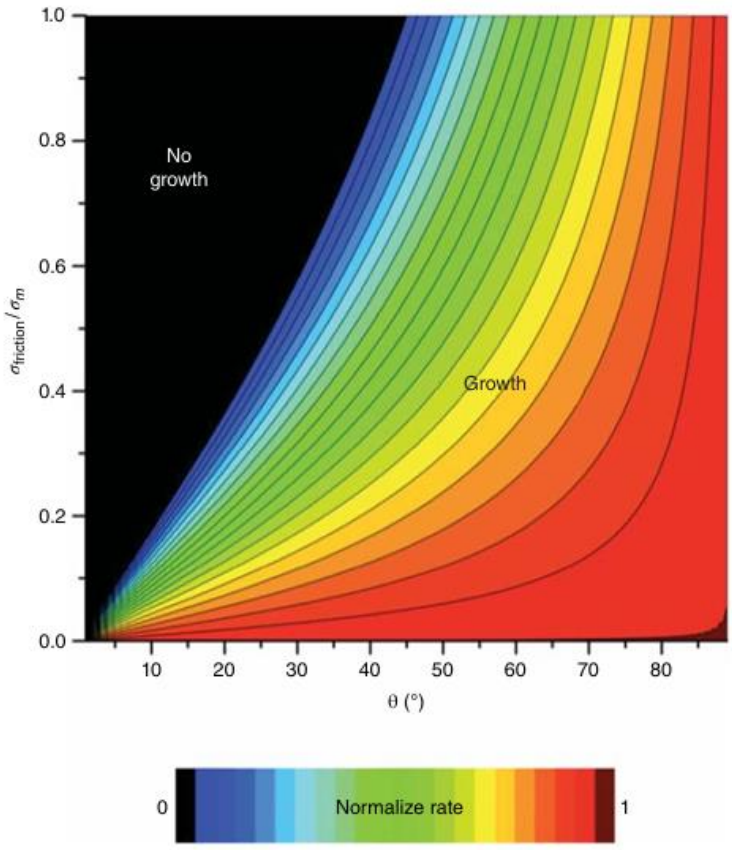

Figure 1.4 Effect of surface grain geometry and grain boundary sliding on whisker growth rate [57].

The growth rate is normalized by the maximum growth rate and projected as a contour on the plot as a function of θ and $\sigma_{friction}/\sigma_m$. The region of interest is $60° < \theta < 90°$, corresponding to those observed from cross sections of whiskers. For high $\sigma_{friction}/\sigma_m$ or small θ whisker growth requires higher stresses from accretion, which leads to lower growth rates and short whiskers. For low $\sigma_{friction}/\sigma_m$ or large θ grain

growth requires lower stresses from accretion, which leads to higher growth rates and long whiskers.

1.2.2 Whisker Formation Behavior of Sn-based Alloy

Adding alloying elements including lead (Pb) to tin (Sn) finishes can mitigate tin whisker formation, as was reported in the 1960s by Glazunova and Kudryavtsev [8] and by Arnold [9]. Even Sn-Pb alloys can produce whisker growth under the right stress. Chason et al. [25] reported that whisker formation from electrodeposition Sn-10Pb alloy films on multilayer samples fabricated on Si substrate. In general, the effect of tin-lead alloy on inhibiting whisker growth is obvious. Most researchers believe that whether alloying can change the structure of tin from columnar grain to equiaxed grain is the key to whether whiskers can be suppressed. For instance, Pb, Bi, and In adding have been reported to change the grain structure of Sn-based alloy to equiaxed, which also shows a positive effect on mitigating whisker formation [26-28].

A theory proposed by Boettinger et al. [26] states that if many oblique or parallel grain boundaries are located within the deposit (such as Sn-Pb alloy film), creep is relatively uniform, and no hillocks/whiskers would occur. Averaged over many grains transport between interior grain boundaries with different normal stresses would allow uniform swelling of the deposit to relieve compressive stress. For the columnar structures (such as Sn-Cu alloy film), the Sn flows toward the free surface based on coble creep theory. The Sn atoms accumulation is localized to oblique surfaces near but under the free surface that forces the grain upward. Moreover, the lack of lateral grain boundary mobility of the columnar structure of Sn-Cu caused by precipitate boundary pining is

considered to promote whisker growth by maintaining a laterally small grain. Fig. 1.5 shows the columnar and equiaxed structures.

1.2.3 Whisker Failures Report

Tin whiskers pose a serious reliability risk to electronic assemblies [7,29]. Many cases have been reported where tin whiskers have caused system failures in earth- and space-based applications. There are reports of at least three tin whisker-induced short circuits that resulted in the complete failure of on-orbit commercial satellites [30]. There have also been whisker-induced failures in medical devices [31], weapon systems [32], power plants [33], and consumer products [7-9].

If a tin whisker initiates a short in an application environment possessing high levels of current and voltage, then a destructive phenomenon known as a Metal Vapor Arc can occur. The conditions conducive to the formation of an MVA include but are not limited to, ambient pressure, temperature, and the presence or absence of materials capable of suppressing the arc. During the MVA event, the tin whisker undergoes a phase transition from a solid to a plasma state, consisting of highly conductive metal ions that surpass the electrical conductivity of the solid-state whisker. This ionized state facilitates the formation of an electrical arc capable of carrying significant currents for durations that can extend for several seconds. This arc is sustained until it is either interrupted by circuit protection mechanisms, such as fuses and circuit breakers, or extinguished through other natural processes. For example, past experiments have demonstrated that at atmospheric pressures of about 150 torrs, a tin whisker could initiate a sustained metal vapor arc where the supply voltage was approximately 13 Volts (or greater) and the supply current was 15 Amps (or greater). The phenomenon is further influenced by

environmental factors such as air pressure, with experimental observations indicating a lower power threshold for arc initiation and maintenance in reduced pressure conditions. This has significant implications for space-based applications where vacuum conditions prevail, as demonstrated by incidents of MVA on commercial satellites leading to operational failures due to blown fuses.

The general risks fall into four categories:

a. Stable short circuits

Stable short circuits usually occur in low-voltage and high-impedance circuits. In such circuits, insufficient current may be available to fuse the whisker open, resulting in a stable short circuit. Depending on a variety of factors including the diameter and length of the whisker, it can take more than 50 milliamps (mA) to fuse open a tin whisker.

b. Transient short circuits

At atmospheric pressure, if the available current exceeds the fusing current of the whisker, the circuit may only experience a transient glitch as the whisker fuses open.

c. Metal Vapor Arc

Tin whiskers can initiate a metal vapor arc through a process involving the growth and eventual bridging of tin whiskers between conductive surfaces. This process occurs when tin whiskers grow and eventually bridge conductive surfaces, leading to short circuits and potentially catastrophic failures.

d. Debris/Contamination

Whiskers or parts of whiskers may break loose and bridge isolated conductors or interfere with optical surfaces.

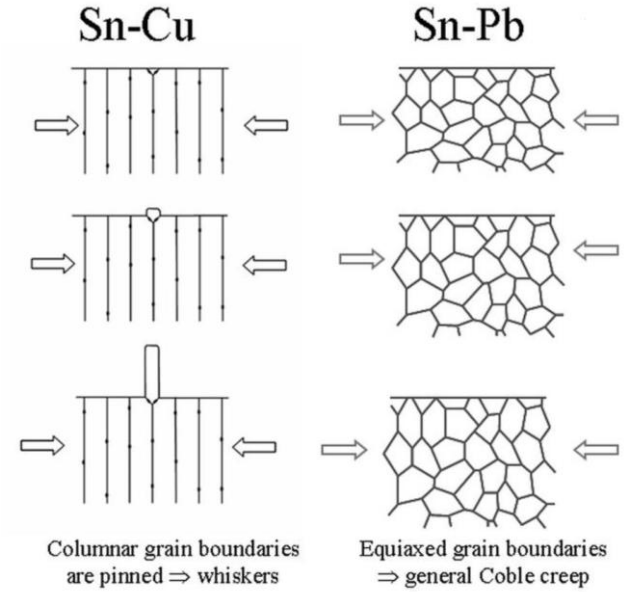

Figure 1.5 Effect of grain shape and mobility on whisker and hillock formation

1.2.4 Mitigation Strategies

The underlying uncertainties and associated lack of predictability of the Sn whisker growth create a challenging environment for risk management. To date, some effective methods, such as conformal coatings [35], Ni barrier layers [34], and SnPb [26] or SnBi [27] alloying, have been proven to mitigate tin whisker formation to some extent. However, there are still many difficulties to overcome.

A conformal coating uses an insulating protective coating to cover the shape and contour of the object. The risks and benefits of conformal coatings for Sn have been studied by Goddard using Uralane 5750 coating [35-36]. Woodrow and Ledbury [37] measured the whisker suppression of a variety of spray coatings on brass coupons plated with 150 micro inches of Sn. The studies suggest that many conformal coatings are not

predictably reliable for whisker mitigation in systems with long-term life expectancies unless an extremely thick coating is applied.

Ni barrier layer is thought to reduce the compressive stress by preventing Cu atoms from diffusing to Sn to form SnCu intermetallic compound. Schetty et al. [38] found that neither Sn film exhibited whisker growth when depositing pure Sn and Sn-10Pb over nickel-plated copper alloy substrates. Additionally, Xu et al. [39] reported that a plated Ni layer under plated Sn films was effective in blocking whiskers after 6 months of incubation at 50 ^{o}C. A control specimen without a plated Ni underlayer grew whiskers after only 3 months. Application of a Ni barrier layer has been found to reduce the build-up of compressive stress in the Sn film and, over time, develop tensile stress in the film. The tensile stress in the Sn is most likely due to the interfacial diffusion between Sn and Ni. The solubility of Ni in Sn and Sn in Ni has been calculated to be 0.005 at % and 11.0 at % respectively. The faster diffusion of Sn atoms into the Ni creates a material deficiency in the Sn film, leading to a buildup of tensile stress in the Sn film. There are many reports that an underlying Ni layer mitigates whisker growth, but Sn whiskers have also been produced in the presence of a Ni barrier layer especially when mechanical stress is applied.

Conformal coatings may not uniformly cover all surface irregularities, potentially leaving vulnerable sites for whisker growth. Nickel barrier layers, though effective in some contexts, can be compromised by factors such as layer thickness, grain size, and the potential for intermetallic compound formation, which can influence their effectiveness. Alloying with lead or bismuth, while historically effective, raises environmental and health concerns, particularly in light of regulations such as the Restriction of Hazardous

Substances Directive (RoHS), which limits the use of lead in electronic and electrical equipment.

1.3 Electroplating method

1.3.1 Electroplating basic

Electroplating represents a pivotal technique in the domain of materials science and engineering, facilitating the deposition of a metal layer onto a substrate through an electrochemical process. This process is fundamentally driven by the migration of metal ions within an electrolytic solution, bridging from a positively charged anode to a negatively charged cathode under the influence of an applied electrical current. The operational principle behind electroplating involves the dissolution of metal from the anode, which then oxidizes into ions that are free to move through the solution. Upon reaching the cathode, these ions undergo reduction, precipitating as a solid metal coating on the object placed at the cathode.

This method is particularly crucial in the context of advanced wafer-level packaging technologies within the semiconductor industry. Electroplating is employed for the fabrication of conductive features such as bumps, pillars, and redistribution layers, essential for integrated circuit connectivity. Additionally, it plays a critical role in the filling of Through-Silicon Vias (TSVs), which are key components in the creation of three-dimensional integrated circuits. These applications underscore the versatility and precision that electroplating offers for microscale and nanoscale fabrication processes.

In the specific case of tin (Sn) electroplating, the process begins with the anodic oxidation of solid tin metal into tin ions, which subsequently dissolve into the electrolyte solution. This transformation from a solid state to an ionic state facilitates the migration

of tin ions toward the cathode, where they are then reduced and solidified to form a coherent metal layer. The schematic representation of this process, as illustrated in Figure 1.6, provides a visual understanding of the electroplating mechanism, highlighting the transition of tin from the anode, through the electrolyte solution, and onto the cathode surface.

As shown in Fig. 1.6, on the anode side, the tin metal is oxidized, and the tin atoms become tin ions and enter the solution.

$$Sn \rightarrow Sn^{2+} + 2e$$

The tin ions diffuse to the copper cathode under the concentration gradient. Tin ions are reduced to tin atoms at the cathode and adsorbed on the copper surface.

$$Sn^{2+} + 2e \rightarrow Sn$$

Based on the Nernst equation 1.2, the potential E of the Sn^{2+}/Sn electrode is defined by

$$E = E^0 + \frac{RT}{zF} \ln a\,(Sn^{2+}) \tag{1.7}$$

where R, T,z, and F are the gas constant, absolute temperature, number of electrons, and Faraday's constant (96,487C), respectively.

The current-potential relationship has a limit where the rate of deposition reaction is limited by the transport of M^{z+} ion, in this case is Sn^{2+}. A general current-potential relationship is shown in Figure 1.7. The maximum current density is given by

$$i_L = \frac{nFD}{\delta} c_b \tag{1.8}$$

where D is the diffusion coefficient of the Sn^{2+}, c_b is the bulk concentration of Sn^{2+} in the solution, δ is the diffusion layer thickness, n the number of electrons involved

in the reaction, and F the Faraday constant. To calculate the diffusion maximum current density i_m for the deposition of a metal ion Sn^{2+} at a cathode in an unstirred solution, the diffusion layer thickness δ is assumed 0.05 cm, the concentration of Sn^{2+} ions in the bulk is 0.2 mol/L, and the diffusion coefficient D of Sn^{2+}, in the unstirred solution, is 2 x 10^{-5} $cm^2\ s^{-1}$.

Using Eq. (1.8), we calculate that the maximum diffusion current density for electroplating Sn in this case is

$$i_L = \frac{nFD}{\delta} c_b = \frac{2\times 96487\times 2\times 10^{-5}\times 0.2\times 10^{-3}}{0.05} = 0.0154\ A\ cm^{-2} \qquad (1.9)$$

For uniform plating, stirring is required practically. In the stirred electrolyte solution, the diffusion layer thickness δ and the maximum current density i_L depend on the nature of stirring. The diffusion layer δ can be calculated by

$$\delta = \frac{1.61 D^{1/6} \nu^{1/6}}{\sqrt{\omega}} \qquad (1.10)$$

and the maximum current density can be calculated by

$$i_L = \frac{0.62 nFaD^{2/3} c}{\nu^{1/6}} \sqrt{\omega} \qquad (1.11)$$

where D is the diffusion coefficient, υ the coefficient of viscosity, ω the rotation angular speed, c the concentration of solution, and a the disc surface area. In this study, when rotation speed is 250 rpm, we get δ = 30 um and i_l = 30.71 $A\ cm^{-2}$

The combination of low cost, simplicity, versatility, and precision makes electroplating an indispensable technique within the electronic manufacturing industry. Moreover, the precision afforded by electroplating, in terms of thickness control and

uniformity of the deposited layers, is crucial for ensuring the performance and reliability of electronic devices.

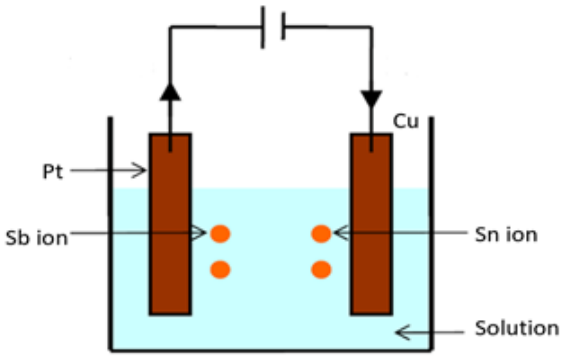

Figure 1.6 Schematic of electroplating bath

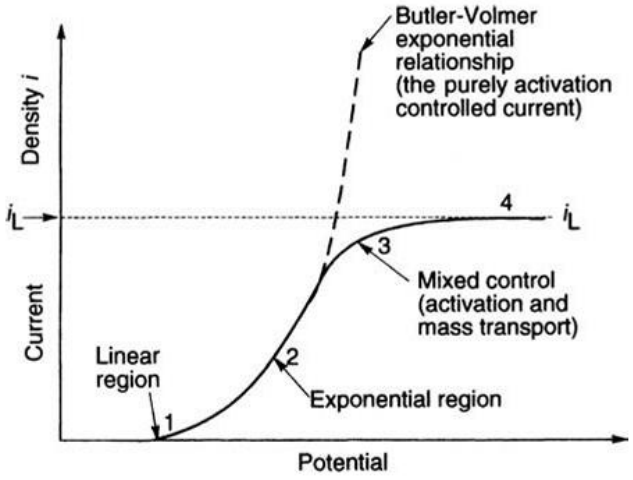

Figure 1.7 Four regions in the general current-overpotential relationship: 1, liner; 2, exponential; 3, mixed control; 4, maximum current density region.

1.3.2 Electroplating of Tin-based Alloys

The transition to lead-free tin-based alloys in electroplating presents a significant technical challenge, primarily due to the substantial differences in standard electrode potentials between tin (Sn) and potential co-plating metals. This issue is less pronounced in traditional Sn–Pb (tin-lead) plating systems, where the electrode potentials of Sn (-0.136 Volts) and Pb (-0.126 Volts) are relatively close, facilitating their co-deposition from Sn–Pb anodes with uniformity and predictability akin to pure metal plating processes. This near parity in electrode potentials enables a synergistic deposition process, yielding consistent alloy compositions across the plated surfaces.

Conversely, in lead-free alloy systems, the co-plating metals often possess more noble standard electrode potentials compared to tin. This disparity introduces several complications in achieving uniform and defect-free alloy deposits, which are critical for the performance and reliability of the plated components. Among the common issues encountered in the electroplating of tin alloy solutions are:

a. Preferential Deposition at Low Current Densities: At lower current densities, the metal with the more noble electrode potential tends to deposit preferentially, leading to variations in the alloy composition as a function of current density. This results in non-uniform properties across the plated layer, which can affect the performance characteristics of the final product.

b. Immersion Deposits and Anode Maintenance: The more noble additive metal may form immersion deposits on the tin anode, necessitating regular replenishment of the additive metal in liquid concentrate form and frequent anode maintenance. This increases the operational complexity and maintenance requirements of the plating process.

c. Formation of Immersion Deposits Post-Plating: Interruption of the current while plated parts remain in the bath can result in the formation of immersion deposits on the plated layer by the additive metal. This phenomenon can degrade solderability or, if the deposits form within the plated layer, lead to interlayer adhesion failures, compromising the integrity and functionality of the plated component.

d. Oxidation of Divalent Tin (Sn2+) to Tetravalent Tin (Sn4+): The presence of a more noble additive metal can catalyze the oxidation of Sn2+ ions in the electrolyte to Sn4+, thereby reducing the stability of the plating bath. This transformation affects the efficiency and consistency of the plating process, requiring more rigorous monitoring and control of bath chemistry.

Addressing these challenges necessitates a comprehensive understanding of the electrochemical behavior of the metals involved, as well as the development of advanced plating bath formulations and process controls. Innovations in electrolyte composition, anode materials, and plating techniques are critical for overcoming the difficulties posed by the disparate electrode potentials of tin and its alloying partners in lead-free systems. Such advancements will be essential for ensuring the continued evolution of electroplating technologies in alignment with environmental regulations and the demand for high-performance, lead-free electronic components.

1.4 Literature review

In the previous sections, individual literatures reporting the mechanisms, risks of tin whiskers, and means of mitigation have been presented. From a historical standpoint, more literatures in these areas are further summarized as follows.

In 1951, Campton et al. from Bell Laboratories first reported a series of long-term investigations into the general topic of whisker formation [8]. Whisker growth was also found on electroplated Sn, Ag, Zn, and Al, but not only on Cd. The research provided the first statement that whiskers formed spontaneously. The conclusion was that whisker growth is not only limited to electroplated surfaces but also to solid metals. Most of the research since Compton's paper in 1951 has begun to focus on the electroplating of tin and tin alloys on various substrates, as tin and tin alloy plating has become the preferred choice for electronic components due to the favorable combination of contact resistance, corrosion resistance, low cost, and solderability.

In 1952, Peach attempted a qualitative explanation for the cause and mechanism of the growth of whiskers observed on cadmium and tin [40]. He stated that Sn or Cd atoms migrated through a screw dislocation at the center of the whisker and subsequently deposited themselves at the whisker tip.

In 1959, Arnold first reported the beneficial whisker mitigation effect when alloying Sn coating with Pb [9]. The paper stated that whisker formation occurred if SnSb alloy was subjected to high compressive stresses, which was proven the main source of whisker formation. In 1964, Pitt and Henning reported that whiskers formed due to clamped-pressure environments on hot-dipped SN and Sn-50Pb deposited on copper and steel substrates [41]. The results showed that whisker densities decreased with increasing Pb content.

In 1974, Britton from the International Tin Research Institute Ltd stated that Sn-Pb deposits at least 8 μm thick are probably safe and suitable for most purposes where

whisker growth may be a hazard [42]. The paper claimed that 1% of Pb is sufficiently effective to prevent whiskers formation.

In 1975-1976, a set of publications by Dunn of the European Space Agency strongly recommended that surfaces that are prone to stress-induced whisker growth (such as Sn, Cd, and Zn) be excluded from spacecraft design [8,29]. The suggested alternative surface treatment is the Sn-Pb alloy of 60Sn/40Pb. Dunn was the first to suggest that pure Sn plating should not be used for critical applications such as spacecraft. However, no mandatory or regulatory stance was taken against Dunn's proposal, which proved to be very unfortunate in the years to come, as several major reliability failures in USAF equipment were attributed to tin whiskers.

In 1986, Nordwall, Capitano, and Devaney discussed the US military's first experience with whiskers growing from tin-coated hybrid circuits [30]. The whiskers break off, falling into active circuitry and causing the circuit to short out. The U.S. Air Force discovered the problem while sifting12 years old failed radar system. Analysis revealed numerous bridging whiskers (up to 2.5mm long, some of the longest ever observed in an electronic circuit) causing electrical shorts. In 1989, Corbid [43] of Hi-Rel Laboratories claimed that reflowing could not prevent whisker growth as previously noted in earlier studies by examining the use of Sn in miniature electronic packages. The question of whether reflowing helps to mitigate whisker formation remains open today.

In 1990, Cunningham and Donahue of the Raytheon Company presented a paper at the SAMPE conference on Sn whiskers, which compared whisker growth from Sn and Sn-Pb subjected to mechanical stresses at elevated temperatures [44]. The results showed that the process which produced the fewest whiskers was 60/40 Sn/Pb with reflow, which

again, combined an elevated temperature with Pb-containing Sn. The first published paper from a connector company that dealt with reliability problems involving Sn whiskers was a 1993 work by Diehl [45] from Burndy Connector Corporation. Diehl also concluded that the addition of Pb was necessary to ensure that Sn electroplating would not produce whiskers. His directive was subsequently adopted by all of Burndy Corporation's Sn plated connector products.

In 1999, whisker problems arose in ultrafine pitch circuits, reported by Ishii et al. [46]. The ultrafine circuits referred to a pitch of 50 lm, corresponding to a lead-frame spacing with gaps of 20 lm or less between adjacent leads. The pure Sn lead-frames were experiencing a high incidence of shorting due to whiskers (the problem was reported to be mitigated by annealing at 150 C for 2 h). At the beginning of the 21st century, General Electric issued a service bulletin stating that whisker problems had been found on certain GD relays in field service for over 10 years. The recommended corrective action was to brush off and vacuum up the removed whiskers. Around the same time (2001), in a different case study, Stevens [47] of the Foxboro Company reported whisker-induced relay failures (used in nuclear facilities). After eight years in service, the relays failed due to Sn whiskers. The relay finishes were originally Sn–Pb, but due to cost savings, the finishes were switched to pure Sn in 1983. Since the failed relays were used in nuclear facilities, a total field replacement action was initiated immediately.

In 2002, the Government-Industry Data Exchange Program (GIDEP) issued an Agency Action Notice on Sn whiskers authored by Khuri [48] from the Department of the Navy to remind the electronics industry of the potential risks associated with the use of pure Sn-plated finished on electronic assemblies. The notice recommended that pure

Sn finishes be avoided at all costs and that the use of Sn–Pb solders be utilized. Due to current mandated regulations involving the use of Pb in electronic assemblies, it has become more difficult to solve the whisker problem by use of Pb-containing alloys. We discuss this subject in the next section.

In 2005, Boettinger [26] investigated the development of whiskers and hillocks on electrodeposited layers of Sn, Sn-Cu, and Sn-Pb. It was found that all deposits exhibit initial compressive stress post-plating, with Sn–Cu showing the highest due to rapid Cu6Sn5 intermetallic compound formation. Over time, this stress evolves differently across the materials due to factors like grain structure, with Sn–Cu and Sn showing surface disturbances such as whiskers and hillocks, whereas Sn–Pb deposits remained undisturbed due to their equi-axed grain structure and lower initial compressive stress. The paper suggests that whisker and hillock growth results from the relaxation of compressive stress through localized creep, and it proposes mitigation strategies based on the alloying elements' influence on deposit stress and structure. This research provides significant insights into preventing whisker growth and enhancing the reliability of electronic components.

In 2009, Sobiech [49] investigated the spontaneous growth of Sn whiskers on tin-coated Cu surfaces, a critical issue for electronic device reliability. Through synchrotron white beam micro Laue diffraction measurements, the research identifies local in-plane residual strain gradients around the roots of growing Sn whiskers as the driving force for whisker formation. This growth is facilitated by negative in-plane and out-of-plane strain gradients, which arise due to the formation of Cu6Sn5 intermetallic compounds along the Sn grain boundaries. The findings suggest that whisker growth is not merely a result of

compressive strain but is significantly influenced by the specific three-dimensional strain gradients at the whisker nucleation site. This work provides valuable insights into the mechanics of Sn whisker formation, offering a foundation for developing strategies to mitigate whisker-related failures in electronics.

In 2014, J. Stein [50] identified the crystallographic directions parallel to the whisker-growth axes by combining focused ion beam (FIB) microscopy for physical growth angles and EBSD for crystallographic orientations of 55 whiskers. The findings reveal that Sn whiskers preferentially grow along low-index directions of the beta-Sn crystal structure.

In 2020, Jagtap [51] reviewed the scientifically challenging and technologically important problem of Sn whisker growth, especially in the light of relatively new insights gained in the recent past, intending to provide a quick overview of the important results and stimulating future studies. In particular, the mechanisms of whisker growth by critically examining the roles of stress and its regeneration, oxide layer, diffusion conduits, and crystal anisotropy in creating conditions conducive to whiskering were discussed. In addition, recent proposals for effectively mitigating whisker growth in Sn coatings were provided.

1.5 Dissertation objectives and tasks

In the new paradigm of highly integrated electrical and electronic systems, especially with particular application conditions such as in the electrical vehicles (EV) and 3D packed system-on-chip (SOC), reliable electrical connections play an increasingly critical role. Recent studies have led to great interest in antimony (Sb) as a substitute to Pb and other elements in tin plating.

Sn–Sb alloy is one of the potential alternate materials considered for replacing Pb-containing alloys for soldering in electronic packaging. The Sb has the effect of imparting strength and hardness to the alloy. Mathew's [52] work on the Sn-Sb alloys shows that these materials exhibit superior tensile and creep properties over eutectic Sn–Pb solder. The tensile strength of the solder was enhanced with an increasing antimony content related to an improved solid solution strengthening when alloying Sn grains with Sb. Moreover, the melting temperature of Sn–5Sb solder (245 °C) is about 62 °C higher than eutectic Sn–Pb solder (183 °C) and has proven to be more suitable for higher-temperature applications such as step soldering technology. The superior reliability of soldering connections using SnSb solders against thermo-mechanical stress in comparison to Sn-Ag or Sn-Ag-Cu-based solders was shown between chip and substrate, but also between substrate and copper baseplate. A strongly suppressed deterioration of Sn-Sb-based solder in comparison to Sn-Ag-based solder was observed when storing the solders at high temperatures. Further, an increasing Sb content in Sn-Sb-based solders resulted in an enhancement of the thermal cycling reliability of large-area solder joints. Finally, Sn-Sb-based solders provide economic advantages due to their competitive price in comparison to SnPbAg, SnAg, or SAC solders.

In the chip packaging industry, solder is deposited on the substrate by electroplating and then formed by the reflow process. However, in the current research on the properties of SnSb alloys, SnSb alloys are synthesized by metallurgical methods. Therefore, it is very important to find a method for preparing SnSb alloy by electroplating.

The main work of this dissertation includes three parts as described below:

Develop Sn-xSb Electroplating Solution: This step involves formulating an electroplating solution containing tin and a certain amount of antimony. The tin-antimony electroplating solution enables the synthesis of a tin-antimony electroplating alloy in a single step.

Design a Fixture to Accelerate Whisker Growth: This step involves creating a fixture or setup that facilitates or speeds up the growth of tin whiskers.

Explore the Mitigation Mechanism: Finally, the process aims to investigate methods or mechanisms to mitigate or prevent the growth of tin whiskers.

Figure 1.8 outlines a process involving the development of a tin-antimony (Sn-xSb) electroplating solution and the design of a fixture to accelerate whisker growth, ultimately leading to the exploration of a mitigation mechanism for whisker growth.

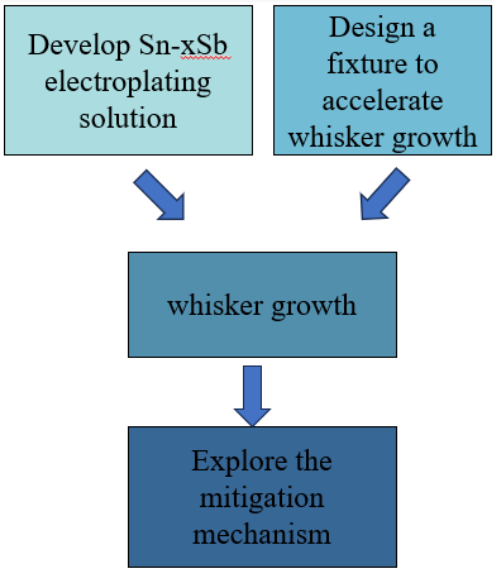

Figure 1.8 The objective flow chart of this study

CHAPTER TWO

EXPERIMENTAL PREPARATION

2.1 Review of whiskers growth accelerating methods

The incubation period for Sn whiskers can extend over several months, presenting a challenge for experimental investigation and understanding of the phenomena. To expedite the observation and study of whisker growth, researchers employ various methodologies designed to accelerate the process. Figure 2.1 shows several commonly used methods to accelerate whisker growth. They are applying external mechanical stress (Figure 2.1 a and b), thermal cycling (Figure 2.1 c), and inducing intermetallic compounds (Figure 2.1 d). Among the most prevalent approaches is the aging of tin-plated copper (Cu) samples under conditions of ambient or elevated humidity. This method capitalizes on the naturally occurring intermetallic compound (IMC) induced stresses that promote the formation of whiskers.

In the context of tin-plated copper systems, the mechanism underlying accelerated whisker growth involves the diffusion of copper atoms into tin, especially under conditions of elevated temperature. This diffusion process favors the formation of the intermetallic compound Cu6Sn5. Considering the molar volumes of copper and tin at 7 cm^3/mol and 16 cm^3/mol, respectively, the formation of Cu6Sn5, with a molar volume of 118 cm^3/mol, signifies a considerable increase in volume. This volumetric expansion leads to the buildup of internal compressive stress within the tin layer, which in turn acts as a driving force for the emergence of tin whiskers.

However, this method, while instrumental in facilitating the observation of whisker growth, is also marked by its slow progression, with the process unfolding over protracted durations that can sometimes extend to a year or more. Moreover, the experimental replication of whisker growth under these conditions often yields inconsistent results. The variability in whisker morphology, distribution, and growth dynamics poses significant challenges for researchers aiming to develop a comprehensive understanding of the factors influencing whisker formation and to devise effective mitigation strategies. This inherent unpredictability underscores the complexity of the whisker growth phenomenon and the need for continued investigation into the environmental and material conditions that precipitate the formation of these conductive structures.

To speed up the evaluation period, a variety of external methods have been developed for generating internal stresses at a faster rate. These methodologies encompass both thermal and mechanical strategies to generate the requisite stresses for whisker formation. One approach to induce thermal stresses is to thermally cycle Sn-plated samples [17]. This method consists of rapid sample cooling and heating cycles that induce compressive and tensile stresses, respectively (Fig 2.1 c). While effective, the rapidly grown whisker population using this method is not necessarily representative of that found on naturally aged samples. In addition, for coatings with a thermal expansion coefficient that mismatches with the Sn plating, thermal cycling could lead to coating delamination. Since this may not occur under normal operating conditions, non-representative results on the coating efficacy could be obtained.

Routes to mechanically induce stresses include bending [53], scratching [54], and indentation [55-56]. The latter approach has been successfully used to accelerate whisker growth using both nanoscale and microscale indenters . Nano-indentation generates very localized compressive stresses; however, this only leads to the growth of a single whisker from the nanoscale-indented region. While this approach is quite attractive for in-situ studies of the whisker growth mechanisms, it is not optimal for evaluating coatings because the nano-indenter must break through the coating to apply direct stress to the Sn plating. In this region, the coating is removed or damaged and proper evaluation of its efficacy for stopping whisker growth cannot be achieved. Micro-indentation, which can consist of a ball-shaped indenter on the order of 1 mm in diameter, has been shown to be more effective than nano-indentation for growing a larger whisker and hillock population over a broader area. This approach increases the overall stress that is transferred to the weaker grain boundaries, and loads would be more cumulative causing the nodule diameter to remain continuous, and, thus, promoting upward whisker growth.

The application of nanoscale and microscale mechanical stress inducement techniques, such as indentation, has been explored as a method to increase compressive stress within metallic coatings, potentially accelerating whisker formation for research purposes. However, these techniques have shown limited utility in whisker research due to specific practical challenges.

The first major challenge arises from the nature of the indentation process itself. The indentation creates a dent that is primarily vertical in orientation, making it exceedingly difficult to prepare a flat surface sample within the deformed area for subsequent microscopic examination or analysis. This limitation significantly restricts the

ability to directly observe and study the initiation and growth of whiskers in the area most affected by the induced stresses.

The second challenge pertains to the whiskers that develop away from the immediate vicinity of the indentation dent. After the surface of the sample is polished to facilitate observation, pinpointing the original location of these whiskers becomes problematic. The polishing process, necessary for preparing the sample for microscopic analysis, can alter the surface topology to such an extent that identifying the exact spots from which whiskers have grown is often not feasible. This has led scholars to primarily understand the mechanism of whisker growth through the study of individual whiskers. However, they have been unable to formulate comprehensive laws governing whisker growth on a larger physical scale, such as the millimeter scale.

Given these obstacles, researchers frequently resort to analyzing cross-sectional samples to study whisker growth. This approach involves examining a slice of the sample material, allowing for the observation of whisker development within the cross-section. However, this method inherently limits the observable area to a small number of grains within the sample, which may not adequately represent the overall whisker growth behavior across the entire surface. This limitation underscores the need for innovative experimental setups and fixtures designed to overcome these challenges. By enabling more effective preparation and examination of samples, such advancements could significantly enhance the capacity to study whisker growth mechanisms, distribution, and characteristics in detail, thereby contributing to the broader understanding of whisker phenomena and the development of mitigation strategies.

Due to the limitations of the above methods for accelerated growth of whiskers, and the availability of metrological tools for observation and characterizations of whisker growth, a unique mechanism is designed to apply well controlled normal forces to the sample for stress induction that's necessary for the accelerated tin whisker growth.

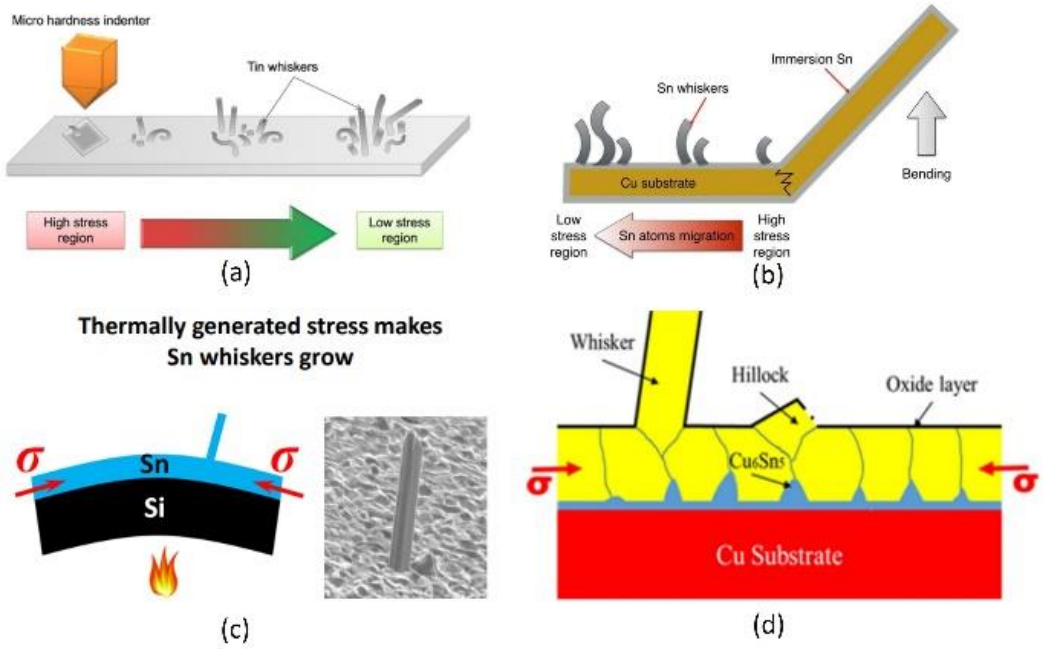

Figure 2.1: Tin whiskers growth accelerating methods: (a) Indentation, (b) Bending, (c) Thermal cycling, (d) IMC formation on the interface.

2.2 Fixture design

The incubation period for the growth of tin (Sn) whiskers is significantly influenced by environmental conditions and exhibits considerable variability. In this study, an innovative fixture design is proposed, specifically engineered to expedite the

incubation and subsequent growth of Sn whiskers through the deliberate application of continuous mechanical stress. The design principle of the fixture is founded on a sandwich configuration, incorporating two flat acrylic plates. The first plate features a flat surface, while the second plate is characterized by a V-notch with precise dimensions of 20 mm in length and 5 mm in width, as illustrated in Fig 2.2a. This configuration is designed to ensure the uniform distribution of pressure, specifically calibrated at 35 MPa, across the surface of the sample. This pressure is sustained over an extended duration, potentially up to 24 weeks, at ambient temperature conditions. The implementation of this fixture is expected to provide a controlled and accelerated environment for the study of Sn whisker growth, thereby contributing valuable insights into the mechanisms underpinning this phenomenon.

In the pursuit of maintaining a uniform application of stress throughout an experiment designed to study Sn whisker growth, the experimental setup includes acrylic plates that are securely affixed using screws. This methodical assembly ensures that there is no displacement or relaxation of the force applied to the sample. As a result, this configuration creates a distinct bifurcation on the sample surface, dividing it into two separate zones. The area directly beneath the V-notched plate is preserved in its original, as-plated condition, free from any mechanical deformation. Conversely, the section positioned under the flat acrylic plate is subjected to pronounced pressure, leading to noticeable deformation.

The central hypothesis driving this experimental inquiry suggests that the interface between these two distinct zones — particularly, the transition from the undeformed, as-plated region to the mechanically stressed, deformed area — will act as

the critical nucleation site for the growth of Sn whiskers. This process is anticipated to unfold as the induced stress relaxes, a concept depicted in the illustrative Fig 2.2b. By concentrating on this demarcation, the research aims to methodically uncover the mechanisms that underpin the formation of Sn whiskers when subjected to persistent mechanical stress. This endeavor seeks to augment the academic discourse surrounding the factors that govern whisker growth dynamics in tin and tin-alloy coatings, thereby enriching the scholarly understanding of this complex phenomenon. This enhanced insight is pivotal for devising more effective strategies to mitigate the risks associated with whisker growth in electronic components and systems.

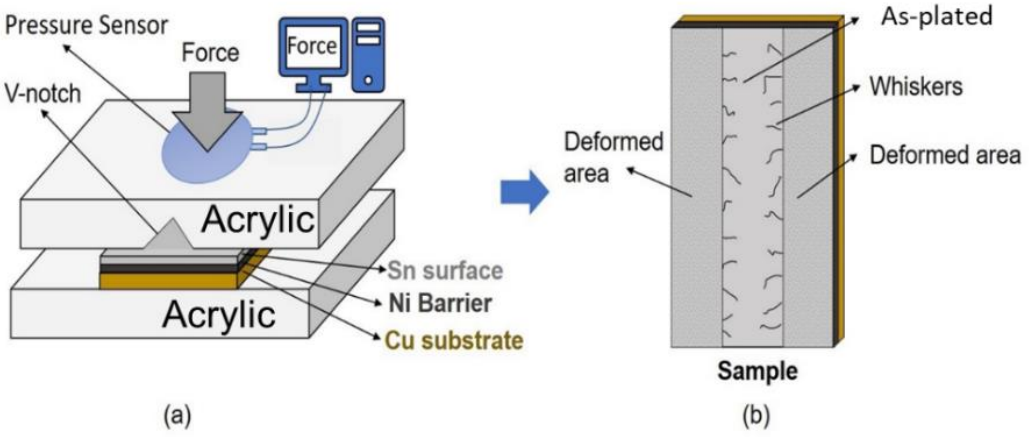

Figure 2.2: Schematic of fixture for whisker acceleration, (a) fixture to apply mechanical stress, and (b) sample surface after removed fixture.

2.3 Sample preparation

2.3.1 Electroplating

The journey toward desired tin whisker mitigation starts from the optimal atomic arrangements when tin films is formed. In this study, electroplating method is chosen for tin and tin alloy film deposition. Prior to electroplating, Cu substrates, (99.99%, Mccarts) with dimensions of 40 mm × 10 mm × 1mm were immersed in sulfuric acid (10%) for 15 seconds to remove the oxide layer and were rinsed in DI water. Next, a Ni coating was electroplated on the Cu substrate from a Nickel sulfate plating bath. Ni as a barrier layer can avoid the formation of IMC (Cu6Sn5) between the Sn and Cu layers. Electroplating Ni was performed at a constant current density of 50mA/cm^2 in 60 ml of solution at 55 °C for 10 mins. A pure Ni sheet (99.999%) was used as an anode. The final Ni layer had a thickness of 5um.

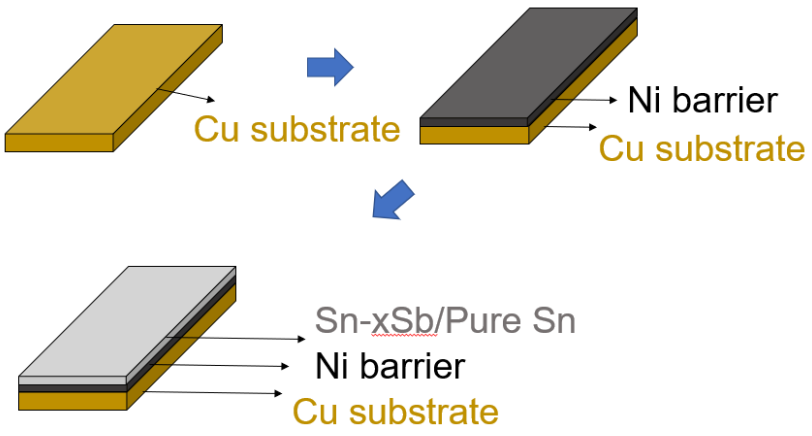

Figure 2.3: Schematic diagram of the electroplating preparation process

For the Sn-xSb deposits, the constant current density was 50mA/cm^2, and the solution temperature was 35°C. A pure Sn sheet (99.999%) was used as an anode. Pure Sn samples were prepared from a tin MSA plating bath. The final Sn layer had a thickness of 12um. Fig 2.3 shows the schematic diagram of the electroplating preparation process of the sample.

2.3.2 EBSD sample preparation

Electron Backscatter Diffraction (EBSD) has been a powerful tool widely used in grain and micro stress characterization for various crystals. The analytical tool perfectly fitting this study requires stringent sample preparation for effective diffraction pattern generation. Based on the material combinations and their respective properties, some special polishing parameters have been attempted for whisker samples. The preparation of the EBSD sample involved a meticulous process comprising mechanical polishing and ion milling to ensure optimal surface conditions for analysis. The initial mechanical polishing was performed using an AutoMet 2000 Power Heads semi-automatic system from Buehler, designed to facilitate precise grinding and polishing. Subsequent to mechanical preparation, the samples were subjected to ion beam polishing, utilizing the Gatan Ilion II system. This critical procedure aims at the meticulous removal of the superficial oxide stratum, unveiling the material's inherent structure requisite for efficacious EBSD examination. Ion milling presents a critical advantage by ensuring the integrity of the sample's surface is maintained, free from the potential distortions introduced through mechanical preparation techniques.

To maintain the structural integrity and surface purity of the samples throughout the preparatory stages, a procedure involving the application of an epoxy solution,

solubilized in acetone, was employed as a protective measure during the intricate processes of cutting and thinning. This protective coating was subsequently dissolved using acetone, a step meticulously executed to prevent any residual contamination. A subsequent delicate drying phase employing compressed air was implemented, a measure critical in preserving the pristine condition and cleanliness of the sample, thereby underscoring the comprehensive and methodologically rigorous approach adopted to ensure the prepared samples meet the exacting criteria essential for precise and accurate EBSD analysis.

To mount the sample in preparation for ion milling, Ag (silver) paint was utilized, chosen for its superior electrical and thermal conductivity, rapid setting time, ease of removal, and stability under cryogenic temperatures. The specific product selected for this study was Ted Pella Fast Drying Silver Paint, Product No.16040-30. The rapid curing properties of this Ag paint necessitated swift specimen mounting to prevent insecure attachment, which could lead to detachment during the ion polishing phase.

Given the unique material characteristics and the critical nature of the surface preparation for EBSD analysis, the study explored specialized polishing parameters tailored to the whisker samples. This approach was informed by the materials' properties and the need to achieve a high-quality surface finish, essential for accurate EBSD scanning and subsequent analysis. Figure 2.4 a and b illustrates the whisker growth region before and after ion polishing with the sample preparation method mentioned above. It can be seen that the whiskers are effectively removed after ion polishing, leaving behind only the whisker roots. Additionally, the ion polishing process reveals the

crystal texture of the electroplated surface, providing a clearer view of the underlying microstructure.

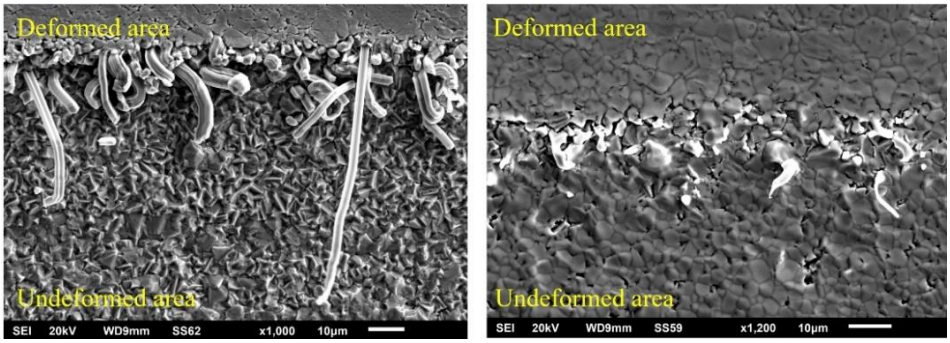

Figure 2.4 Surface polished sample of a whisker growth region: (a) before ion polishing, (b) after ion polishing

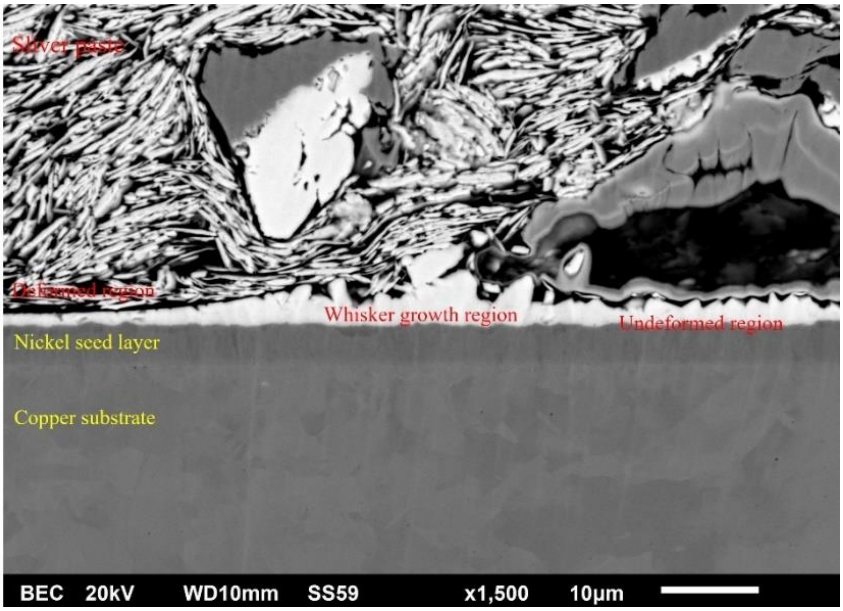

Figure 2.5 Cross-section polished sample of a whisker growth region

Figure 2.5 shows the cross-section of a polished area of a sample after ion polishing. It can be seen that the sample is divided into four layers from top to bottom, namely the silver paste used to paste the sample, the tin-antimony electroplating layer, the nickel seed layer and the copper substrate. The polished area is very smooth, and the crystal structure can be clearly seen.

Table 2.1 delineates the steps and parameters for the preparation of surface and cross-sectional samples via ion polishing. During the preparation of cross-sectional samples, the polishing temperature is rigorously maintained at -100 °C using liquid nitrogen. This measure is crucial to mitigate temperature elevations that could induce crystal changes, such as recrystallization, during ion bombardment. The sample rotation speed is precisely set at 0.5 RPM, and the ion beam bombardment fan angle is configured to 80 degrees to facilitate the polishing of a larger surface area.

Table 2.1 Ion polishing parameters and steps

	Cross-section sample	Surface sample
Ion polishing temperature	-100 C	-100 C
Rotation speed	0.5 RPM	0.5 RPM
Ion polishing wedge	80 degrees	80 degrees
Ion polishing steps	a. 150 mins at 7 Kev b. 30 mins at 1Kev c. 60 mins at 0.5 Kev	a. 15 mins at 1 Kev b. 30 mins at 0.5Kev c. 60 mins at 0.1 Kev

The ion polishing procedure is segmented into three distinct phases. Initially, rough polishing is conducted with an energy setting of 7 keV for a duration of 150 minutes to efficiently remove the surface oxide layer. Subsequently, intermediate polishing is executed at 1 keV for 30 minutes to smoothen the previously rough-polished area. The final phase involves fine polishing at an energy level of 0.5 keV for 60 minutes, aimed at exposing stress-free crystal textures. This meticulously outlined protocol ensures the precise preparation of samples, preserving their microstructural integrity while preventing thermal damage throughout the polishing process. The steps for preparing a surface sample are similar, and the polishing time depends on the thickness of the material being removed.

2.4 Whiskers analysis methods

The growth dynamics of Sn whiskers and the surface microstructure of the applied coatings were meticulously examined using a Scanning electron microscope (SEM) (JEOL 6520), to acquire high-resolution images elucidating the topographical and compositional details of the specimens. Preparation of samples for EBSD analysis was adeptly executed utilizing a Gatan Ilion II system, with the process being conducted at temperatures below -100°C to mitigate any potential alterations in grain structure attributable to ion beam interactions during sample preparation. The EBSD analysis itself was performed with a Tescan Mira3 SEM operating under low vacuum conditions, enabling the precise determination of the crystallographic orientation of the material's grains. This analysis was carried out at an accelerated voltage of 20 keV, and high-resolution mapping was achieved with a step size of 0.05 µm, covering a scanning area of 150 µm in length and width. Additionally, Energy Dispersive Spectroscopy (EDS) was

employed to assess the distribution of elements within the specimens, and X-ray Diffraction (XRD) measurements were conducted over a range of 20 to 90 degrees using a Rigaku device to investigate the crystallographic structure further. For morphological studies, an SEM model JSM-6510 was utilized, further contributing to the comprehensive characterization of the specimen's microstructure.

CHAPTER THREE

ELECTROPLATING SOLUTION

3.1 Tin electroplating solution

In this study, pure tin samples were prepared as a control group. Sn methane sulfonic acid (MSA) solution was used to electroplate pure tin sample for whisker growth. The Sn MSA bath was prepared up to a volume of 60ml, and the plating was conducted at 80 ℃. The Sn MSA electrolyte was composed of analytical MSA (0.1mol/L), pure Sn MSA (0.2 mol/L), SnSO4 (0.2 mol/L), Polyethylene glycol (0.01 mol/L), and Triton X-100 (3ml/L). Sodium hydroxide is used to adjust the pH of the plating solution. The pH was about 3.5. Triton X-100 served as a wetting agent to diminish the solution's surface tension and enhance its spreading capabilities. Concurrently, PEG functioned as a leveling agent, facilitating the deposition of a coating characterized by smoothness and minimal crack formation.

Illustrated in Figure 3.1 is the morphology of tin as prepared via the described solution. SEM pictures show that the pure tin coating is smooth and void-free. Figure 3.2 presents an EBSD inverse pole figure (IPF) map of a pure Sn sample, revealing that the tin coating predominantly exhibits a <110> crystal orientation as a result of the specified electroplating method. Additionally, the EBSD result (as shown in Fig 3.3) revealed that the Sn coating possesses an average grain size of 4.99 μm, indicative of the microstructural characteristics imparted by the electroplating solution's composition and the conditions under which the electroplating was conducted.

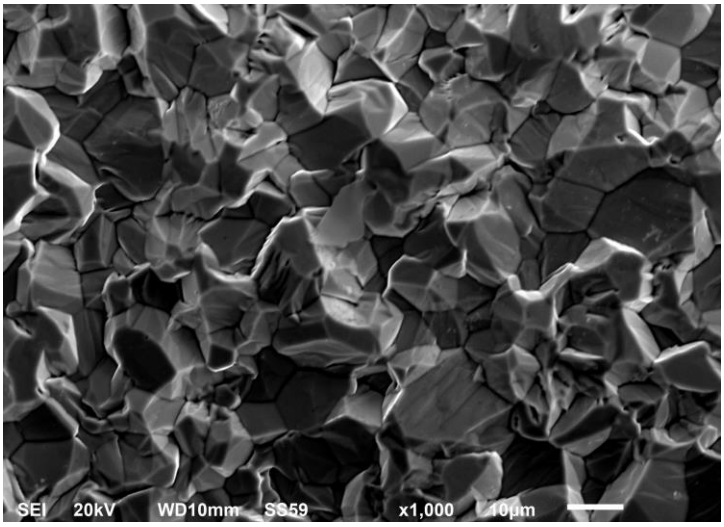

Figure 3.1: SEM image of pure tin surface at 1000x magnification

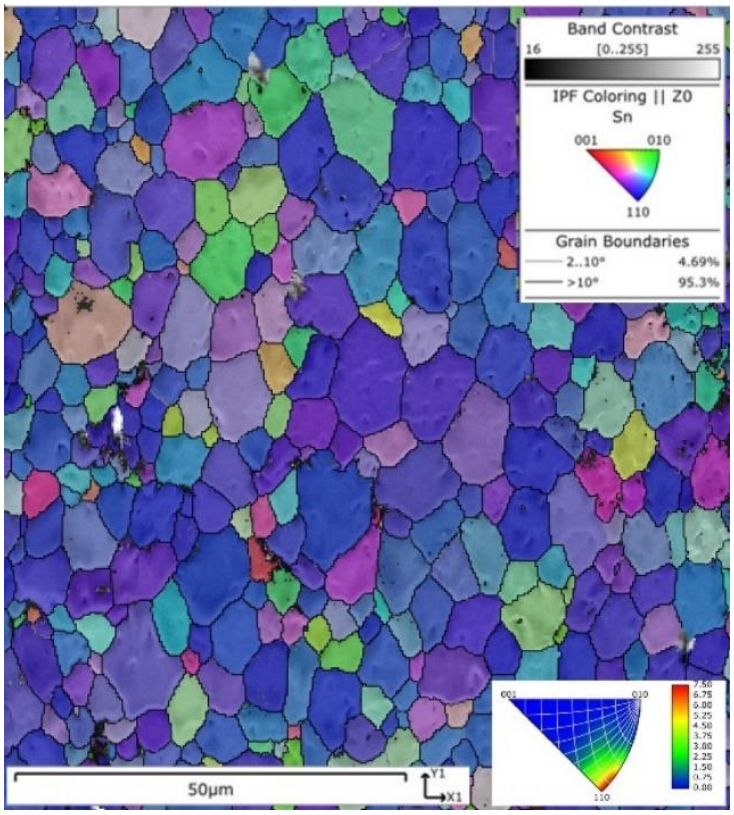

Figure 3.2: EBSD IPF of pure tin surface

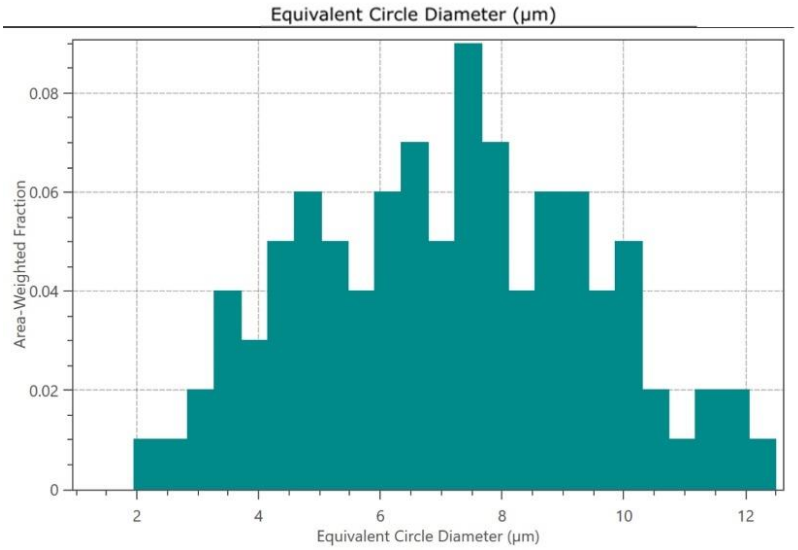

Figure 3.3: Grain size distribution of pure tin prepared by Sn MSA solution

3.2 Nickel electroplating solution

A nickel sulfur solution was used to electroplate the pure nickel seed layer on the Cu substrate. The Ni sulfur bath was prepared up to a volume of 60ml, and the plating was conducted at 55 ℃. Nickel sulfur electrolyte was composed of analytical Sulfuric acid (0.2mol/L), pure Nickel Sulfur (0.2 mol/L), Boric acid (0.2 mol/L), Nickel chloride (0.2 mol/L), and SDS (0.02 mol/L). The pH was about 3.5. Boric acid was used as a pH buffer which could suppress the hydrogen evolution reaction during Ni electroplating. Nickel chloride was used to improve the conductivity of the plating bath and prevent anode passivation. Figure 3.4 shows the Ni seed layer morphology prepared by the above solution. Figures 3.5 (a) and (b) show that the nickel seed layer prepared by the above method has a mean grain size of 1.5 um. The thickness was 10 um. Figure 3.5 (c) shows the EDS results of the Ni seed layer.

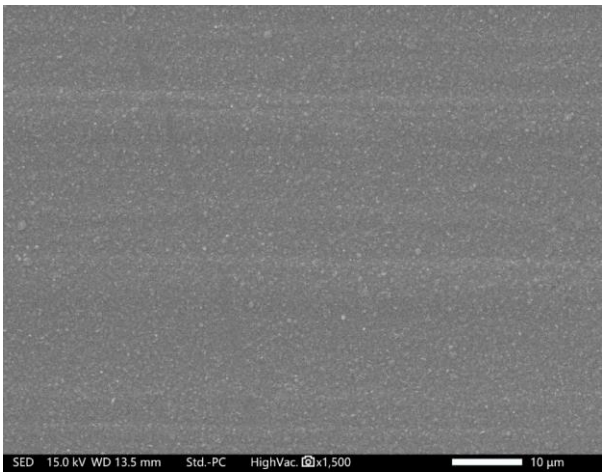

Figure 3.4: SEM image of Nickel seed layer surface under 1500 magnification

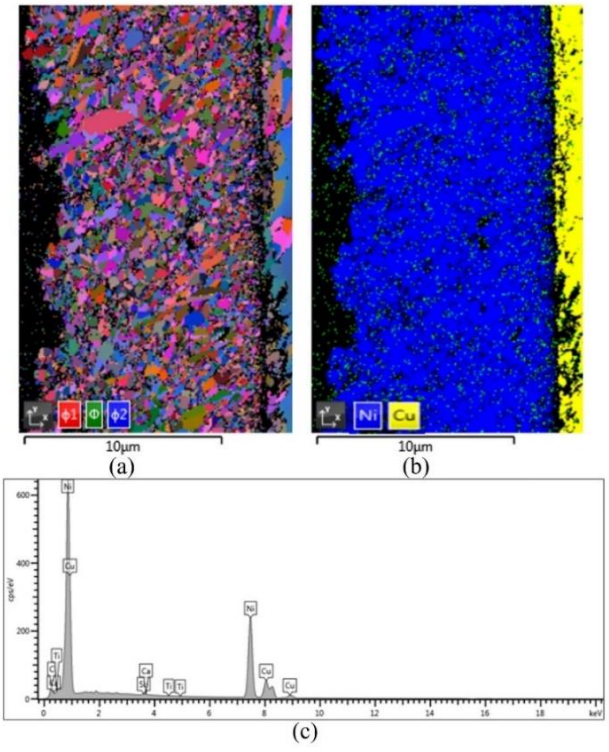

Figure 3.5: Nickel seed layer Crystallography and Composition: (a) EBSD IPF, (b) Phase map, (c) EDS spectrum

3.3 Tin-antimony co-electroplating solution

Developing a new electroplating solution involves careful experimentation and consideration of various factors. In this study, to develop a SnSb plating solution, the following factors need to be determined.

a. Selection of Metal salts: For the Sn component of the alloy, commonly used Sn salts are tin sulfate (SnSO4), tin chloride (SnCl2), and tin methane sulfonic acid (Sn MSA). For the Sb component, commonly used Sb salts are antimony acetate (Sb acetate), antimony potassium tartrate (Sb K tartrate), and antimony fluoride (Sb fluoride). The combination and concentration of Sn and Sb salts are based on their electroplating properties and compatibility with the plating bath. The ratio of Sn to Sb will affect the final alloy properties.

b. Selection of buffer agent: Tin(II) ions tend to hydrolyze in an aqueous solution, and form an insoluble basic salt:

$$SnCl2\ (aq) + H2O\ (l) \rightleftharpoons Sn(OH)Cl\ (s) + HCl\ (aq)$$

Buffer helps maintain a stable pH level in the electroplating bath and contributes to the overall stability of the plating bath by preventing excessive changes in pH due to by-products generated during plating.

c. Selection of chelating agents: For Sn–Sb plating, Sn has a standard reduction potential of -0.136 Volts and Sb is 0.212 Volts. Hence the Sn and Sb cannot be co-electroplating using Sn–Sb anodes in the same manner as for pure metal plating because the standard electrode potentials of Sn and Sb are too great.

d. Chelating agents can be applied to form stable complexes and reduce the potential difference between Sn and Sb. Also, by forming complexes, the chelating agents increase the solubility and stability of the metal ions in the plating solution.

e. Selection of leveling agents. Leveling agents are used in plating baths to provide substantial uniformity of the surface.

3.3.1 Investigation of the effects of metal source on tin-antimony alloy morphology

In this section, a total of 9 combinations are formed with three popular tin metal sources and three antimony sources. Table 3.1 summarizes the 9 systems composed of three tin metal salts and three antimony metal salts in this study. They are solution 1 (Sb acetate and SnCl2), solution 2 (Sb acetate and Sn MAS), solution 3 (Sb acetate and SnSO4), solution 4 (Sb K tartrate and SnCl2), solution 5 (Sb K tartrate and Sn MSA), solution 6 (Sb K tartrate and SnSO4), solution 7 (Sb fluoride and SnCl2), solution 8 (Sb fluoride and Sn MSA) and solution 9 (Sb fluoride and SnSO4).

Solution 1 is composed of analytical Sb acetate (0.1mol/L), acetate acid (0.2 mol/L), Sn chloride (0.2 mol/L), chloride acid (0.4 mol/L), and sodium acetate (0.02 mol/L). The pH value was approximately 2.5. During the electroplating procedure employing solution 1, a significant generation of bubbles was observed at the cathode across various current densities, accompanied by the precipitation of hydrogen gas, which precluded the deposition of the metallic coating. This phenomenon is attributable to the divergent reduction potentials of the metal ions present in the solution, wherein the disparity in these potentials is notably large. Consequently, with the increment of current density, there ensues the formation of black particulate matter, which subsequently adheres to the cathode surface (as shown in Fig.3.6). At low current densities, the current

efficiency is suboptimal, leading to an incomplete and non-uniform coating surface (Fig.3.6 a). As the current density increases, tin ions begin to undergo electrochemical reduction. However, in the absence of an effective complexing agent in the solution, antimony ions remain unreduced, resulting in a coating comprised exclusively of tin (Fig.3.6 b). When the current density is further elevated, an intense reduction reaction ensues on the cathode surface, causing a rise in pH and the decomposition of organic compounds, which ultimately leads to the formation of a black precipitate (Fig.3.6 c).

Solution 2 is composed of analytical MSA (0.2mol/L), Tin MSA (0.2 mol/L), Sb acetate (0.2 mol/L), acetate acid (0.2 mol/L), and sodium acetate. The pH was about 2.6. During the electroplating process using solution 2, the cathode produces a large number of bubbles under different current densities, hydrogen gas precipitates, and the coating cannot be deposited. This is because the two metal ions in the solution have different reduction potentials, and more importantly the reduction potential difference is too large. There is no effective metal coating formed on the surface of the sample, other than some black residue from the decomposition of organic matter when the current density is small (Fig.3.7 a). When the current increases, black particles form and absorb the cathode surface (as shown in Fig.3.7c).

Solution 3 is composed of analytical sulfuric acid (0.2mol/L), Sn sulfuric (0.35 mol/L), Sb acetate (0.1 mol/L), acetate acid (0.1 mol/L), and sodium acetate with an overall pH of about 2.7. During the electroplating process, the cathode produces a large number of bubbles under different current densities, hydrogen gas precipitates, and the coating cannot be deposited. When the current increases, black particles form and absorb the cathode surface (as shown in Fig.3.8).

Solution 4 is composed of analytical Sb tartrate (0.1mol/L), Sn chloride (0.2 mol/L), Chloride acid (0.2 mol/L), and tartaric acid (0.4 mol/L). The pH was about 3.5. For solution 4, a white coating formed on the cathode surface during the electroplating process, and the EDS data proved that the coating was 100% tin (as shown in Fig.3.9). At low current density, the coating can be seen to peel off (Fig.3.9 a). This likely shows the result of a low current density, where the electroplating is incomplete and has started to peel off due to insufficient current efficiency, resulting in a weak bond between the coating and the substrate. As the current density increases, the coating becomes smoother (Fig.3.9 b and c) and the bond between the coating and the substrate becomes stronger. Antimony cannot be deposited under different parameters such as temperature, pH, and current density. The reason is that in this system, even though tin can undergo a reduction reaction, antimony is unstable to form an effective complex. The considerably large potential difference prevents the antimony reduction reaction from occurring.

Table 3.1 Combinations of different tin and antimony salts

	SnCl2	**Sn MSA**	**SnSO4**
Sb acetate	Solution 1	Solution 2	Solution 3
Sb K tartrate	Solution 4	Solution 5	Solution 6
Sb fluoride	Solution 7	Solution 8	Solution 9

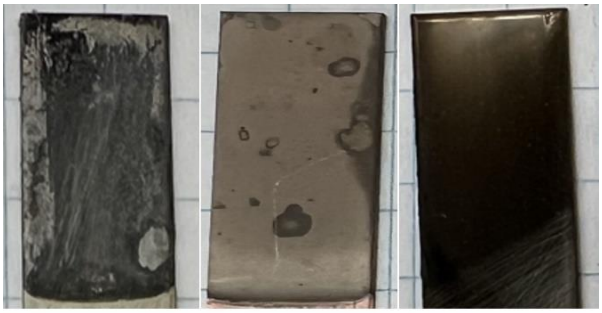

Figure 3.6: Sn-xSb sample prepared with solution 1 under different current densities: (a) 0.19 A/dm^2, (b) 0.38 A/dm^2, (c) 0.76A/dm^2

Solution 5 is composed of analytical MSA (0.2mol/L), Tin MSA (0.2 mol/L), Sb K tartrate (0.4 mol/L), and tartaric acid (0.4 mol/L). The pH was about 2.5. Similar to solution 4, a pure tin film was deposited on the cathode using solution 5, but antimony could not be deposited under different parameters such as temperature, pH, and current density, and the coating was uneven (as shown in Fig. 3.10).

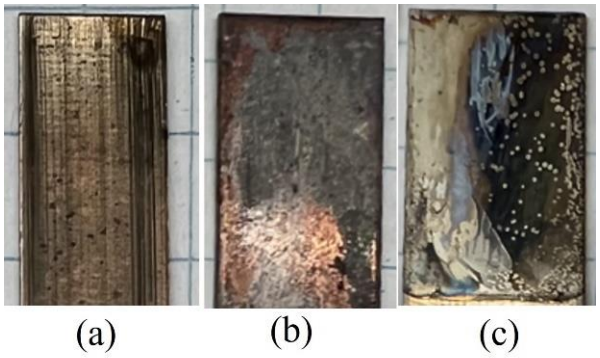

Figure 3.7: Sn-xSb sample prepared with solution 2 under different current densities: (a) 0.19 A/dm^2, (b) 0.38 A/dm^2, (c) 0.76A/dm^2

Figure 3.8: Sn-xSb sample prepared with solution 3 under different current densities: (a) 0.19 A/dm^2, (b) 0.38 A/dm^2, (c) 0.76A/dm^2

Solution 6 is composed of analytical Sulfuric acid (0.2mol/L), tin sulfuric (0.2 mol/L), (0.2 mol/L), Sb K tartrate (0.2 mol/L) and tartaric acid (0.02 mol/L). The pH was about 2.7. For solution 6, neither tin nor antimony can be deposited on the cathode surface. After electroplating is completed, some gray particles are formed on the cathode surface, which are easily washed away by water. The formation of gray particles may be due to the decomposition of organic matter due to excessive current and low pH value. (As shown in Figure 3.11).

Solution 7 is composed of analytical Sb fluoride (0.2mol/L), Sn chloride (0.2 mol/L), Citric acid (0.2 mol/L) and Chloride acid (0.2 mol/L). The pH was about 3.0. For solution 7, a relatively complete coating was deposited on the cathode surface, but the coating was rough and blistered. This was because, during the electroplating process, metal ions were deposited too fast and accompanied by the formation of bubbles, resulting in high porosity in the coating and poor bonding force of the coating. The

coating deposition rate is uneven due to poor surface wetting properties. (As shown in Fig.3.12). EDS results show that the coating indeed contains both tin and antimony.

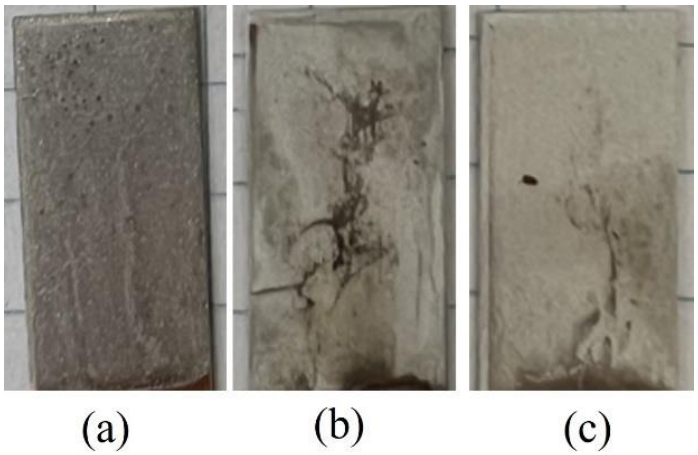

Figure 3.9: Sn-xSb sample prepared with solution 4 under different current densities: (a) 0.19 A/dm^2, (b) 0.38 A/dm^2, (c) 0.76A/dm^2

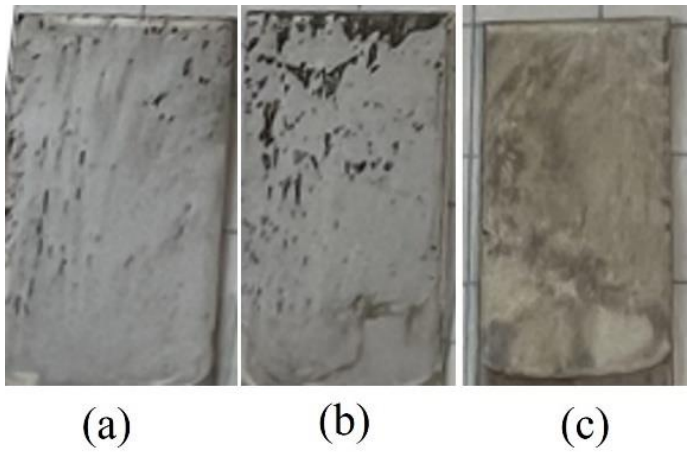

Figure 3.10: Sn-xSb sample prepared with solution 5 under different current densities: (a) 0.19 A/dm^2, (b) 0.38 A/dm^2, (c) 0.76A/dm^2

Solution 8 was composed of analytical MSA (30 ml/L), Tin MSA (0.2 mol/L), Sb fluoride (0.2 mol/L), and sodium acetate (0.2 mol/L). The pH was about 2.4. A pure tin film was deposited on the cathode using solution 8, but antimony could not be deposited (as shown in Fig.3.13).

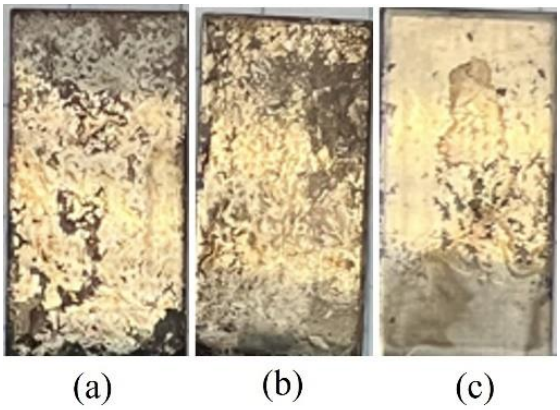

Figure 3.11: Sn-xSb sample prepared with solution 6 under different current densities: (a) 0.19 A/dm^2, (b) 0.38 A/dm^2, (c) 0.76A/dm^2

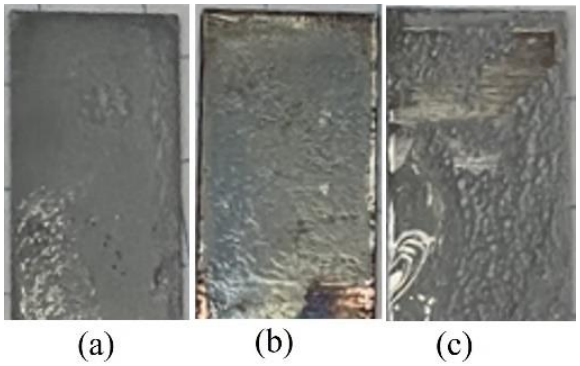

Figure 3.12: Sn-xSb sample prepared with solution 7 under different current densities: (a) 0.19 A/dm^2, (b) 0.38 A/dm^2, (c) 0.76A/dm^2

Solution 9 is composed of analytical Sulfuric acid (0.2mol/L), Sb fluoride (0.2 mol/L), tin sulfate (0.2 mol/L), and sodium citrate. The pH was about 2.5. For solution 9, black particles form and absorb the cathode surface (as shown in Fig.3.14).

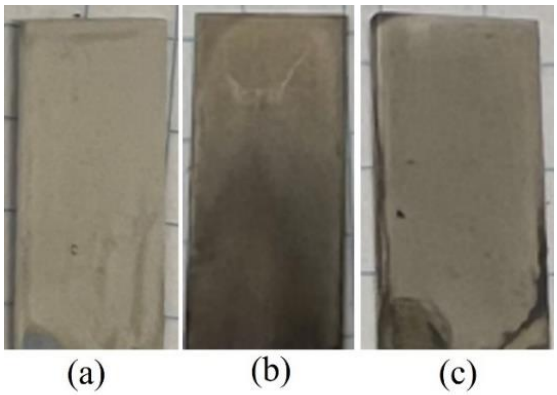

Figure 3.13: Sn-xSb sample prepared with solution 8 under different current densities: (a) 0.19 A/dm^2, (b) 0.38 A/dm^2, (c) 0.76A/dm^2

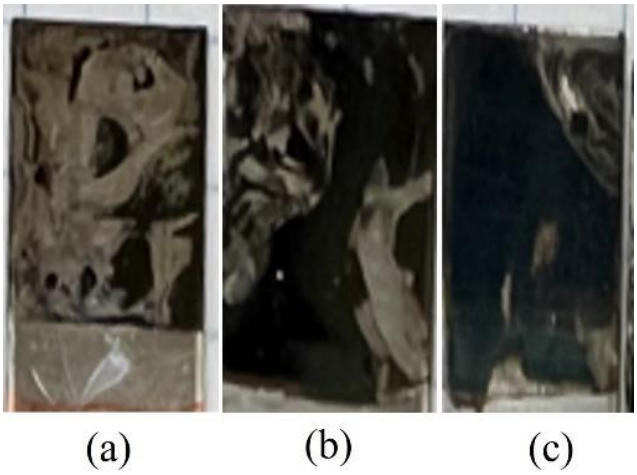

Figure 3.14: Sn-xSb sample prepared with solution 9 under different current densities: (a) 0.19 A/dm^2, (b) 0.38 A/dm^2, (c) 0.76A/dm^2

Table 3.2 provides a detailed summary of the surface quality and elemental composition of samples prepared using solutions 1 through 9, as analyzed by EDS. The analysis reveals that the samples prepared with solutions 1 and 7 exhibit the presence of both tin and antimony on their surfaces. In contrast, the samples prepared with solutions 2, 5, and 8 are composed exclusively of tin. Furthermore, the samples prepared with solutions 3, 4, 6, and 9 are found to contain only antimony. These findings underscore the influence of different solution formulations on the resulting surface compositions and highlight the critical role of solution chemistry in the electroplating process.

The above samples were prepared without any plating additives. This will cause several problems. Without levelers, high-current-density areas tend to receive more deposition, resulting in uneven coatings with peaks and valleys. The coating thickness will vary across the surface, potentially compromising the integrity and durability of the electroplated layer. The absence of levelers may lead to a less smooth and less shiny surface, reducing the visual appeal of the electroplated object. Without buffers, areas near the cathode can experience significant pH changes, which can adversely affect the deposition process. pH fluctuations can lead to the formation of undesirable phases or compounds in the coating, resulting in poor adhesion and increased brittleness.

When both leveler additives and buffers are absent, the combined effects can severely degrade the electroplating process and the quality of the final coating. Issues such as severe non-uniformity, poor adhesion, increased surface roughness, and inconsistent physical and chemical properties can arise, rendering the electroplated coating ineffective for its intended application.

Table 3.2 Summary of Solution 1-9

	Sn metal	Sb metal	Deposition state	Composition
Solution 1	SnCl2	Sb acetate	Gray, uniform	Sn and Sb
Solution 2	Sn MSA	Sb acetate	Gray, uniform	Pure Sn
Solution 3	SnSO4	Sb acetate	No coating, and black particles formed	Sb
Solution 4	SnCl2	Sb K tartrate	No coating, and black particles formed	Sb
Solution 5	Sn MSA	Sb K tartrate	Whiter coating, very thin, blistering	Pure Sn
Solution 6	SnSO4	Sb K tartrate	No coating, and black particles formed	Sb
Solution 7	SnCl2	Sb fluoride	Gray, uniform, blistering	Sn and Sb
Solution 8	Sn MSA	Sb fluoride	Whiter, uniform	Pure Sn
Solution 9	SnSO4	Sb fluoride	No coating, and black particles formed	Sb

3.3.2 Investigation of the effects of chelating agents on tin-antimony alloy morphology

The incorporation of chelating agents in electroplating solutions represents a strategic approach to modulating the electrochemical environment, particularly in stabilizing metal ions within aqueous solutions. Chelating agents achieve this by complexing with metal ions, thereby reducing the propensity for these ions to form

insoluble metal hydroxides, which can precipitate out of solution and negatively impact the plating process. This section delves into a more detailed examination of Solution 1 and Solution 7, both of which demonstrated the potential for depositing coatings that incorporate both Sn and Sb elements, despite the practical limitations of these coatings. In this section, solution 1 consists of Sb acetate (0.2mol/L), Sn chloride (0.2 mol/L), and chloride acid (0.2 mol/L). Solution 7 consists of Sb fluoride (0.2mol/L), Sn chloride (0.2 mol/L), and chloride acid (0.2 mol/L). Electroplating was conducted with 60 ml solution 1 at 30 °C for 10 mins. The pH value of the solution was around 3.0. Citric acid, sodium gluconate, ammonium citrate, lactic acid, EDTA (Ethylenediaminetetraacetic acid), tartaric acid, ascorbic acid, and potassium sodium tartrate were studied.

Figure 3.15 shows an SEM image of the Sn-xSb sample prepared with different chelation agents in solution 1: (a) Citric acid, (b) ascorbic acid, (c) ammonium citrate, (d) sodium gluconate (e) lactic acid, (f) EDTA, (g) tartaric acid, (h)potassium sodium tartrate. As shown in Figure 3.15 (a), under the action of citric acid, the coating exhibits a spherical morphology. Correspondingly, under the action of lactic acid and ammonium citrate, the coating showed a needle-like morphology and a square morphology respectively. EDS results proved that 100% Sn element on Figure 3.15 (b), (d), (f), (g), and (h) samples, which indicate ascorbic acid, sodium gluconate, EDTA, tartaric acid, and potassium sodium tartrate dose not chelate either tin ions or antimony ions.

Different from the combination of tin chloride and antimony acetate, tin chloride, and antimony fluoride exhibits a needle-like or leaf-like morphology. These needle-like or leaf-like morphologies are dendrites deposited during the electroplating process. Combined with the EDS results, the needle-like or leaf-like structure is 100% tin.

Figure 3.16 shows SEM images of the Sn-xSb sample prepared with different chelation agents in solution 7: (a) Citric acid, (b) ascorbic acid, (c) ammonium citrate, (d) sodium gluconate (e) lactic acid, (f) EDTA, (g) tartaric acid, (h)potassium sodium tartrate.

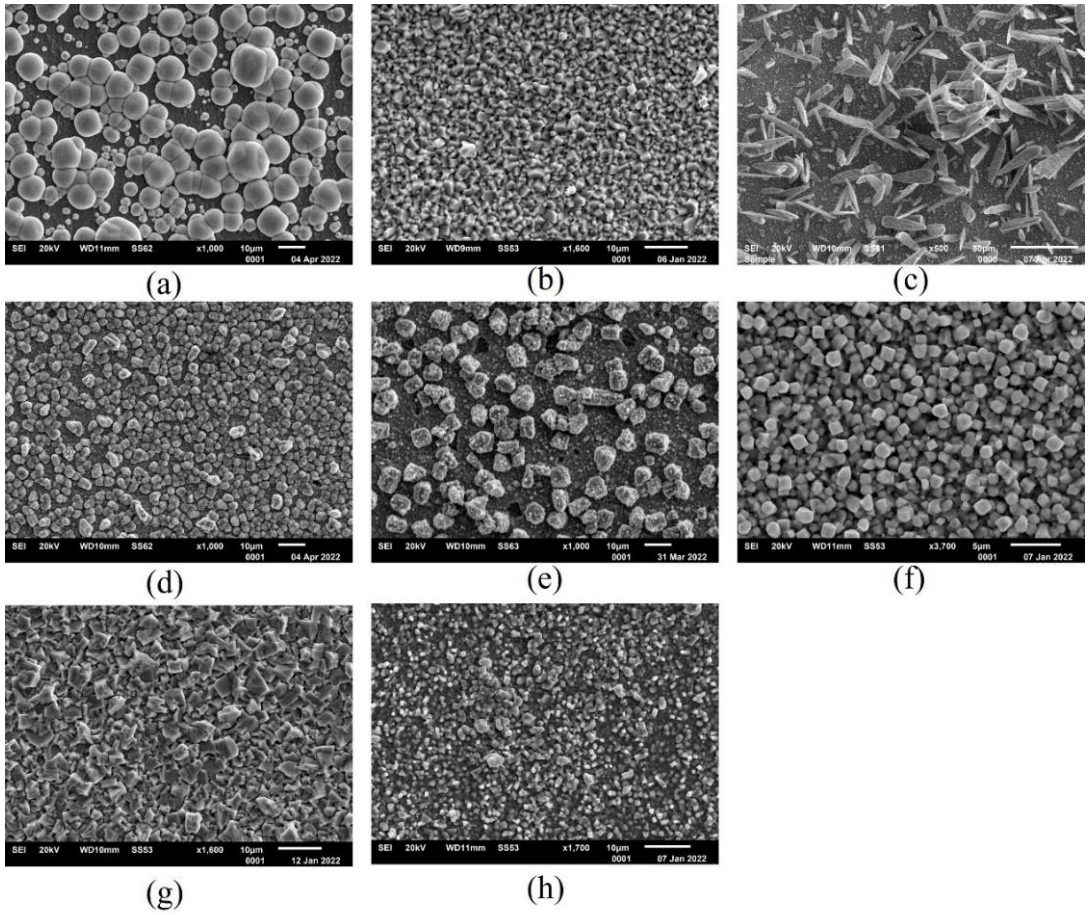

Figure 3.15: SEM image of Sn-xSb sample prepared with different chelation agents in solution 1: (a) Citric acid, (b) ascorbic acid, (c) ammonium citrate, (d) sodium gluconate (e) lactic acid, (f) EDTA, (g) tartaric acid, (h)potassium sodium tartrate

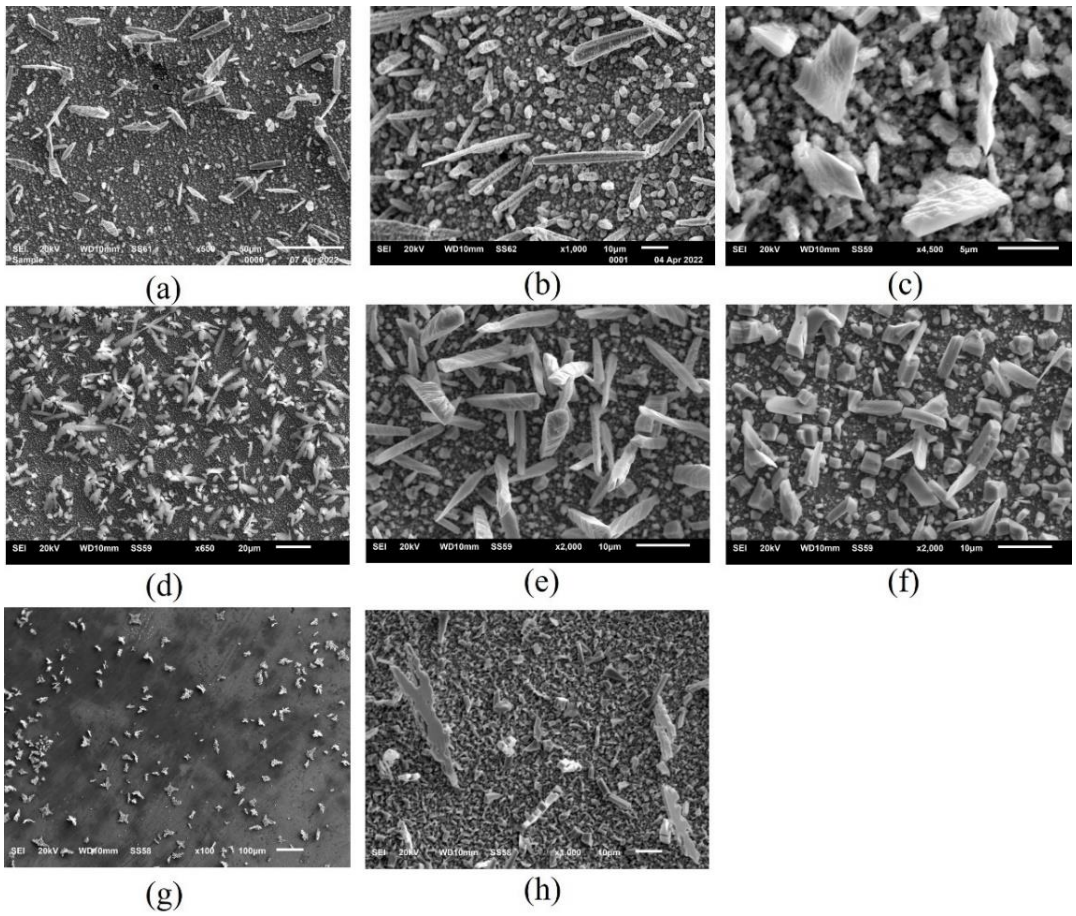

Figure 3.16: SEM image of Sn-xSb sample prepared with different chelation agents in solution 7: (a) Citric acid, (b) ascorbic acid, (c) ammonium citrate, (d) sodium gluconate (e) lactic acid, (f) EDTA, (g) tartaric acid, (h)potassium sodium tartrate

3.3.3 Investigation of the effect of leveling agent on tin-antimony alloy morphology

Based on the experimental results in the previous chapter, solution 1 with lactic acid was used for studying the effect of the leveling agent on the Sn-xSb morphology. PEG (Polyethylene glycol), Thiourea, TPAB (pentyl ammonium bromide), 2-4 naphthol were studied. Fig. 3.17 shows an SEM image of the Sn-xSb sample prepared with different leveling agents in solution 1: (a) PEG, (b) Thiourea, (c) TPAB, (d) 2-4 naphthol.

The use of PEG, Thiourea and TPAB increases the internal stress of the coating, thus cracks to form on the surface of the deposition material. It can be found from figure 3.17 (d) that the use of 2-4 naphthol makes the coating exhibit a triangular morphology. The formation of ravines rather than cracks on the surface proves that the ions made some adjustments during the reduction process to reduce internal stress.

3.3.4 Investigation of surfactant on tin-antimony alloy morphology

An electroplating leveling agent is a chemical additive used in the electroplating process to improve the surface finish and uniformity of the deposited metal layer. The primary functions of a leveling agent include smoothing surface defects, enhancing surface brightness, controlling deposition rate, and improving adhesion. Based on the experimental results in the previous section, solution 1 with additional 2-4 naphthol was used for studying the effect of surfactant on the Sn-xSb morphology. Figure 3.18 shows an SEM image of the Sn-xSb sample prepared with different leveling agents in solution 1: (a) Triton-X 100, (b) PVA, (c) Gelatin, (d) saccharin. The leveling effects of using Triton-X100, Gelatin, and saccharin on the deposition surface are significant. The difference is that the morphology of the coating formed under the action of the three is different. Under the action of Triton X-100, the morphology of the coating is triangular. Under the action of gelatin, there are squares in the coating. Under the action of saccharin, the coating shows a spherical morphology. PVA also levels the coating to a certain extent, but the coating is deposited with a cube morphology in different directions.

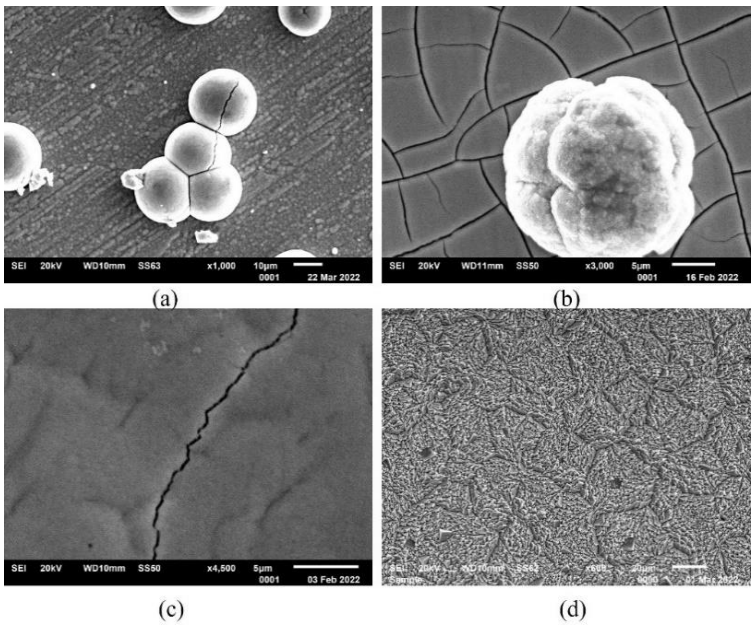

Figure 3.17: SEM image of Sn-xSb sample prepared with different leveling agents in solution 1: (a) PEG, (b) Thiourea, (c) TPAB, (d) 2-4 naphthol

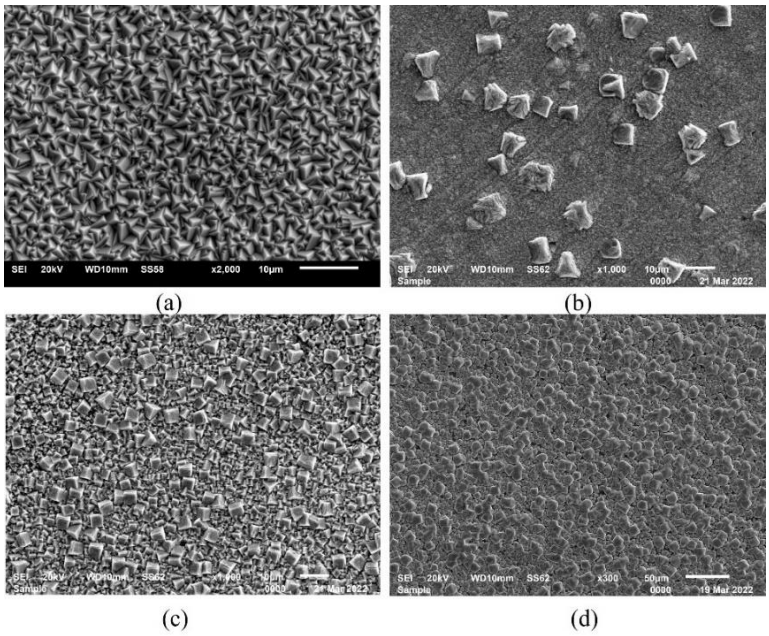

Figure 3.18: SEM image of Sn-xSb sample prepared with different surfactant agents in solution 1: (a) Triton-X100, (b) PVA, (c) gelatin, (d) saccharin

3.3.5 Effects of electroplating conditions on tin-antimony alloy morphology

Figure 3.19-3.21 plots the deposition rate of Sn-3Sb, Sn-10Sb, and Sn-15Sb coatings as a function of current density for a plating time of approximately 30 minutes. It can be seen that the deposition rate increased linearly with current density and that the concentration of Sb in the bath did not affect this rate.

The deposition rates increase with an increase in temperature at all current densities. This is evident as the curves for 45°C and 60°C lie above the curve for 30°C. This trend could be attributed to the enhanced ion mobility and increased electrochemical activity at higher temperatures, which can accelerate the reduction of metal ions to form the alloy coating. The deposition rate appears to reach a plateau or a slightly declining trend as the current density increases from 0.5 A/dm² to 1.62 A/dm² for all temperatures. This suggests that beyond a certain current density, the efficiency of ion deposition does not increase significantly with current. It may also indicate the onset of limiting factors such as mass transport limitations or side reactions (like hydrogen evolution) becoming more prevalent at higher current densities. At the highest current density shown (0.74 A/dm²), the deposition rate does not differ greatly between the temperatures of 45°C and 60°C, whereas it is slightly lower at 30°C. This might suggest that the deposition process is approaching a diffusion-limited regime, where the temperature dependency becomes less pronounced due to the rate-limiting step being the transport of ions to the cathode surface rather than the charge transfer itself.

Figure 3.22 is a plot of Sb content in coating as a function of electroplating solution pH. As shown, the amount of Sb content in the coating decreased sharply with increasing solution Ph. When the solution pH reaches 3.5, the coating is completely Sn,

and no more Sb is deposited. At lower pH value of approximately 1.8, the Sb content in the coating is at its highest, nearing 30%.

This trend could be indicative of the increasing competition between hydrogen evolution and metal deposition reactions at higher pH levels. At lower pH values, the concentration of H^+ ions is greater, potentially suppressing the reduction of Sb^{3+} ions and resulting in a higher Sb content in the coating. As the pH increases, the reduced concentration of H^+ ions might allow for more hydrogen evolution, which competes with Sb^{3+} ion reduction, leading to a lower Sb content in the coating.

Figure 3.23 is a plot of Sb content in coating as a function of Sb concentration in the electroplating solution. Initially the weight percentage of the coated Sb is almost linearly proportional to the Sb ion concentration in the solution. The slope drops when the solution concentration reaches approximately 20%.

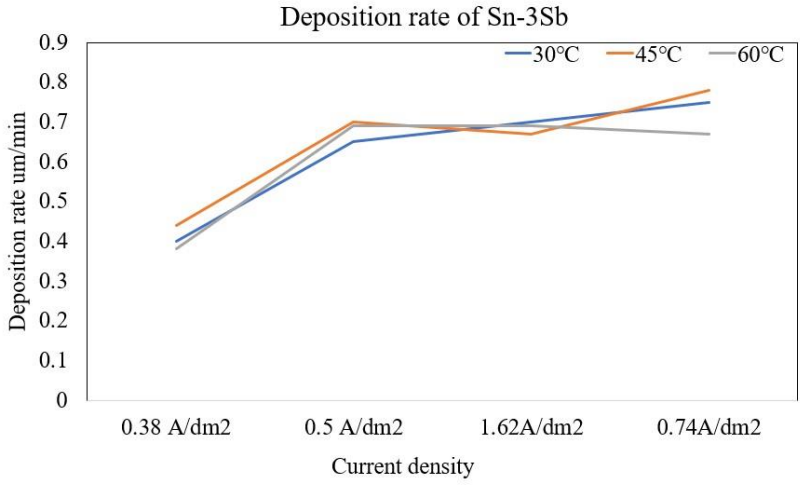

Figure 3.19: Sn-3Sb coating deposition rate as a function of current density

Figure 3.20: Sn-10Sb coating deposition rate as a function of current density

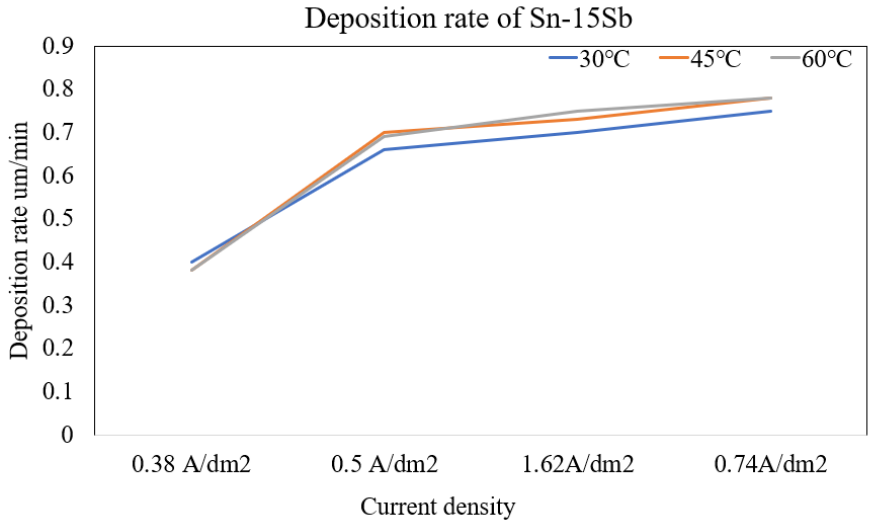

Figure 3.21: Sn-15Sb coating deposition rate as a function of current density

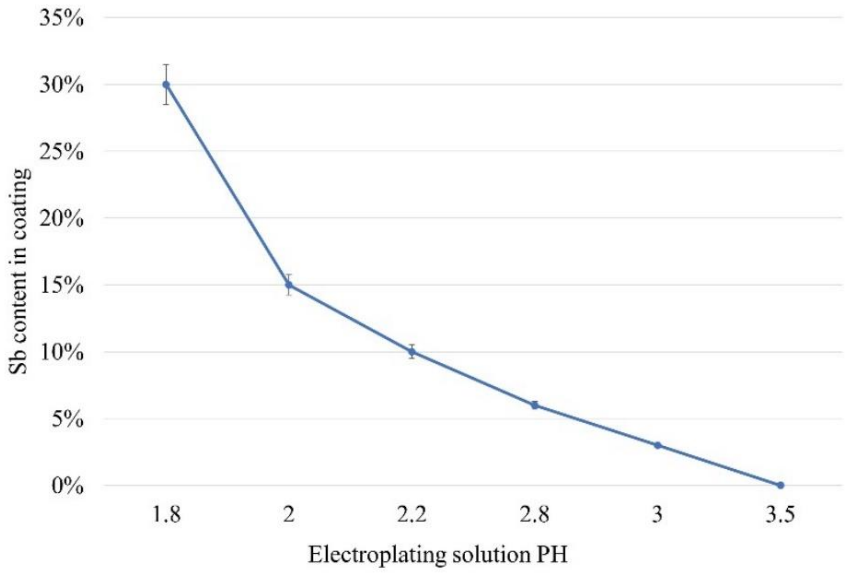

Figure 3.22: Sb content on Sn-xSb films as a function of electroplating solution pH

Figure 3.23 shows an initial steep increase in Sb content within the coating as the concentration of Sb in the solution rises from 5 Wt% to 20 Wt%. This suggests a relatively efficient incorporation of Sb from the solution into the coating at lower concentrations. As the Sb concentration in the solution continues to increase beyond 40 Wt%, the rate of increase in Sb content in the coating begins to taper off, indicating a diminishing return on the Sb concentration in the solution. This plateau effect, where the Sb content in the coating levels out around 40-50 Wt% despite further increases in Sb solution concentration, suggests that the electroplating system may be approaching a saturation point. Beyond this point, additional Sb ions in the solution may not be deposited onto the substrate as efficiently, possibly due to limitations in the electroplating process or the formation of competing Sb-containing species within the solution.

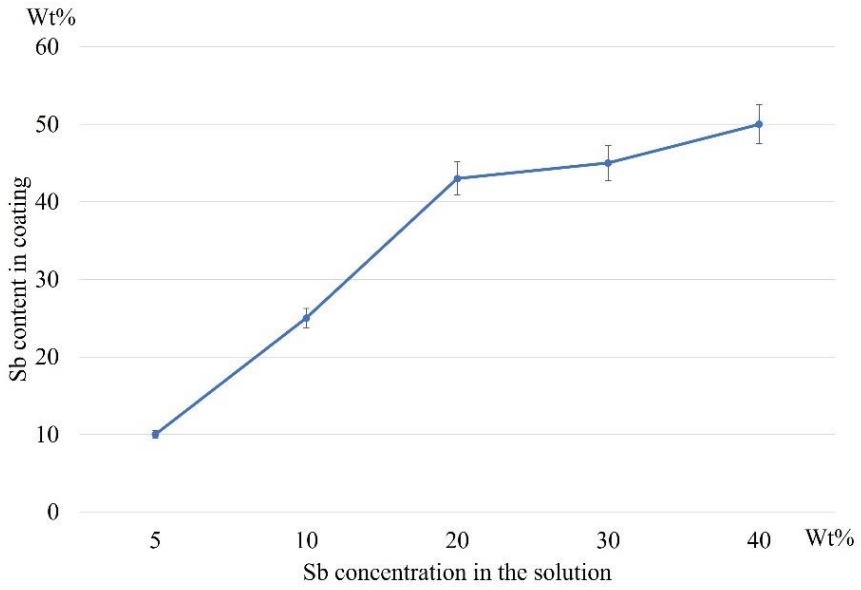

Figure 3.23: Sb content on Sn-xSb films as a function of Sb concentration in the solution

Table 3.3 summarizes how different additives affect the composition of the coating. As can be seen from the table, in solutions containing citric acid, ammonium citrate or lactic acid, EDS results show that the coating contains both tin and antimony. Citric acid can positively impact the electroplating of Sn-Sb alloys by acting as a complexing agent and buffer. It stabilizes the electroplating bath, controls the deposition process, improves surface morphology, and enhances the overall quality and corrosion resistance of the coatings. However, its use requires careful optimization to maximize benefits and minimize potential drawbacks [58].

Ammonium citrate has been reported to form complexes with tin and antimony ions in the electroplating bath. This complexation helps stabilize the metal ions in

solution, preventing their precipitation and ensuring a consistent supply of ions for deposition [59].

Lactic acid positively influences the electroplating of Sn-Sb alloys through its roles as a complexing agent and pH stabilizer. It helps stabilize the electroplating bath, controls the deposition process, improves surface morphology, and enhances the quality and corrosion resistance of the coatings. However, its use requires careful optimization to maximize its benefits and minimize potential drawbacks, ensuring a high-quality and reliable electroplating process. From the samples prepared with ascorbic acid, sodium gluconate, EDTA, tartaric acid or potassium sodium tartrate, only Sn elements was detected.

Table 3.3 Summary of EDS results on Sn-xSb coating with different additives

additives	EDS
citric acid	Sn and Sb
ascorbic acid	Pure Sn
ammonium citrate	Sn and Sb
sodium gluconate	Pure Sn
lactic acid	Sn and Sb
EDTA	Pure Sn
tartaric acid	Pure Sn
potassium sodium tartrate	Pure Sn

CHAPTER FOUR

TIN WHISKERS RESULTS AND ANALYSIS

4.1 Whiskers growth results

4.1.1 Morphology

The morphology of as-plated pure Sn and Sn-xSb samples is shown in Fig. 4.1a-d. From Fig.4.1a, the deposits of the pure Sn sample display a relatively uniform and equiaxed grain morphology characteristic. The uniformity suggests a stable growth process without the influence of alloying elements. With the introduction of a small amount (3.42 wt%) of Sb (as shown in Fig.4.1 b), there is a discernible change in grain morphology. The grains appear to be smaller and more numerous than in pure Sn, which indicates that the addition of Sb influences the nucleation rate and growth kinetics of the Sn crystal structure. At a higher Sb concentration (10.78 wt%), the grains seem to become even more refined, and there is an observable change in grain shape, suggesting that Sb acts as a grain refiner and alters the preferred growth direction of the Sn grains. This change could also signify a shift in the alloy's physical properties, such as increased hardness or tensile strength. At this concentration (14.93 wt% Sb), the grain structure becomes even more complex, with a mixture of refined grains and some larger, more irregular formations. This could be a result of further changes in the alloy's crystallographic texture due to the increased Sb content.

From these SEM micrographs, it is evident that the addition of Sb has a marked effect on the microstructure of the Sn deposits. Increasing Sb content correlates with a decrease in grain size and a transition to more complex grain structures, which could

have significant implications for the mechanical and electrical properties of the Sn-Sb alloy coatings. Such information is vital for applications where specific microstructural characteristics are desired to achieve optimal performance in electronic soldering, plating, or barrier layer applications.

Figure 4.2 (a-c) shows the evolution of the surface morphology over 24 hours, 1 week, and 4 weeks progressive changes. Initially, the surface may appear relatively smooth but over time, changes such as oxidization or recrystallization could occur, leading to the growth of whiskers or hillocks as can be seen in subsequent images. It can be seen from Figure 4.2 c that Sn whiskers grew up to 73 um on the pure tin sample，whereas for the Sn-xSb alloy samples, no whiskers or hillocks were observed within the same time frame, as shown in Fig.3 (d-l). The direction of whisker growth is not straight, and whiskers may grow in any direction.

With a small amount of Sb (3%), Figure (d-f) for storage at 1 week, 3 weeks, and 24 weeks show that the Sb addition impacts the aging process. The addition of Sb can affect the grain structure and the diffusion rates on the surface, potentially leading to different morphologies as compared to pure Sn. It can be seen that hillock begins to grow in the third week. In the 24th week, a large number of hillocks grow along the boundary between deformation and non-deformation, and the length can reach 25 microns and the width can reach 15 microns, much less than 250 microns whiskers for the pure Sn sample. The results indicate that Sn whiskers and hillocks are significantly suppressed under pressure after co-electroplating with Sb.

The observation made from Figure 4.3 regarding the 24-week time point suggests that the variation in Sb concentration across the samples does not markedly influence the

suppression of hillock formation. Despite the presence of varying Sb levels, the uniformity in the number and dimensions of the hillocks implies that Sb's role in hillock inhibition is not significantly effective under the conditions presented.

This could be an indication that the mechanism by which Sb impacts Sn's microstructure does not directly correlate with hillock prevention over an extended period of storage at room temperature. Hillock formation is a complex phenomenon that can be influenced by numerous factors, such as internal stress, grain boundary energy, and surface diffusion rates. The presence of Sb might influence some of these factors but not sufficiently to alter the kinetics of hillock formation discernibly after a prolonged period.

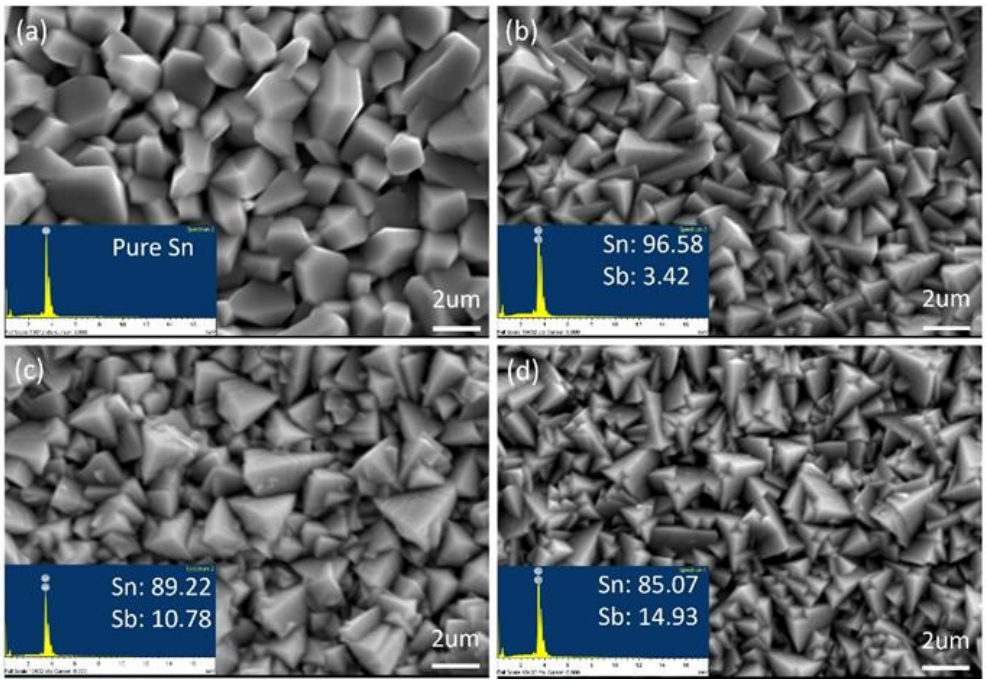

Figure 4.1. SEM morphologies of as-plated pure Sn and Sn-xSb samples: (a) pure Sn, (b) Sn-3Sb, (c) Sn-10Sb, and (d) Sn-15Sb.

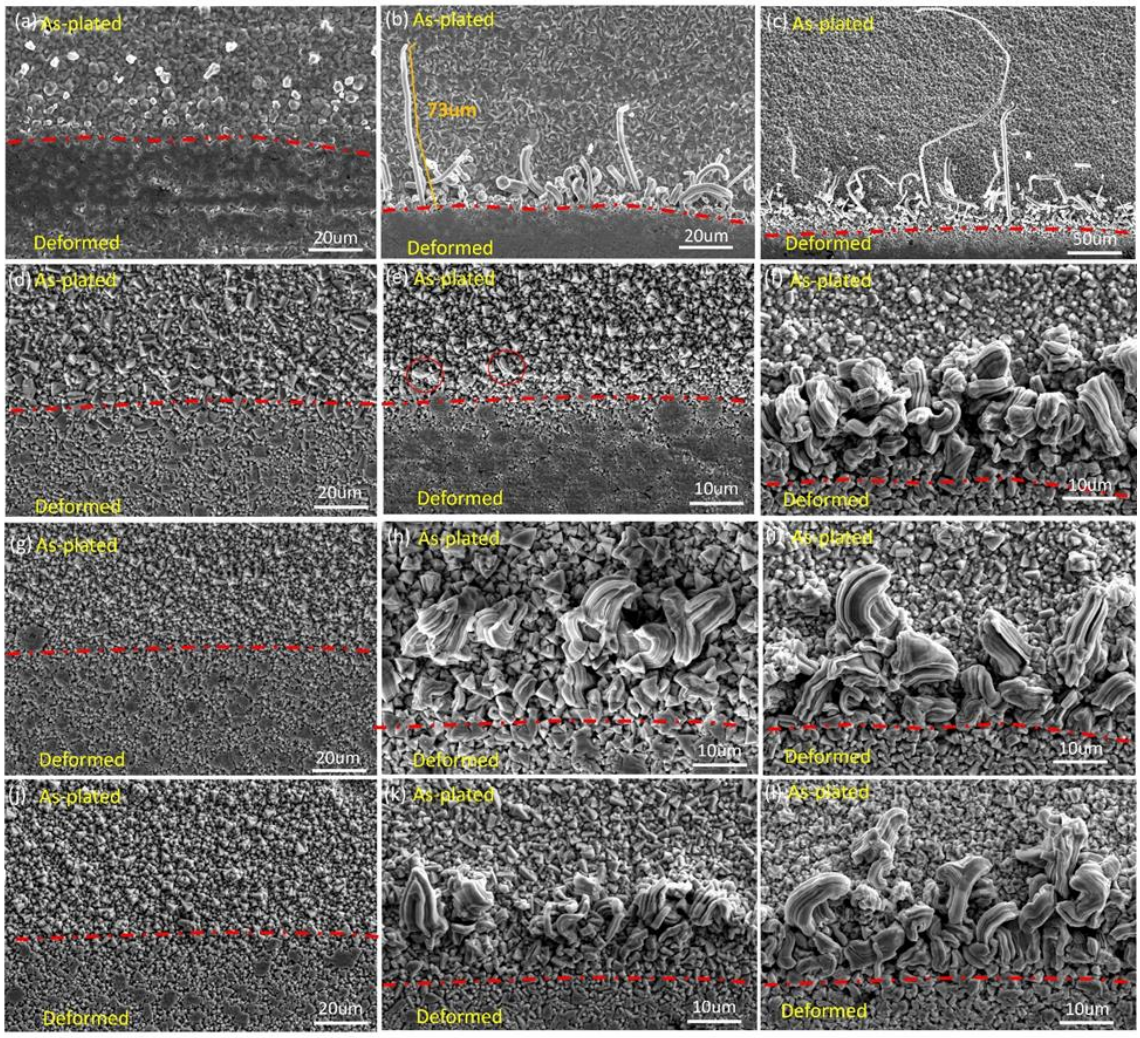

Figure 4.2: Surface morphology evolution of pure Sn and Sn-xSb under room temperature: (a-c) pure Sn storing for 24 hours, 1 week, and 4 weeks respectively, (d-f) Sn-3Sb sample storing for 1 week, 3 weeks and 24 weeks respectively, (g-i) Sn-10Sb sample storing for 1 week, 12weeks and 24 weeks respectively, and (j-l) Sn-15Sb sample storing for 1 week, 12 weeks and 24 weeks respectively.

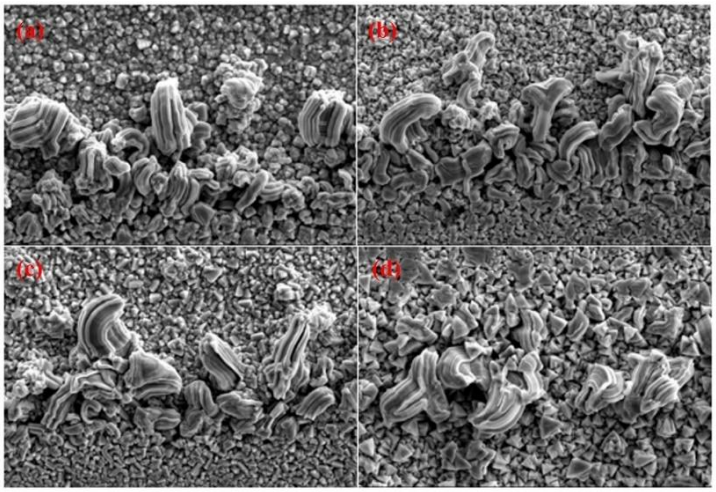

Figure 4.3: Surface morphology of hillocks distribution on and Sn-xSb sample for 24 weeks at room temperature (a) Sn-3Sb, (b) Sn-5Sb, (c) Sn-10Sb and (d) Sn-15Sb

4.1.2 Whisker length

In this study, the stress diffusion model was used to study whiskers growth. Whiskers are grown driven by the stress diffusion of atoms to the whisker root. Assume that there is a diffusion field of radius *b* around a whisker of diameter 2*a*. During steady state, the stress field, σ, can be described by the following 2D continuity equation (in a cylindrical coordinate system):

$$\nabla^2\sigma = \frac{\partial^2\sigma}{\partial r^2} + \frac{1}{r}\frac{\partial\sigma}{\partial r} = 0 \tag{4.1}$$

This has a solution of the form:

$$\sigma = B\sigma_0 \ln\frac{r}{a} \tag{4.2}$$

Where $B = [\ln(b/a)]^{-1}$ and σ_0 is the stress in the Sn film due to the chemical reaction. Assuming that σ_0 is constant because the stress is sustained by the chmical reaction, and it decays only when the reaction is over.

If the following boundary conditions are imposed:

$$\sigma = \sigma_0 \, at \, r = a$$

$$\sigma = 0 \, at \, r = b \tag{4.3}$$

Then the flux of atoms is driven by the gradient in the chemical potential of atoms $\mu = -\sigma(r)\Omega$, where Ω is the molar volume of Sn, can be given as:

$$j_v = -\frac{D_{gb}}{kT}\nabla\mu \tag{4.4}$$

Where D_{gb} is the grain boundary diffusivity, k is the Boltzmann constant and T is the absolute temperature. The total volume of the material that can be transported with a flux of atoms j_v in time dt can be given as:

$$j_v A\Omega dt = 2\pi a^2 dh \tag{4.5}$$

This predicts that the growth rate of tin whiskers, dh/dt driven by the stress of the atoms will be as follows:

$$\frac{dh}{dt} = \frac{D_{gb}\Omega\partial\sigma}{kT}\Big|_{r=a} \tag{4.6}$$

The kinetics of the tin whiskers growth predicted using the above equation agree with the experimental results as shown in Fig 4.4-4.5. Figure 4.4 shows the whisker growth rates predicted using this model for two different values of σ_w(the threshold stress for whisker nucleation) for a range of possible strain rates. For volumetric strain rates, de/dt, within the range of 10^{-6} to 10^{-8} which aligns with intermetallic compound (IMC) growth kinetics, the model forecasts steady-state whisker growth rates between 6×10^{-12} and 2×10^{-11} m/s. This prediction aligns well with the reported whisker growth rate in Fig.4.5 of approximately 1.7×10^{-11} m/s.

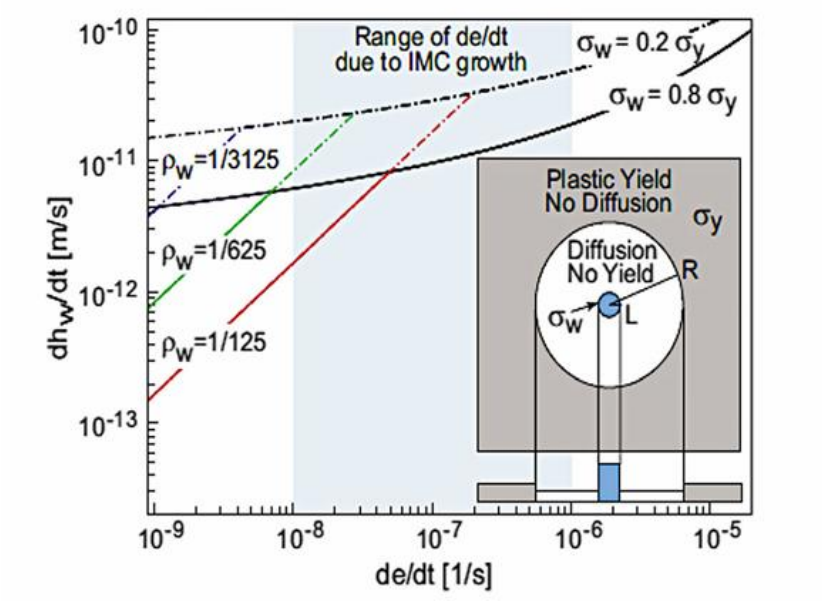

Figure 4.4 Whisker growth rates predicted using the analytical model for two different values of stress [60].

Figure 4.5 shows a comparison of average whisker length for pure tin and Sn-xSb (x=3 wt%, 5wt%, 10wt%, and 15wt%.) samples over 24 weeks. For pure tin samples, whiskers began to grow around the seventh day, the growth rate began to increase rapidly in the third week and began to decrease in the twelfth week. This is because whiskers are a process of releasing internal stress. After the whiskers break through the obstruction of the oxide film, the internal stress will be released rapidly, which is manifested as rapid growth of the whiskers. The internal stress release of the coating will gradually decrease which is manifested as a decrease of whisker growth rate. For Sn-xSb samples, we note that no whisker growth was observed but hillocks began to form in the third week. The hillock can range in width from 3-10 um, which is much larger than the typical whisker diameter. Hillocks were observed on all Sn-xSb samples and there was not much

difference in their size. The data indicate that the Sb content did not have a significant effect on hillock formation. Also, the addition of tin has a very positive effect on inhibiting whisker growth.

Comparing the trends, the graph suggests that while pure Sn is prone to whisker/hillock growth under these conditions, the addition of Sb at concentrations of 3%, 10%, or 15% appears to mitigate this growth effectively. The lack of any discernible difference between the Sn-Sb alloys implies that the presence of Sb at these levels is sufficient to inhibit growth and increasing the concentration of Sb beyond 3% does not provide additional benefits in terms of suppressing the average length of whiskers/hillocks.

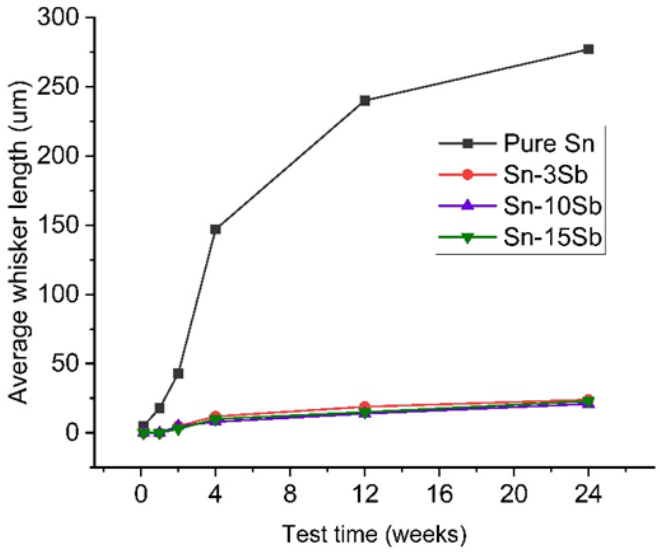

Figure 4.5: Average whiskers/hillocks length as a function of storage time

4.1.3 Whisker Density

Figure 4.6 shows the comparison of whisker density for the pure Sn, Sn-3Sb, Sn-5Sb, Sn-10Sb, and Sn-15Sb electroplated films over 24 weeks. Noted that all samples were stored on ambient. The line of pure Sn shows a dramatic increase in the number of whiskers/hillocks over time, with a particularly steep rise between weeks 4 and 24. The alloys exhibit a vastly different behavior compared to pure Sb. For Sn-3Sb, Sn-5Sb, Sn-10Sb, and Sn-15Sb, the whisker/hillock density remains relatively low and changes little over the entire duration of the study.

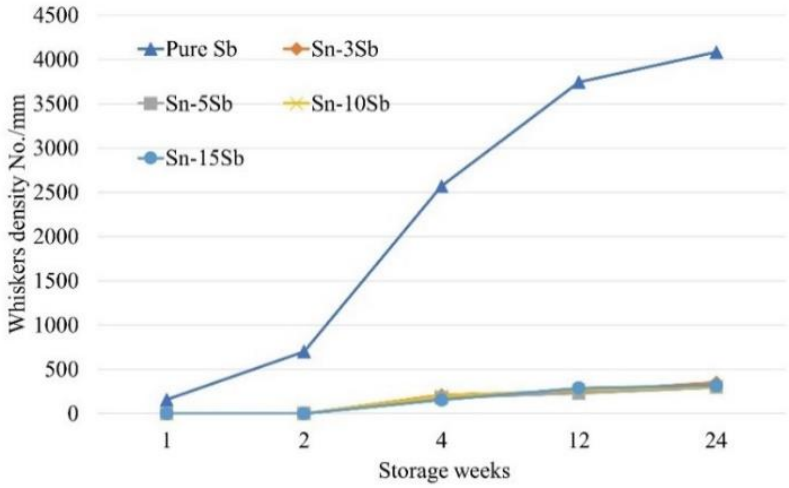

Figure 4.6: Whiskers/hillocks density as a function of storage time

The whiskers density were investigated using SEM images at an incidence angle of 10^0 to enhance contrast at an accelerating voltage pf 20 KV, and utilizing the Image-J image analysis program to count the number of whiskers. The composition of whiskers

or hillocks were investigated using EDS operating at 20 KV. At least five images were utilized to obtain statistical information on whiskers density. In this study, we define a whisker as one with an aspect ratio greater than 5, to distinguish it from hillocks, protrusions or other formations that were present but were stocky with an aspect ratio typically less than 2.

The constant low density of whiskers/hillocks across the Sn-Sb alloy samples, irrespective of the Sb concentration, indicates that even a small amount of Sb (3%) added to Sn may be sufficient to inhibit whisker/hillock formation. Furthermore, increasing the Sb content in these alloys up to 15% does not show a significant change in the density, which suggests that the initial addition of Sb has a pronounced effect, with limited incremental benefit from adding more Sb.

4.2 Tin whiskers growth mechanism

4.2.1 Surface EBSD

Figures 4.7, 4.8, and 4.9 show a representative EBSD color-coded orientation map of pure Sn sample obtained from 4 weeks of storage at -15C, room temperature, and 40C, respectively. The pole figures are color-coded to represent the intensity of each orientation within the sample. The yellow line presents the low-angle grain boundaries (LAGBs) with a misorientation in the range of 1°-10° and the black line presents the high-angle grain boundaries (HAGBs) with a misorientation over 10°. The EBSD image is divided into two areas: deformed area and undeformed area, corresponding to applying pressure and not applying pressure. Figures 4.7, 4.8, and 4.9 reveal that the dominant crystallographic texture of the Sn plating electroplated using the process condition mentioned in chapter three was (110). A comparison of deformed areas and undeformed

areas reveals that the crystallographic orientation of the tin phase does not change before and after deformation. However, tin grains become significantly larger after deformation.

Figure 4.10 shows a Sn grain size distribution before and after deformation. It can be seen that the grain growth rate is faster at low-temperature conditions. From Figure 4.10 a, at -15C temperature, deformation seems to result in a broader grain size distribution, with a tail extending to larger diameters, indicating grain growth due to deformation. At room temperature, the effect of deformation on grain size appears to be less pronounced than at -15°C but still noticeable with a slightly broader distribution in the deformed state. The histograms for 40°C show significant grain growth in the deformed state, with a very pronounced shift towards larger grain sizes. This indicates that deformation at higher temperatures promotes considerable grain growth. The grain growth in the deformed areas could be due to mechanisms like grain boundary migration, where boundaries move to reduce the total boundary energy, especially at higher temperatures. The deformation at -15°C and 40°C leading to different distributions suggests temperature-dependent mechanisms are at play, like increased atomic mobility at higher temperatures.

Figure 4.11 is a pole figure map of Sn grains before and after deformation after storage for 4 weeks under different temperature conditions. The tin in the undeformed area shows a highly concentrated (110) crystal orientation. In comparison, the crystal orientation of tin in the deformed area diffuses from (110) to the surroundings. This change in crystal orientation is the twisting or tilting of tin grains to release internal stress. The concentration of the (110) orientation in the undeformed area and its diffusion after deformation suggests that deformation causes a realignment of the crystal lattices.

This could be indicative of recrystallization or grain boundary migration phenomena where grains rotate to accommodate the stress applied.

From Figure 4.11 (a-b), the deformed area shows more spread in intensity, indicating a deformation-induced realignment of grains. In comparison, the undeformed area has more concentrated intensities around specific poles, indicating a stronger preferred orientation and less internal stress or strain. The room temperature pole figures (as shown in Figure 4.11 b-c) show the effect of deformation is less pronounced than at -15°C. At 40°C, the deformed area (Figure 4.11 e) shows broadened poles, indicating that higher temperatures may facilitate grain rotation or recrystallization, relieving stress and causing texture randomization. The undeformed area (Figure 4.11 f) maintains a relatively sharp texture, similar to that seen at -15°C.

Figure 4.12 is an inverse pole figure map of Sn grains before and after deformation after storage for 4 weeks under different temperature conditions. The colors in each IPF map represent the intensity of a particular crystallographic direction that is parallel to the sample reference frame. The color scale, indicating multiples of a random distribution, shows the frequency of grains oriented in a particular direction. It can be seen from the figure that in the deformation area, the crystal direction of tin is concentrated from (110) to (100), that is, the tin grains rotate along the in-plane axis. This can indicate which (100) crystallographic directions are more favorable under mechanical stress. Also, this kind of in-plane rotation could be indicative of certain slip systems being activated under stress.

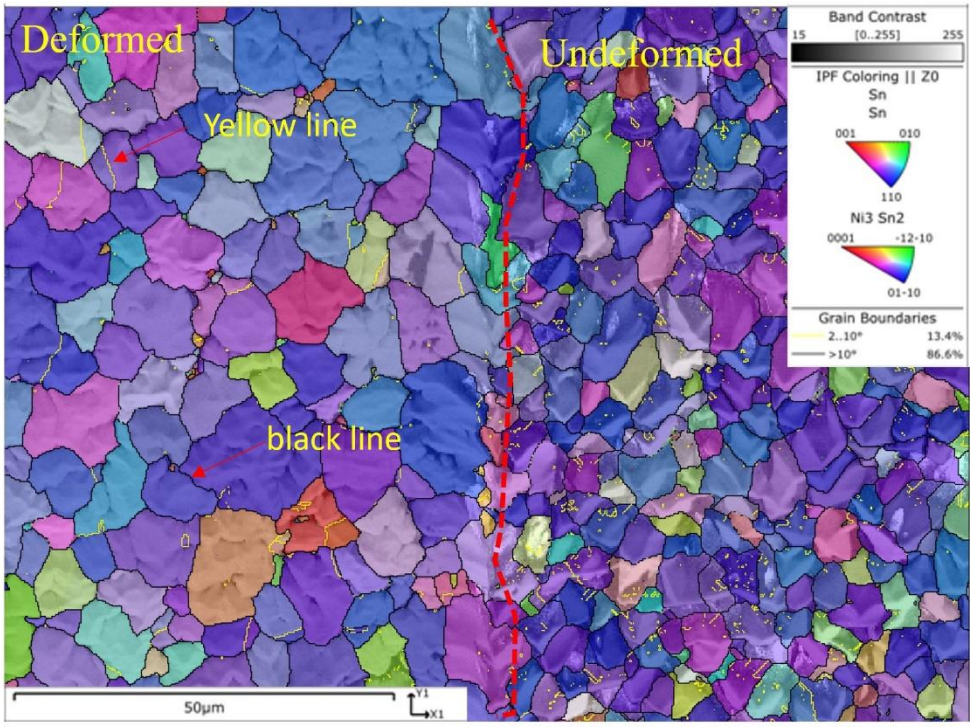

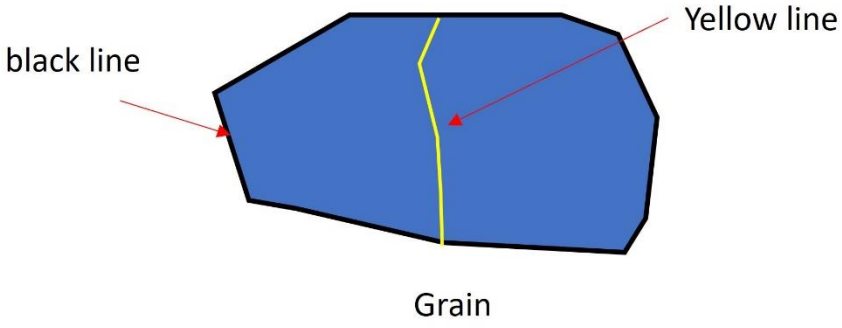

Figure 4.7: Grain map of the surface of pure tin coating from Sn MSA solution on -15^0 C for 4 weeks

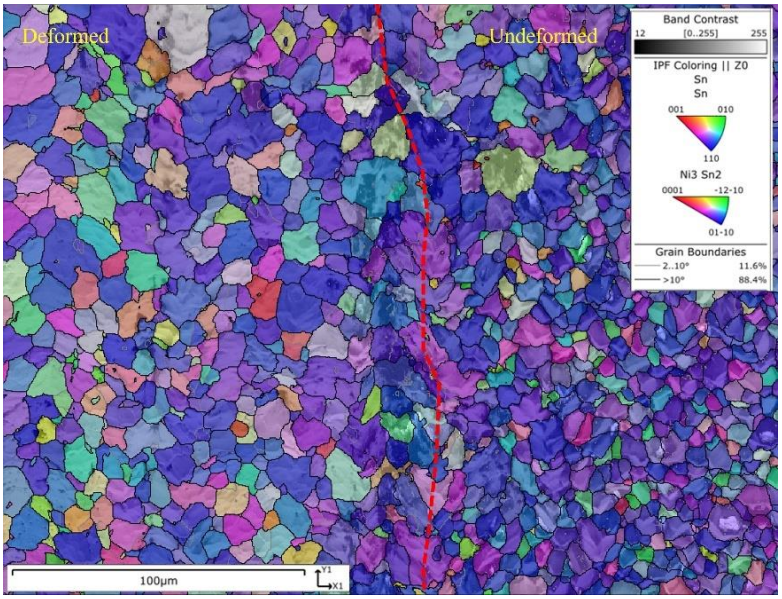

Figure 4.8: Grain map of surface of pure tin coating from Sn MSA solution on ambient for 4 weeks

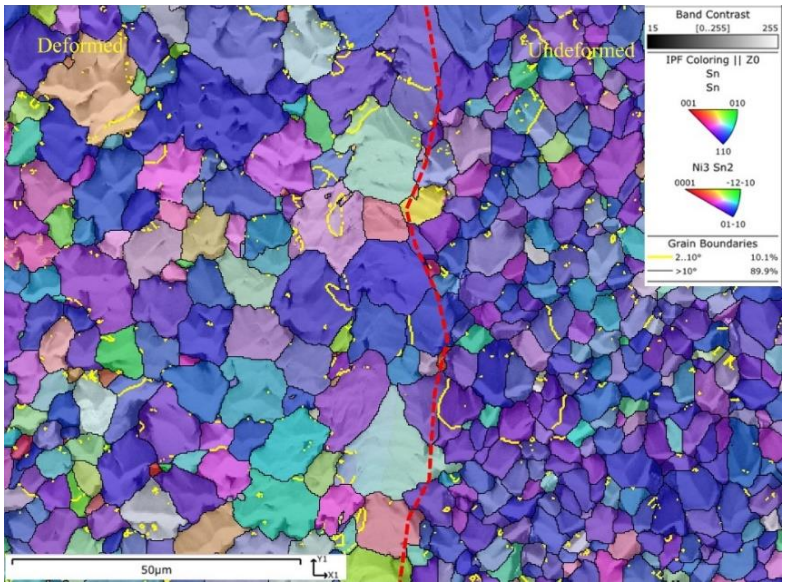

Figure 4.9: Grain map of the surface of pure tin coating from Sn MSA solution on 40^0C for 4 weeks

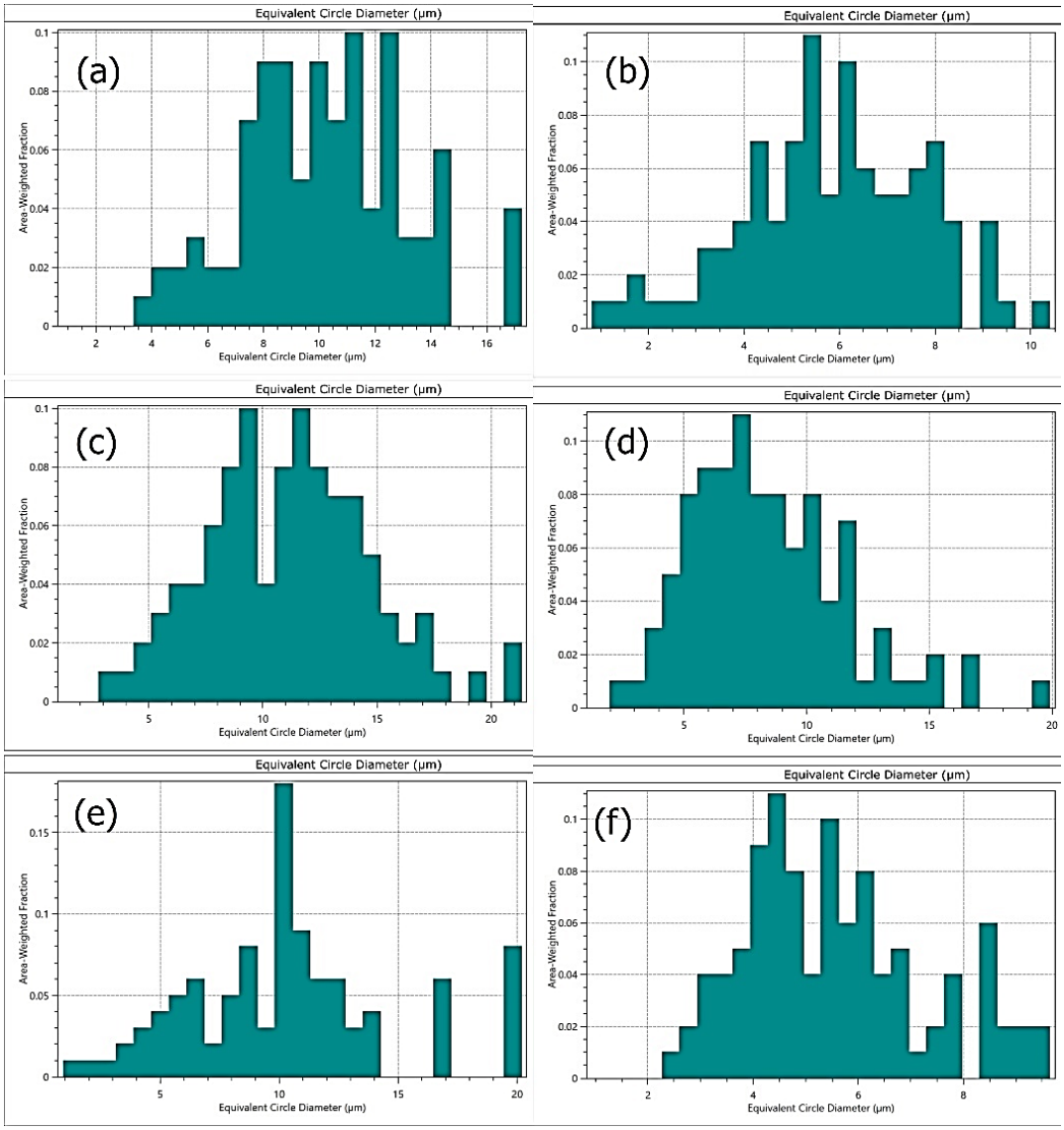

Figure 4.10: Sn grain size distribution map pure tin coating from Sn MSA solution storage for 4 weeks under different temperatures (a) deformed area at -15C, (b) undeformed area at -15C, (c) deformed area at room temperature, (d) undeformed area at room temperature, (e) deformed area at 40C, (f) undeformed area at 40C,

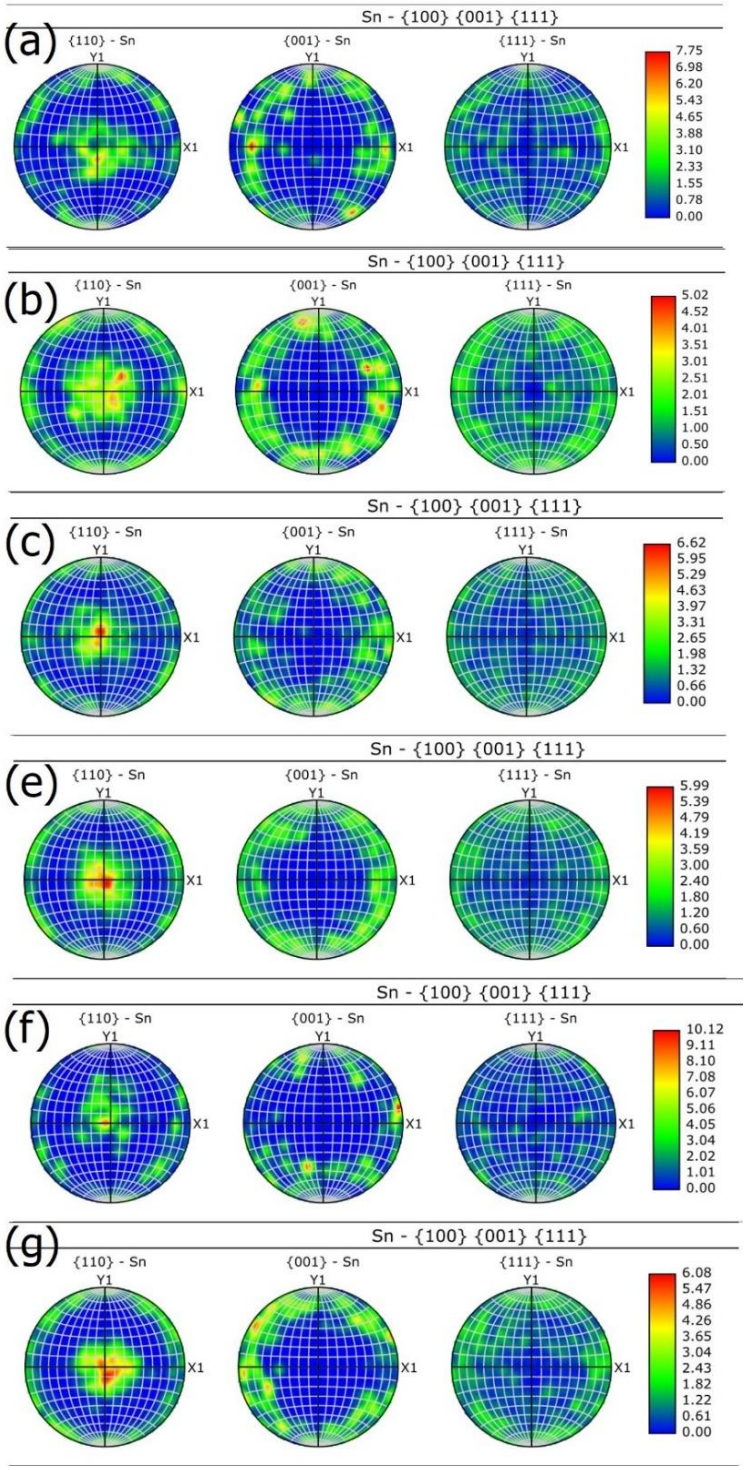

Figure 4.11: Sn grain pole figure map of pure tin coating storage for 4 weeks under different temperature (a) deformed area at -15C, (b) undeformed area at -15C, (c) deformed area at room temperature, (d) undeformed area at room temperature, (e) deformed area at 40C, (f) undeformed area at 40C,

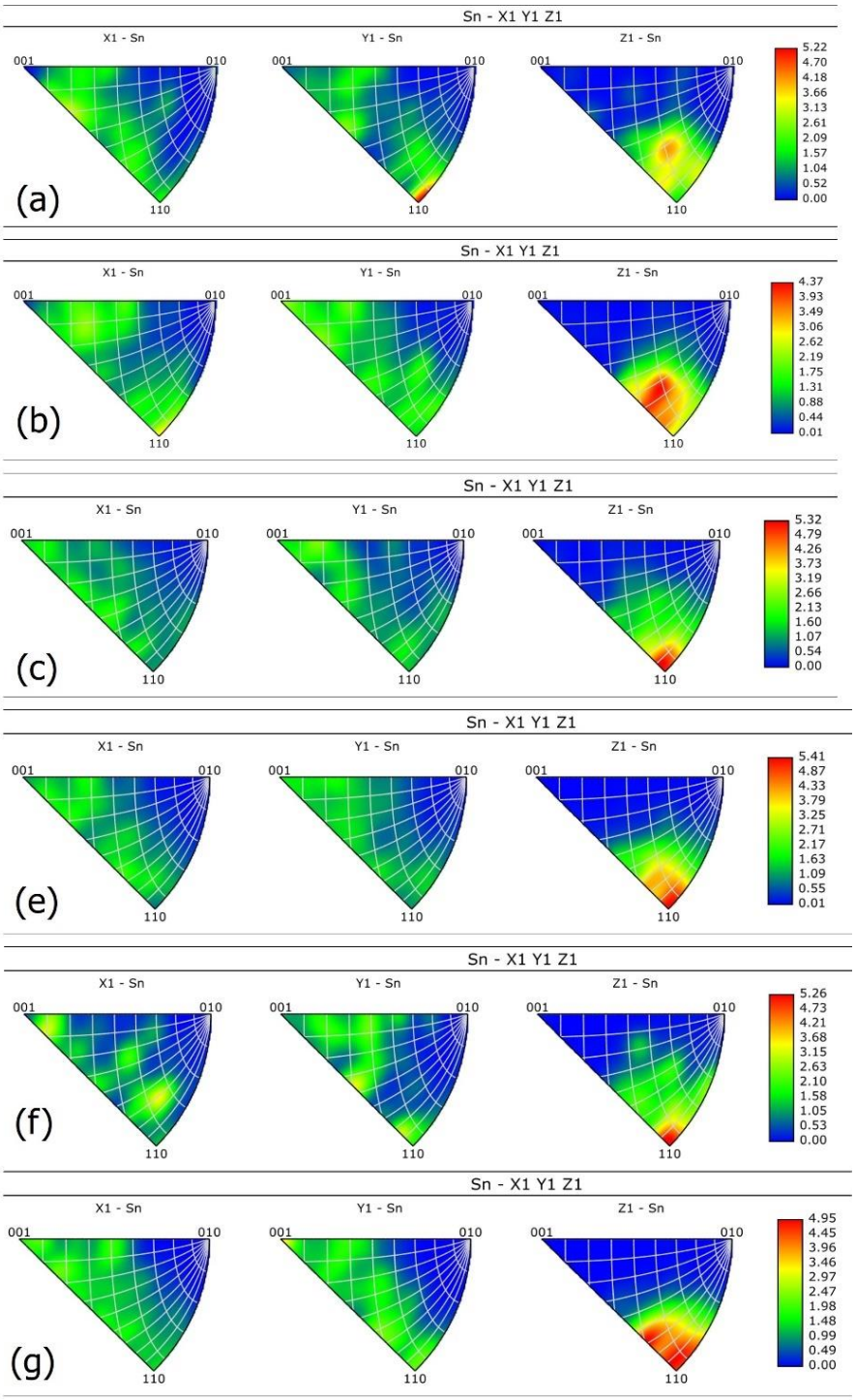

Figure 4.12: Sn grain inverse pole figure map of pure tin coating storage for 4 weeks under different temperature (a) deformed area at -15C, (b) undeformed area at -15C, (c) deformed area at room temperature, (d) undeformed area at room temperature, (e) deformed area at 40C, (f) undeformed area at 40C,

4.2.2 Cross-section results

Figure 4.13 presents a cross-sectional inverse pole figure analysis of a pure tin sample after a storage period of 4 weeks at -15°C. The analysis reveals a distinctive pattern of grain boundary formation related to whisker growth. Specifically, the region where whisker growth is observed exhibits a higher concentration of low-angle grain boundaries. These boundaries are most prevalent in the area experiencing whisker growth, followed by the deformation zone, with the non-deformed regions showing the least concentration of such boundaries. This distribution suggests that the mechanical stress induced in specific areas influences the formation of low-angle grain boundaries, which are indicative of the initial stages of plastic deformation.

Complementing this analysis, a KAM map, depicted in Figure 4.14, underscores the correlation between internal stress levels and whisker growth areas. The map indicates that the regions of whisker growth are subject to the highest internal stresses, reinforcing the hypothesis that stress concentration is a significant driver of whisker formation.

Further comparative analyses are provided in Figures 4.15 - 4.18, which offer cross-sectional inverse pole figures of pure tin samples stored for 4 weeks at room temperature and 40°C, respectively. These figures illustrate a notable decrease in the formation of low-angle grain boundaries in the whisker growth areas at elevated temperatures. This observation can be attributed to the increased propensity for grain boundary slippage at higher temperatures, which serves as a mechanism for stress relief. Consequently, the thermal conditions under which tin samples are stored have a profound effect on the microstructural changes associated with whisker growth, with elevated

temperatures facilitating grain boundary movement and thereby potentially mitigating the formation of whiskers by allowing the material to relieve stress more efficiently.

Figure 4.19 is a schematic of Sn whisker growth principle. In the deformed area, all directions of tin grains are constrained, so grain twisting and tilting cannot occur. Under the action of compressive force, dislocations are formed and aggregated to form new small-angle grain boundaries. In the whisker growth area, dislocation accumulates. According to Coble's theory, when a unit grain is subjected to tensile force in the out-plane direction, the free surface generates vacancies. In the plane direction, the grains are subjected to compressed force and the atomic density at the grain boundaries increases. Under the influence of the equilibrium between vacancies and atoms, the atoms diffuse to the free surface and form whiskers.

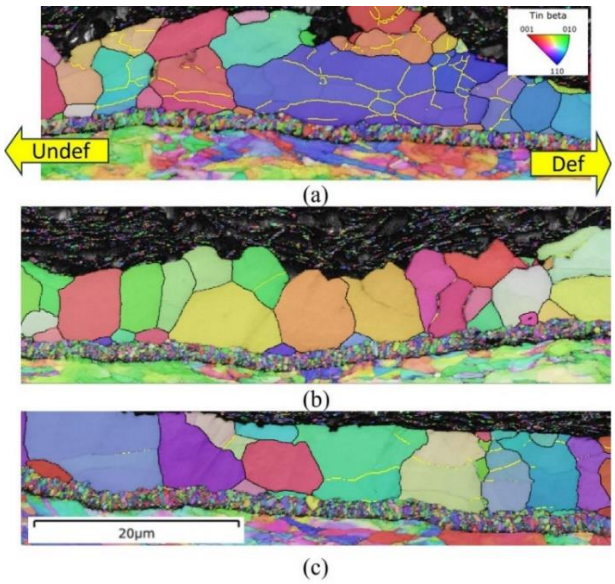

Figure 4.13: Grain maps of cross-sections of pure tin coatings storage at -15^{0}C for 4 weeks: (a) whisker growth area, (b) undeformed area and (c) deformed area.

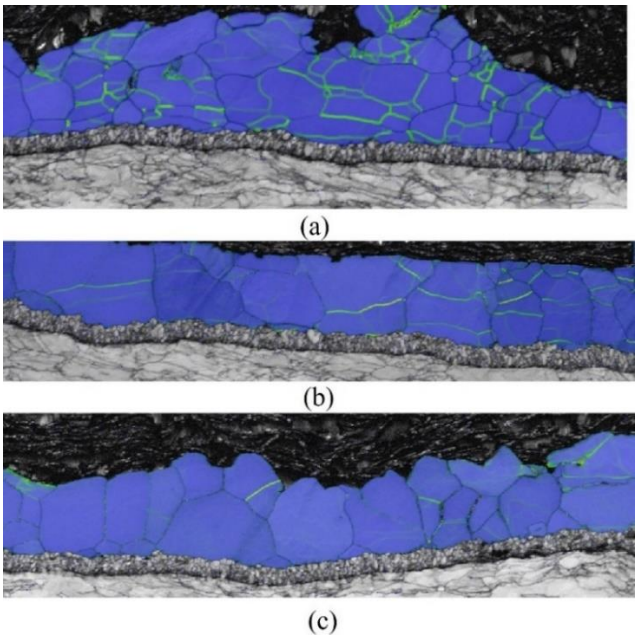

Figure 4.14: KAM maps of cross-sections of pure tin coatings storage at -15^{0}C for 4 weeks: (a) whisker growth area, (b) undeformed area and (c) deformed area.

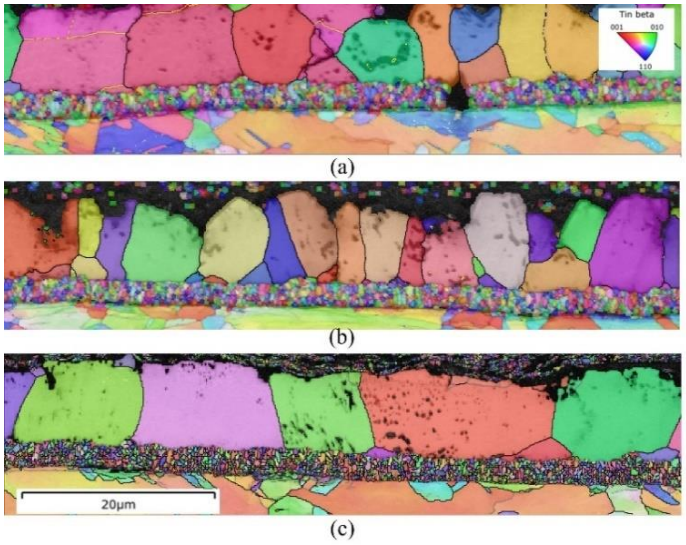

Figure 4.15: Grain maps of cross-sections of pure tin coatings storage at room temperature for 4 weeks: (a) whisker growth area, (b) undeformed area and (c) deformed area.

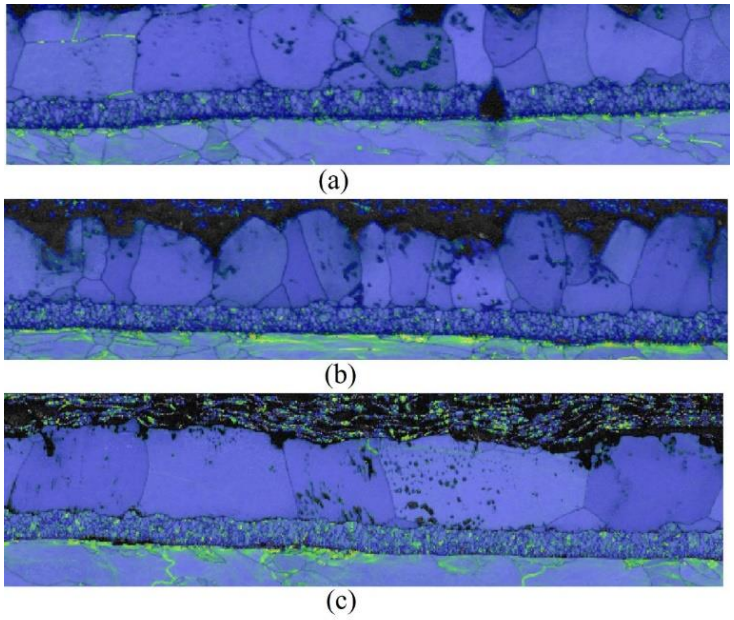

Figure 4.16: KAM maps of cross-sections of pure tin coatings storage at room temperature for 4 weeks: (a) whisker growth area, (b) undeformed area and (c) deformed area.

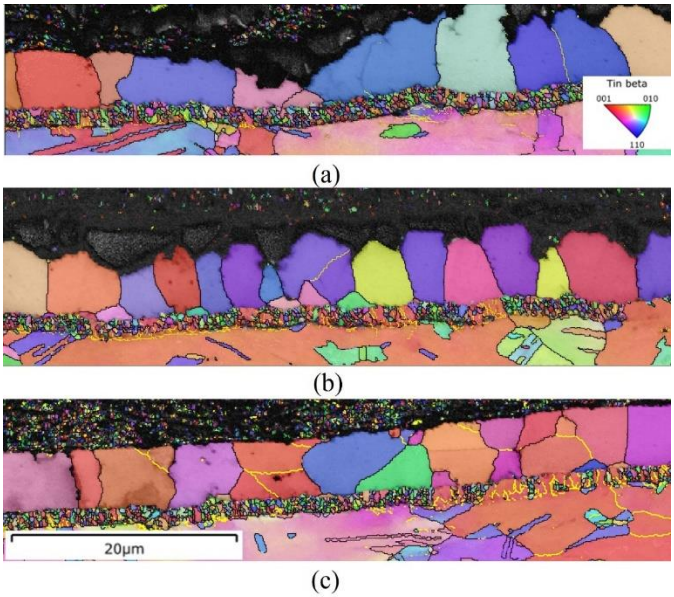

Figure 4.17: Grain maps of cross-sections of pure tin coatings storage at 40 C for 4 weeks: (a) whisker growth area, (b) undeformed area and (c) deformed area.

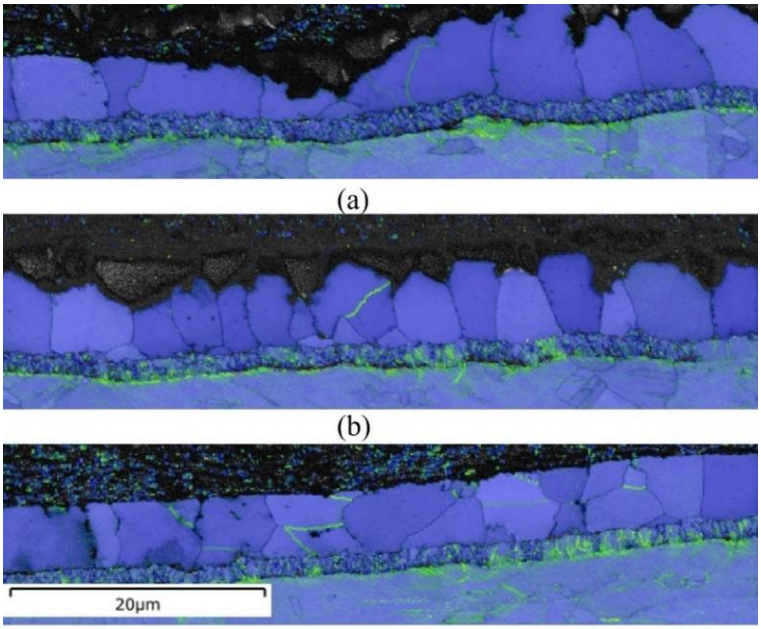

Figure 4.18: KAM maps of cross-sections of pure tin coatings storage at 40C for 4 weeks: (a) whisker growth area, (b) undeformed area, and (c) deformed area.

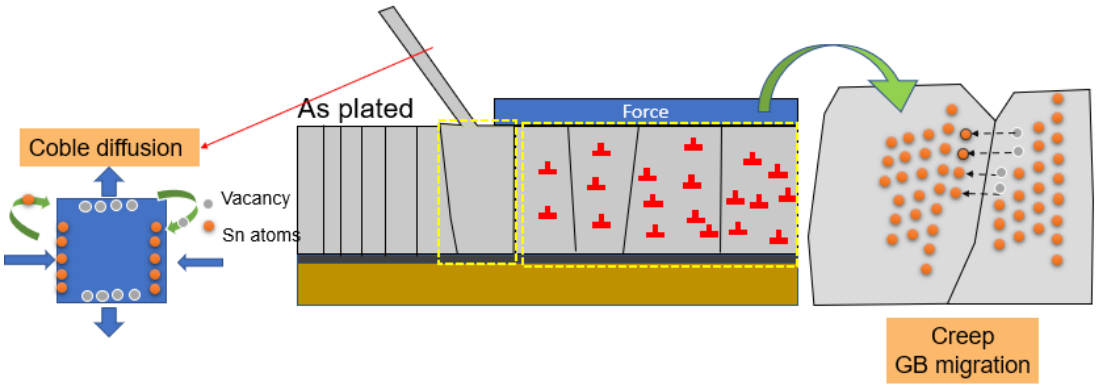

Figure 4.19: Schematic diagram of whisker growth principle

4.3 Whiskers mitigation mechanism

4.3.1 Surface EBSD

Figure 4.20 presents an EBSD color-coded orientation map, illustrating the microstructural changes in pure Sn and Sn-xSb samples. From Figure 4.20, the mean sizes of Sn grains for the three samples are 1.78 um, 1.50 um and 1.64 um, respectively. The significant reduction in Sn grain size with the addition of Sb—from 5.05 μm in pure Sn to approximately 1.5 μm in the Sn-xSb samples—demonstrates the refining effect of Sb on Sn grains. Additions of lead and bismuth, which have inhibitory effects on whiskers, have also been reported to have a refining effect on tin grains [22,30]. However, the grain size does not decrease further with increased Sb content, which suggests a threshold in the refining capacity of Sb addition, corresponding to the above whisker growth results, where whisker suppression does not proportionately escalate with higher concentrations of Sb. Furthermore, Fig. 4.20 reveals a shift in the crystallographic orientation of Sn grains with Sb doping. In the pure Sn sample, the grains predominantly orient in the Z direction close to the (110) plane. With the addition of Sb, this orientation begins to shift. As the Sb content increases from 3% to 10%, the crystal orientation of the Sn grains transitions to (321) and stabilizes. This suggests that the addition of Sb significantly alters the orientation of Sn grains.

Further structural insights are provided by Figures 4.21 and 4.22, which depict the inverse pole figures and pole figures, respectively, for both pure Sn and Sn-xSb samples. The analysis of the tin plating layer in its undoped state exhibits a predominant (110) crystal orientation in the out-of-plane direction. The introduction of a 3% antimony dopant initiates a noticeable shift in the crystal orientation of tin. With increasing

concentrations of antimony, a progressive transition in the crystallographic orientation of tin is observed, culminating in the stabilization of the (321) orientation. This shift in crystal orientation with antimony doping not only highlights the impact of antimony on the structural characteristics of tin but also suggests alterations in the mechanical and possibly electrical properties of the alloy, reflective of the interplay between alloying elements and the resultant microstructural evolution.

As can be seen from Figure Figure 4.23, after the addition of Sb, the Sn grains are refined, but with the increase of Sb element content, the Sn grains are not further refined.

Figure 4.24 shows a grain map of the surface of the Sn-10Sb sample storage for 4 weeks at room temperature. It can be seen that the size of tin grains is almost unchanged after compression deformation, which is contrary to the results of pure tin samples.

A slight rotation of grains is usually observed when Sn undergoing creep deformation [12,31]. In this study, the local misorientation level is presented by kernel average misorientation (KAM). The density of the geometrically necessary dislocations (GNDs) is used to present the dislocation level. The statistics data of average grain size, average KAM, and GNDs are shown in Table 4.2. The KAMave values of the as-plated area, whisker growth boundary, and deformed area of the pure Sn sample are 0.20, 0.37, and 0.22, respectively. Deformed regions exhibit lower KAM values. The GNDs density of the as-plated area, whisker growth boundary, and deformed area of the pure Sn sample are $1.99 \times 10^{8}\ m^{-2}$, $6.59 \times 10^{8}\ m^{-2}$, and $1.53 \times 10^{8}\ m^{-2}$. The GNDs is higher in the whisker growth area, indicating more plastic deformation occurred in the whisker growth boundary area. In contrast, for the Sn-xSb samples, the deformed area shows the highest KAM and GND value among the three areas, indicating that more dislocation occurs in

the deformation region. The occurrence of more dislocations in the deformation zone indicates that DRX is more difficult to occur in the whisker growth area due to grain refinement.

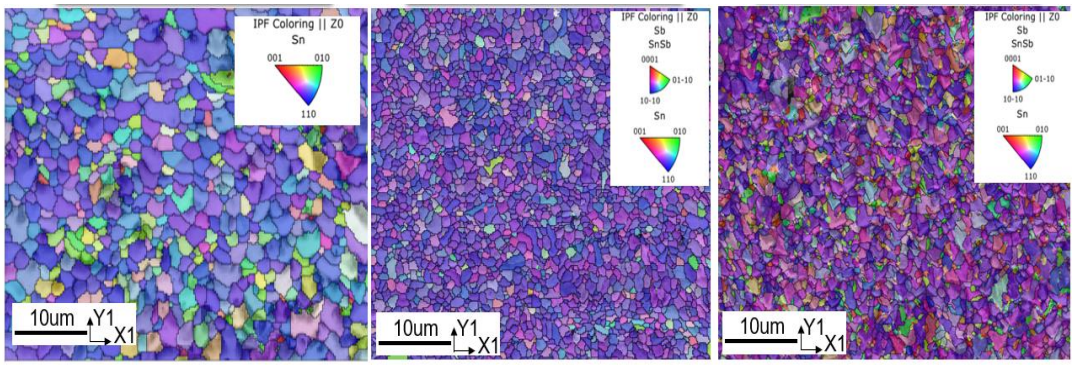

Figure 4.20: Grain map of as-plated surface of pure Sn and Sn-xSb coatings: (a) pure Sn, (b) Sn-3Sb, (c) Sn-10Sb and (d) Sn-15Sb

Table 4.2 Crystallography statistics of pure Sn and Sn-xSb surface samples before and after indentation test storing for 4 weeks at room temperature.

Sample types	Grain Size (um)			Ave. GND×10^8 m^{-2} (Burgers vector =0.5<110>)			Ave. KAM (°)		
	As-plated	Boun-dary	Defo-rmed	As-plated	Boun-dary	Defo-rmed	As-plated	Boun-dary	Defo-rmed
Pure Sn	5.05	6.99	6.82	1.99	6.59	1.53	0.20	0.37	0.22
Sn-3Sb	1.46	1.50	1.52	0.74	0.94	1.19	0.29	0.34	0.44
Sn-10Sb	1.50	1.47	1.41	0.63	0.93	1.17	0.27	0.42	0.56
Sn-15Sb	1.44	1.55	1.51	0.85	1.01	1.23	0.35	0.40	0.49

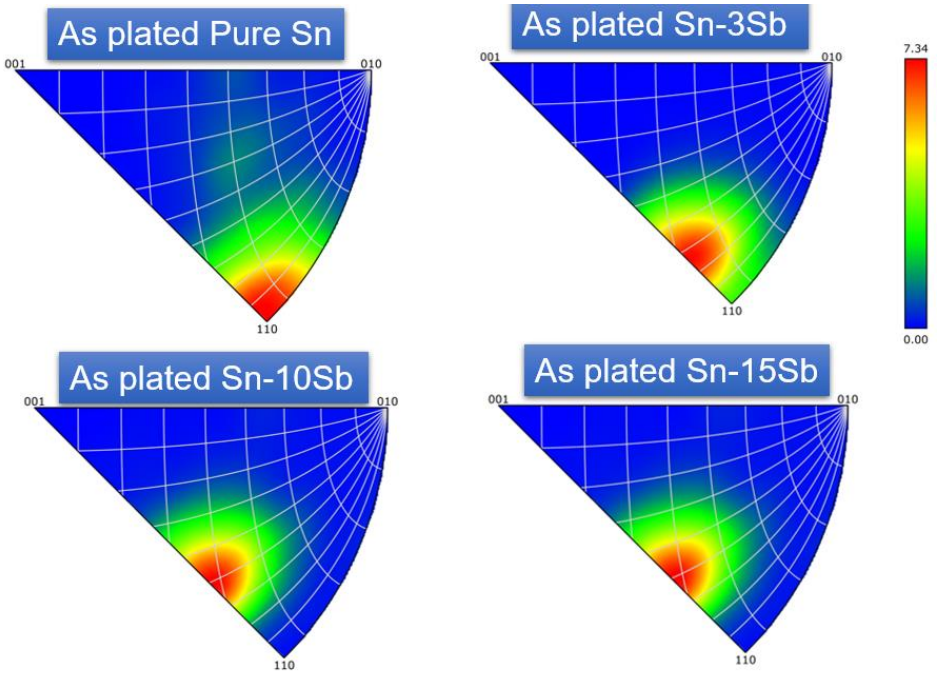

Figure 4.21: Sn phase inverse pole figure of the as-plated surface of pure Sn and Sn-xSb coatings: (a) pure Sn, (b) Sn-3Sb, (c) Sn-10Sb and (d) Sn-15Sb

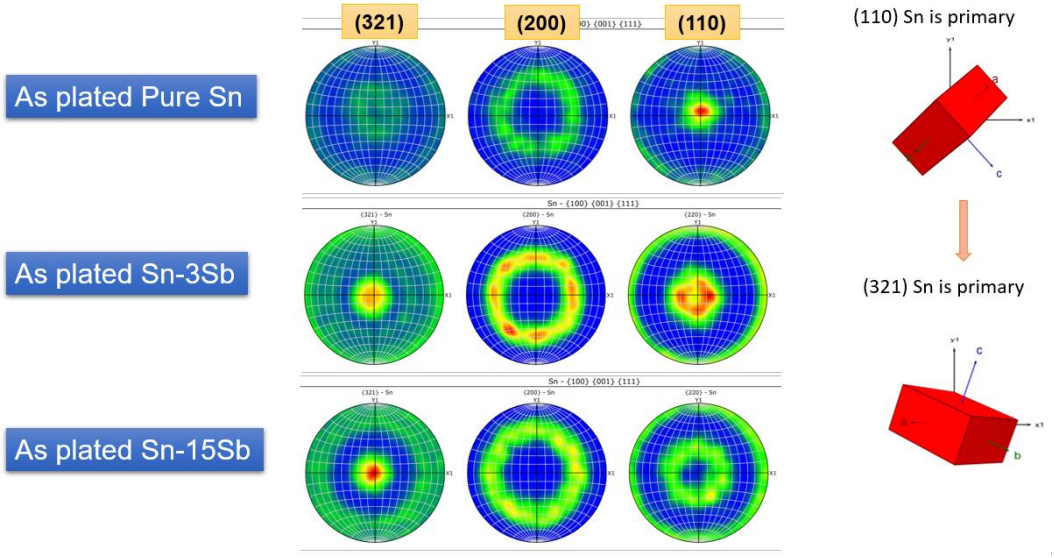

Figure 4.22: Sn phase pole figure of the as-plated surface of pure Sn and Sn-xSb coatings: (a) pure Sn, (b) Sn-3Sb, (c) Sn-10Sb and (d) Sn-15Sb

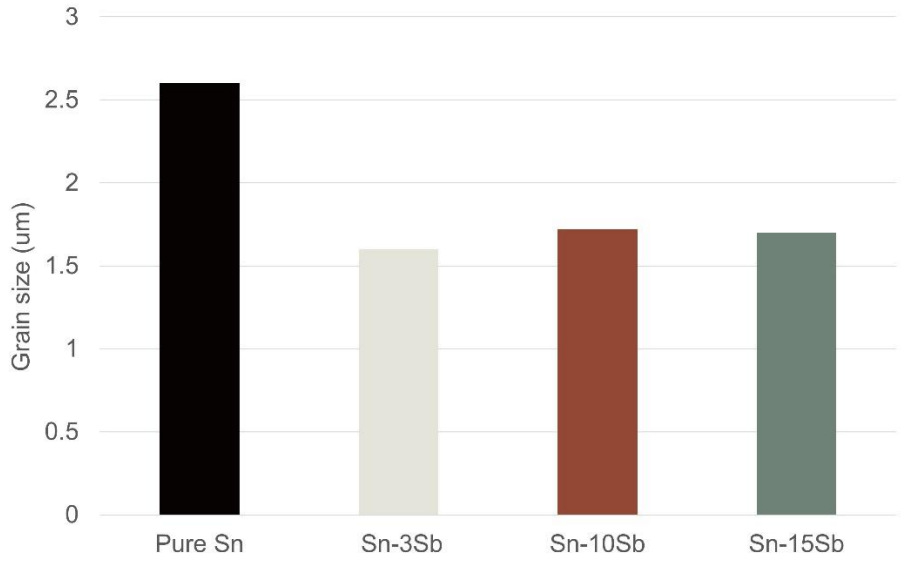

Figure 4.23: Sn grain size as a function of Sb content in the coating

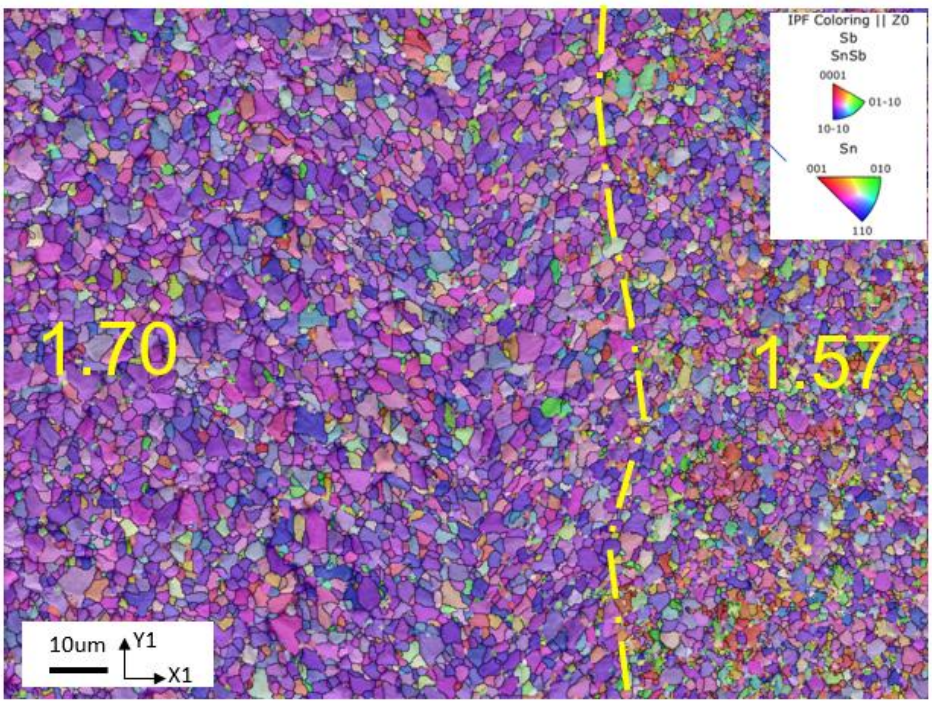

Figure 4.24: Grain map of the surface of Sn-10Sb sample storage for 4 weeks at room temperature

4.3.2 Cross-section results

Figure 4.25 presents a cross-sectional inverse pole figure analysis of an Sn-xSb alloy sample after being stored for four weeks at ambient conditions. This analysis highlights the antimony-doped coating's transition to an equiaxed crystal microstructure, characterized by grains that are approximately equal in dimension along all axes. This microstructural characteristic is noteworthy, as equiaxed grains are often associated with improved isotropic mechanical properties and a more uniform stress distribution within the material, potentially influencing the alloy's resistance to whisker formation.

Figure 4.26 offers a schematic representation of the process involved in mitigating whisker growth within the deformed region of the coating. Upon the application of compressive stress, the grain boundaries within the equiaxed microstructure are prompted to undergo slip movements along the in-plane direction. This mechanism plays a crucial role in alleviating internal stresses that may accumulate as a result of external pressures or thermal mismatches. By enabling the reorientation and movement of grain boundaries, the microstructure can dissipate stress more effectively, thereby reducing the driving forces that lead to whisker nucleation and growth. This schematic diagram elucidates the importance of grain boundary behavior and microstructural adaptation in the context of mechanical stress management, offering insights into the fundamental processes that contribute to the stability and integrity of antimony-doped tin coatings.

Figure 4.25 presents a cross-section inverse pole figure, KAM distribution map, and phase map of Sn-10Sb stored for 4 weeks at room temperature. It can be seen from Fig. 4.25 (a) that the Sb doping coating exhibits an equiaxed crystal microstructure. Compared with the pure Sn sample shown in Fig. 4.13, the Sn-10Sb sample does not

have much LGBS formed in the whisker growth area, which shows that the equiaxed crystal effectively prevents creep deformation and uses grain boundary slip to offset the stress. Additionally, the distribution KAM within the Sn-10Sb sample shown in Fig.4.25(b) is more uniform across the entire sample, as opposed to being concentrated in areas of whisker growth as seen in pure tin. A uniform KAM distribution indicates a more homogeneous internal strain and stress distribution within the grains. Fig. 4.25 (c) shows the phase distribution diagram of the Sn-10Sb sample. The influence of Sb incorporation into a Sn matrix is analogous to the microstructural modifications induced by the addition of lead (Pb) or bismuth (Bi). The introduction of Pb into tin is known to result in the segregation of Pb at the grain boundaries, thereby inhibiting the growth of IMCs at these junctures. In the current study, the absence of segregated Sb at the grain boundaries suggests that the mechanism by which Sb suppresses whisker proliferation is fundamentally linked to the transformation of the grain structure. Specifically, Sb doping leads to the transition from columnar to equiaxed grains, a process augmented by grain refinement.

The formation of a refined and equiaxed grain morphology is beneficial in terms of stress management within the material matrix. This refined microstructure facilitates the uniform distribution and dissipation of compressive stresses, thereby diminishing the driving force responsible for the genesis of tin whiskers. The equiaxed grain structure, as opposed to columnar grains, is intrinsically more isotropic in mechanical behavior, which supports a more homogeneous stress relief throughout the material. Consequently, the alteration of the microstructure through Sb doping is considered to be a strategic

approach to enhance the material's resistance to whisker formation, thus improving its reliability in applications where such phenomena are of critical concern.

Considering that Ni can prevent the interdiffusion of Sn and Cu and SnNi IMCs form very slowly at room temperature [20], the effect of IMCs on whisker growth is ignored. The mitigation of Sn whisker growth by co-electroplating Sb can be attributed to two reasons. First, Sb addition changes the structure of Sn grains from monolater columnar to multilayer equiaxed structure, which is conducive to stress relaxation. Fig.4.26a shows the process of whisker formation from a pure Sn sample with columnar microstructure. Dislocation is first produced by applied stress and then DRX grains with an oblique grain boundary are formed. Continuous stress drives the diffusion of Sn atoms from the base material beneath the oblique grain boundary to the DRX grain, culminating in the protrusion of a whisker. Fig.4.26 b shows the process of whisker inhibition by adding Sb. The equiaxed Sn-xSb samples under stress exhibit grain boundary slip as a significant mechanism for internal stress consumption. This slip at the grain boundaries offsets the stress and slows the diffusion of Sn atoms that are typically induced by internal stress, thereby inhibiting whisker formation. Second, Sb addition changes the Sn grain orientation from (110) to (321). There has been controversy over the preferential orientation of whisker growth, although many studies reported that whiskers are more likely to grow from the (110) or near-(110) grains. In this study, it remains unclear whether the (321) crystal orientation inhibits whisker growth.

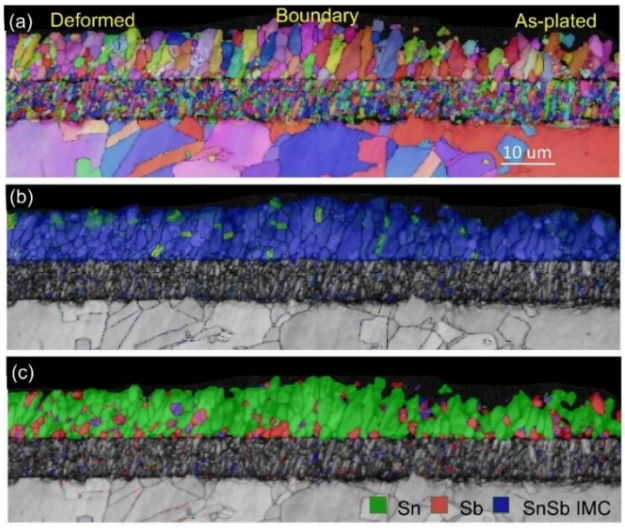

Figure 4.25: Cross-section inverse pole figure of Sn-xSb stored for 4 weeks at room temperature (a) cross-section inverse pole figure, (b) KAM distribution map, and (c) phase map

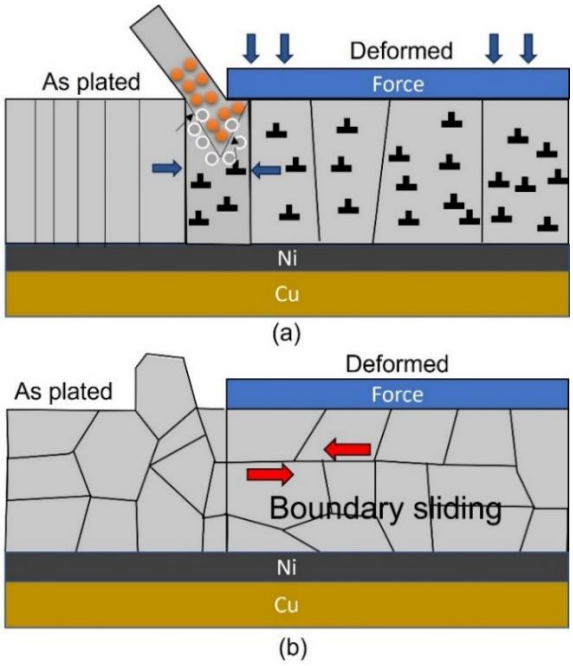

Figure 4.26: Schematic diagram of whisker mitigation principle (a) whisker formation and (b) hillocks formation

CHAPTER FIVE

CONCLUSIONS AND FUTURE WORK

The tin whisker issue represents a significant reliability concern for electronic components and systems. Understanding the causes and mechanisms of whisker growth, along with implementing effective mitigation strategies, is crucial for ensuring the longevity and reliability of electronic devices. As the electronics industry continues to evolve, ongoing research and development are essential to address and manage the risks associated with tin whiskers.

This study introduces an innovative and controllable approach to mitigate the growth of Sn whiskers by electroplating Sn-xSb (x=3 wt.%, 10 wt.%, 15 wt.%) coatings. A tin-antimony electroplating solution, mainly composed of tin chloride and antimony acetate, was developed, enabling the synthesis of a tin-antimony electroplating alloy in one step. A specialized fixture was designed to apply high wide-plane compressive stress, accelerating whisker growth for experimental purposes. Sn whisker mitigation through co-electroplating various Sb additions was investigated by comparing pure matte Sn on Cu substrates with a Ni seed layer. The main conclusions are:

First, the results showed that Sn whiskers were observed only on pure Sn surfaces; no whiskers (only some extrusions/hillocks) were observed on the Sn-xSb films during 6 months of room temperature storage. Whiskers growth was efficiently suppressed by Sb addition as low as 3 wt.%.

Second, the data suggests that the suppression and whisker growth mitigation mechanism involves grain size refinement and a transformation of the grain structure

from columnar to equiaxed configurations. Sb additions also influence grain orientation, shifting from (110) to (321), which is associated with decreased surface energy.

Third, accelerating tests further highlighted the impact of Sb on the microstructural stability of Sn coatings. The grain size in pure Sn samples increased significantly post-indentation, whereas the grain size in Sn-xSb alloys remained relatively stable. This stability is attributed to the formation of horizontal grain boundaries that facilitate stress relaxation more effectively.

These results underscore the critical role of microstructure in the growth of Sn whiskers and highlight the potential of Sb addition as a viable strategy for their mitigation. The study proposes that the microstructural alterations induced by Sb addition not only enhance the mechanical stability of Sn coatings but also contribute to the overall reliability of electronic components by mitigating whisker-related failures.

To build upon the findings of this study, several future research directions are proposed:

- Long-term Stability Analysis:

Extended duration studies could be conducted to evaluate the long-term stability and reliability of Sn-xSb coatings under various environmental conditions, such as temperature cycling and humidity.

- Microstructural Characterization:

Advanced microstructural characterization techniques, such as transmission electron microscopy (TEM) and atom probe tomography (APT), could be used to gain deeper insights into the atomic-scale mechanisms of whisker suppression by Sb inclusion.

- Computational Modeling:

The future effort could focus on developing

computational models to simulate the effects of various alloying elements and microstructural changes on whisker growth, providing predictive insights for designing more robust coatings. In doing so, commercial simulators may be resorted, yet atomic level crystal kinetics should be included with tailored settings.

By pursuing these future research directions, it will be possible to further advance the understanding of tin whiskers, and ultimately achieve mitigation and even total elimination of such a culprit to enormous electrical system failures, thereby enhancing the reliability and performance of electronic devices and systems.

REFERENCES

[1] Cobb, H. L. "Cadmium whiskers." *Monthly Rev. Am. Electroplaters Soc* 33, no. 28 (1946): 28-30.

[2] Mayer, Ludwig, Robert Rickett, and Heinrich Stenemann. "Bismuth Whisker Growth." *Journal of Applied Physics* 33, no. 3 (1962): 982-984.

[3] Brusse, Jay, and Michael Sampson. "Zinc whiskers: hidden cause of equipment failure." *IT professional* 6, no. 6 (2004): 43-47.

[4] Li, Shuai, Yushuang Liu, Peigen Zhang, Yan Zhang, Chengjie Lu, Long Pan, Jianxiang Ding, and Zhengming Sun. "Interface energy-driven indium whisker growth on ceramic substrates." *Journal of Materials Science: Materials in Electronics* 32, no. 12 (2021): 16881-16888.

[5] Lee, B-Z., and D. N. Lee. "Spontaneous growth mechanism of tin whiskers." *Acta Materialia* 46, no. 10 (1998): 3701-3714.

[6] Smetana, Joe. "Theory of tin whisker growth:“The end game”." *IEEE Transactions on Electronics Packaging Manufacturing* 30, no. 1 (2007): 11-22.

[7] Brusse, Jay, Gary Ewell, and Jocelyn Siplon. "Tin whiskers: Attributes and mitigation." *Carts Europe* 16 (2002).

[8] Galyon, George T. "A history of tin whisker theory: 1946 to 2004." In *SMTA International Conference, Chicago*. 2004.

[9] Arnold, S. M. *Repressing the growth of tin whiskers*. 1966.

[10] Puttlitz, Karl J., and George T. Galyon. "Impact of the ROHS Directive on high-performance electronic systems: Part II: key reliability issues preventing the implementation of lead-free solders." *Journal of Materials Science: Materials in Electronics* 18 (2007): 347-365.

[11] Fisher, R. M., L. S. Darken, and K. G. Carroll. "Accelerated growth of tin whiskers." *Acta metallurgica* 2, no. 3 (1954): 368-373.

[12] Chason, Eric, Nitin Jadhav, Fei Pei, Eric Buchovecky, and Allan Bower. "Growth of whiskers from Sn surfaces: Driving forces and growth mechanisms." *Progress in Surface Science* 88, no. 2 (2013): 103-131.

[13] Subramanian, K. N., K. N. Tu, Chih Chen, and Albert T. Wu. "Stress analysis of spontaneous Sn whisker growth." *Lead-Free Electronic Solders: A Special Issue of the Journal of Materials Science: Materials in Electronics* (2007): 269-281.

[14] Xu, Chen, Yun Zhang, Chonglun Fan, and Joseph A. Abys. "Driving force for the formation of Sn whiskers: compressive stress-pathways for its generation and remedies for its elimination and minimization." *IEEE Transactions on Electronics Packaging Manufacturing* 28, no. 1 (2005): 31-35.

[15] Chen, Hao, Hsin Yi Lee, Ching Shun Ku, and Albert T. Wu. "Evolution of residual stress and qualitative analysis of Sn whiskers with various microstructures." *Journal of materials science* 51 (2016): 3600-3606.

[16] Ashworth, Mark A., Geoffrey D. Wilcox, Rebecca L. Higginson, Richard J. Heath, Chanqing Liu, and Roger J. Mortimer. "The effect of electroplating parameters and substrate material on tin whisker formation." *Microelectronics Reliability* 55, no. 1 (2015): 180-191.

[17] Dittes, Marc, Pascal Oberndorff, Paolo Crema, and Valeska Schroeder. "Tin whisker formation in thermal cycling conditions." In *Proceedings of the 5th Electronics Packaging Technology Conference (EPTC 2003)*, pp. 183-188. IEEE, 2003.

[18] Wei, C. C., P. C. Liu, Chih Chen, and King-Ning Tu. "Electromigration-induced Pb and Sn whisker growth in SnPb solder stripes." *Journal of Materials Research* 23, no. 7 (2008): 2017-2022.

[19] Williams, M. E., K-W. Moon, W. J. Boettinger, D. Josell, and A. D. Deal. "Hillock and whisker growth on Sn and SnCu electrodeposits on a substrate not forming interfacial intermetallic compounds." *Journal of electronic materials* 36 (2007): 214-219.

[20] Kim, K. S., C. H. Yu, S. W. Han, K. C. Yang, and J. H. Kim. "Investigation of relation between intermetallic and tin whisker growths under ambient condition." *Microelectronics Reliability* 48, no. 1 (2008): 111-118.

[21] Su, Peng, Jim Howell, and Sheila Chopin. "A statistical study of Sn whisker population and growth during elevated temperature and humidity tests." *IEEE transactions on electronics packaging manufacturing* 29, no. 4 (2006): 246-251.

[22] Osenbach, J. W., J. M. DeLucca, B. D. Potteiger, A. Amin, R. L. Shook, and F. A. Baiocchi. "Sn corrosion and its influence on whisker growth." *IEEE Transactions on Electronics Packaging Manufacturing* 30, no. 1 (2007): 23-35.

[23] Tu, King-Ning. "Irreversible processes of spontaneous whisker growth in bimetallic Cu-Sn thin-film reactions." *Physical review B* 49, no. 3 (1994): 2030.

[24] Vianco, P. T., and J. A. Rejent. "Dynamic recrystallization (DRX) as the mechanism for Sn whisker development. Part I: A model." *Journal of electronic materials* 38 (2009): 1815-1825.

[25] Chason, E., N. Jadhav, W. L. Chan, L. Reinbold, and K. S. Kumar. "Whisker formation in Sn and Pb–Sn coatings: Role of intermetallic growth, stress evolution, and plastic deformation processes." *Applied Physics Letters* 92, no. 17 (2008).

[26] Boettinger, William J., C. E. Johnson, Leonid A. Bendersky, K-W. Moon, Maureen E. Williams, and Gery R. Stafford. "Whisker and hillock formation on Sn, Sn–Cu and Sn–Pb electrodeposits." *Acta materialia* 53, no. 19 (2005): 5033-5050.

[27] Jo, Jung-Lae, Shijo Nagao, Kyoko Hamasaki, Masanobu Tsujimoto, Tohru Sugahara, and Katsuaki Suganuma. "Mitigation of Sn whisker growth by small Bi additions." *Journal of electronic materials* 43 (2014): 1-8.

[28] Meinshausen, L., S. Bhassyvasantha, B. S. Majumdar, and I. Dutta. "Influence of indium addition on whisker mitigation in electroplated tin coatings on copper substrates." *Journal of electronic materials* 45 (2016): 791-801.

[29] Dunn, B. D. "Whisker formation on electronic materials." *Circuit World* 2, no. 4 (1976): 32-40.

[30] Dunn, B. D. "Whiskers with Special Reference to Spacecraft Systems." *ESA Journal* 11, no. 1988 (1987): 12.

[31] Borgesen, Peter, and Eric Cotts. "Implantable Medical Electronics Assembly Quality and Reliability Considerations." *SMTA NEWS AND JOURNAL OF SURFACE MOUNT TECHNOLOGY* 17 (2004): 25-33.

[32] Meschter, Steven, Michael Osterman, Peter Borgesen, and Indranath Dutta. "Enabling Lead Free Interconnects in DoD Weapon Systems." (2017): 0054.

[33] Chudnovsky, Bella H. "Degradation of power contacts in industrial atmosphere: silver corrosion and whiskers." In *Proceedings of the Forty-Eighth IEEE Holm Conference on Electrical Contacts*, pp. 140-150. IEEE, 2002.

[34] Panashchenko, Lyudmyla, and Michael Osterman. "Examination of nickel underlayer as a tin whisker mitigator." In *2009 59th Electronic Components and Technology Conference*, pp. 1037-1043. IEEE, 2009.

[35] Kadesch, Jong S., Henning Leidecker, and John H. Day. "Effects of conformal coat on tin whisker growth." In *IMAP Conference*. 2000.

[36] Kadesch, Jong S., and Jay Brusse. "The continuing dangers of tin whiskers and attempts to control them with conformal coating." *NASA EEE Links Newsletter* (2001).

[37] Woodrow, Thomas A., and Eugene A. Ledbury. "Evaluation of conformal coatings as a tin whisker mitigation strategy." In *IPC/JEDEC 8th International Conference on Pb-Free Electronic Components and Assemblies*, pp. 18-20. 2005.

[38] Schetty, Rob. "Minimization of tin whisker formation for lead-free electronics finishing." *Circuit World* 27, no. 2 (2001): 17-20.

[39] Xu, Chen, Yun Zhang, Chonglun Fan, and Joseph A. Abys. "Thin Sn over Ni: A Practical and Effective Whisker Mitigation Strategy for Leadframe." *Proceedings of IPC/APEX* (2006).

[40] Peach, Milton O. "Mechanism of growth of whiskers on cadmium." *Journal of Applied Physics* 23, no. 12 (1952): 1401-1403.

[41] Pitt, Charles H., and Robert G. Henning. "Pressure-induced growth of metal whiskers." *Journal of Applied Physics* 35, no. 2 (1964): 459-460.

[42] Britton, S. C. "Spontaneous growth of whiskers on tin coatings: 20 years of observation." *Transactions of the IMF* 52, no. 1 (1974): 95-102.

[43] L. Corbid, Constraints on the use of tin plate in miniature electronic packages, in *Proceedings of the 3rd International Electronics Conference, SAMPE* (1989), pp. 773–778

[44] K. M. Cunningham and M. P. Donahue, "Tin whiskers: Mechanisms of growth and prevention", *Proc. 4th Int. SAMPE Electron. Conf.*, vol. 14, pp. 569-575, 1990-Jun.

[45] Diehl, R. P. "Significant characteristics of tin and tin-lead contact electrodeposits for electronic connectors." *Met. Finish.* 91, no. 4 (1993): 37-42.

[46] M. Ishii, T. Kataoka, H. Kruihara, Whisker problem in ultra-fine pitch circuits, in *Proceedings of the 12th European Microelectronics and Packaging Conference* (1999), pp. 379–385

[47] Stevens, Craig. "Relay failures induced by the growth of tin whiskers. A Case Study." In IEEE Boston Reliability Chapter 38th Annual Spring Reliability Symposium, pp. 1-6. 2001.

[48] J. Khuri, Agency action notice, in Government-Industry Data Exchange Program (GIDEP) (2002)

[49] Sobiech, M., M. Wohlschlögel, U. Welzel, E. J. Mittemeijer, W. Hügel, A. Seekamp, W. Liu, and Gene E. Ice. "Local, submicron, strain gradients as the cause of Sn whisker growth." Applied Physics Letters 94, no. 22 (2009).

[50] Stein, Jendrik, U. Welzel, A. Leineweber, W. Huegel, and Eric Jan Mittemeijer. "The crystallographic growth directions of Sn whiskers." Acta Materialia 86 (2015): 102-109.

[51] Jagtap, Piyush, and Praveen Kumar. "Whisker growth in sn coatings: a review of current status and future prospects." Journal of Electronic Materials 50 (2021): 735-766.

[52] Mathew, M. D., H. Yang, S. Movva, and K. L. Murty. "Creep deformation characteristics of tin and tin-based electronic solder alloys." Metallurgical and Materials Transactions A 36 (2005): 99-105.

[53] Chen, Chih-ming, and Yu-jen Chen. "Growth orientation of the tin whiskers on an electrodeposited Sn thin film under three-point bending." *Materials Letters* 63, no. 17 (2009): 1517-1520.

[54] Kuwano, Noriyuki, Marina Binti Lias, Nur Azmah Nordin, Youhei Soejima, and Ahmad Rafiqan bin Nayan. "Preliminary study on deformation and recrystallization behavior of pure tin for mitigation of whisker growth." *Solid State Phenomena* 273 (2018): 107-111.

[55] Moriuchi, Hiroyuki, Yoshihiro Tadokoro, Masahide Sato, Takeshi Furusawa, and Noboru Suzuki. "Microstructure of external stress whiskers and mechanical indentation test method." *Journal of electronic materials* 36 (2007): 220-225.

[56] Shibutani, Tadahiro, Qiang Yu, Takuma Yamashita, and Masaki Shiratori. "Stress-induced tin whisker initiation under contact loading." *IEEE transactions* on electronics packaging manufacturing 29, no. 4 (2006): 259-264.

[57] Sarobol, P., J. E. Blendell, and C. A. Handwerker. "Whisker and hillock growth via coupled localized Coble creep, grain boundary sliding, and shear induced grain boundary migration." Acta Materialia 61, no. 6 (2013): 1991-2003.

[58] Sun, Yi, Shaoan Cheng, Longxin Li, Zhen Yu, Zhengzhong Mao, and Haobin Huang. "Facile sealing treatment with stannous citrate complex to enhance performance of electrodeposited Ti/SnO2–Sb electrode." Chemosphere 255 (2020): 126973.

[59] Watt, Charles S. "Electrodeposition of Sn-Rich, Au-Sn Solder Films." (2015).

[60] Buchovecky, Eric J. "Numerical simulation of stress generation and whisker growth in tin films." PhD diss., Brown University, 2010.